Till Stratigraphy and Sediment Provenance of the Dessert Lake Drumlin Field Area, West of Great Slave Lake, NT: Implications for Regional Glacial Dynamics Models

by

Wenyao Liang

A thesis

presented to the University of Waterloo

in fulfillment of the

thesis requirement for the degree of

Master of Science

in

Earth Sciences

Waterloo, Ontario, Canada, 2024

© Wenyao Liang 2024

Author’s Declaration

This thesis consists of material all of which I authored or co-authored: see Statement of Contributions included in the thesis. This is a true copy of the thesis, including any required final revisions, as accepted by my examiners.

I understand that my thesis may be made electronically available to the public.

Statement of Contributions

Name of contributors	Contribution
Dr. Martin Ross	Assisted with field work including measuring the striations, research design, lab work, photos, thesis revisions and provided guidance on data interpretation and writing.
Dr. Sam Kelley	Assisted with research design and thesis revisions
Dr. John Johnston	Assisted with research design and thesis revisions
Dr. Philippe Normandeau (Government of the Northwest Territories)	Assisted with fieldwork
Cindy Liu (UW coop student, lab assistant)	Assisted with grain size analysis
Anisha Kakera (UW coop student, lab assistant)	Assisted with grain size analysis

Abstract

The integration of till stratigraphic and sedimentologic studies with landform-based ice flow analysis has considerable potential for advancing our understanding of subglacial processes, particularly those related to subglacial sediment transport and the generation of subglacial landforms such as drumlins. Currently, few drumlin studies incorporate till provenance analysis, which limits our ability to establish relationships with subglacial sediment transport, drumlin forming processes, and the regional glacial history.

Considerable effort has been made to reconstruct the last glaciation, with a particular focus on the geometry of the Laurentide Ice Sheet (LIS) ice margins and their retreat pattern and chronology. However, to comprehend the long-term evolution of the LIS during a glaciation, it is also essential to include the dynamics of ice streams, the positions of ice divides and their migration phases, and related shifts in ice flow. The history of glacial dynamics remains limited in many regions covered by the LIS. This research focuses on the Dessert Lake drumlin field, west of Great Slave Lake (GSL) within National Topographic System (NTS) map 85K. This area presents a significant opportunity to investigate tills and related sedimentary processes within a drumlin field due to road access and the presence of road cuts extending across several drumlins along Highway 3. Additionally, the bedrock geology consists of sufficiently contrasting bedrock units extending approximately perpendicular to the long axis of the drumlins, which is particularly useful for till provenance analysis.

The glacial geology record of western GSL bears evidence for four distinct ice-flow phases of the LIS. These phases are preserved in various forms such as outcrop-scale erosional features, subglacial streamlined landforms, and in the orientation of clasts in different tills (a.k.a. till fabric) preserved within the drumlins, as well as in the composition of the till, which is useful to establish bedrock source regions (provenance). The sequence of ice flows indicates an initial southward (180 to 190 deg.) ice flow phase, followed by a clockwise shift towards westward (260 to 270 deg.) ice flow, then a slight deviation towards southwestward (215 to 245 deg.) flow. The counterclockwise shift is supported by the overprint relationship of southwesterly oriented landforms on westerly oriented landforms. The average direction of the drumlin's long axis is 249 degrees, which is close to the top till fabric of drumlin section 1 (246 deg.). Finally, there is evidence along the shore of western GSL for a late northwestward (320 to 325 deg.) flow, which may have been limited in lateral extent. The till provenance analysis suggests some of the surficial till samples show a dominantly local

provenance, but there is surficial till with a more distal signature such as more abundant Canadian Shield derived clasts. These changes in ice flow corresponded with the overall eastward retreat of the ice margin and the increasing influence of topography due to the diminishing thickness of the ice.

In conclusion, glacial dynamics shifted in the area, and the evidence is well-preserved in both the erosional and depositional records. Till stratigraphy and related ice flow shifts are preserved within the drumlin cores. Since erosional processes are thought to play an important role in the formation of drumlins, it is likely, in the context of stratified drumlins, that the surficial till in the Dessert Lake drumlin field, and perhaps in other similar settings, consist of multiple till sheets deposited under different subglacial transport regimes and pathways and may thus have contrasting bedrock source regions. It is thus critical for applications like mineral exploration and environmental protection to determine if the till in lower stratigraphic positions occurs at the surface in the drumlin field.

Acknowledgements

I would like to express my sincere gratitude to the following individuals and institutions for their invaluable support and contributions to the completion of this Master's thesis.

First and foremost, I am deeply thankful to my thesis advisor, Dr. Martin Ross, for his guidance, expertise, and unwavering support throughout this research journey. The insightful feedback and constructive criticism have been instrumental in shaping the content and direction of this thesis.

I extend my appreciation to the members of my thesis committee, Dr. John Johnston and Dr. Sam Kelley, for their valuable insights and constructive comments, which significantly enhanced the quality of this work. The Northwest Territories Geological Survey funded this project and provided logistic and support for field work. Many thanks are given to Phillipe Normandeau, for his guidance and help in the fieldwork.

I am grateful to the Department of Earth and Environmental Sciences, University of Waterloo, for providing the necessary resources and research facilities. The intellectual environment and academic community have been crucial in fostering my academic and research development.

A special thanks goes to my family, especially my mom and dad, for their unwavering support, understanding, and patience. Their love and encouragement have been my pillars of strength throughout this academic pursuit.

In conclusion, this thesis stands as a collective effort, and I am grateful for the support of everyone who played a role in its completion.

Table of Contents

Author's Declaration ii

Statement of Contributions iii

Abstract iv

Acknowledgements vi

List of Figures x

List of Tables xiii

Chapter 1 Introduction 1

1.1 Research Problem 1

1.2 Study Area 2

1.3 Bedrock Geology 4

1.4 Surficial Geology 5

1.5 Research Objectives 8

1.6 Methodology Overview 8

1.6.1 Field Work 9

1.6.2 Laboratory Data Analysis 16

1.7 Thesis Structure 19

Chapter 2 - An Analysis of Subglacial Landforms in the Birch Lake Area, West of Great Slave Lake (NTS 85K), Northwest Territories 20

2.1 Introduction 20

2.2 Subglacial Landforms in the Study Area 20

2.2.1 Ice Flow Parallel Lineations 22

2.2.2 Subglacial Ribs 23

2.2.3 The Size and Shape Continuum of Subglacial Landforms 23

2.3 Methods 25
2.3.1 Outcrop-scale Ice Flow Indicators 25
2.3.2 Landform-scale Indicators 26
2.4 Results 27
2.4.1 Outcrop Scale Ice-flow Indicators 27
2.4.2 Landform Record 31
2.5 Discussion 38
2.5.1 Southward (180-190 deg.) Ice Flow 38
2.5.2 Westward (260-270 deg.) Ice Flow 38
2.5.3 Southwest (220-235 deg.) Ice Flow 38
2.5.4 Northwest (320 to 325 deg.) Ice Flow 39
2.6 Conclusion 39
Chapter 3 - An Analysis of Till Stratigraphy in the Birch Lake Area, West of Great Slave Lake (NTS 85K), Northwest Territories 41
3.1 Introduction 41
3.2 Methodology 41
3.2.1 Grain Size Analysis 42
3.2.2 Clast Fabrics 43
3.2.3 Clast Lithology Counts 44
3.3 Results 46
3.3.1 Results of Drumlin Sections 46
3.3.2 Results of Surficial Samples 57
3.4 Discussion - Paleo-ice Flow Reconstruction 61
3.4.1 Southward (180-190 deg.) Ice Flow Phase 61

3.4.2 Westward (260-270 deg.) Ice Flow Phase 62
3.4.3 Southwest (215-245 deg.) Ice Flow Phase 62
3.4.4 Northwest (320 to 325 deg.) Ice Flow Phase 63
3.4.5 Integrated Evidence for Ice Flow History 63
3.5 Conclusion 64
Chapter 4 Conclusion 66
4.1 Thesis Contribution 66
4.2 Potential Implications of This Research and Recommendation for Future Research 68
Appendix A 81
Appendix B 91
Appendix C 108
Appendix D 146

List of Figures

Figure 1.1. Map of the study area (outlined in red) from and its location in Canada (inset map). Background satellite image is from the World Imagery Basemap from ESRI. Inset map is from the World Topographic Map from ESRI. 3
Figure 1.2. Bedrock domains around the study area (outlined in red) (Okulitch, 2006). 4
Figure 1.3. Location of Pine Point and Cameron Hills to the Canadian Shield (pink) and WCSB (yellow). Modified from Menzies et al. (2019). 6
Figure 1.4. LIS flow lines, ice margins, and glacial lake extents at different time steps (from Lemmen et al., 1994). The study area is outlined in red. 8
Figure 1.5. Methodology overview flowchart. 9
Figure 1.6. A) Location of drumlin sections. B) Specific positions of section 1 to 3 in the drumlin. Hillshade model is based on the Arctic DEM (2 m) obtained from the Polar Geospatial Centre (https://www.pgc.umn.edu/data/arcticdem/). The water bodies layer was obtained from the Geospatial Extraction tool (https://maps.canada.ca/czs/index-en.html). 12
Figure 1.7. General view of the Stratigraphic section 1 to 4. A) Section 1: west of Hwy 3; B) Section 2: east of Hwy 3; C) Section 3: west of Hwy 3; D) Section 4: west of Hwy 3. 13
Figure 1.8. Location of sample sites in 2020 and 2021. 16
Figure 1.9. Workflow for grain size analysis. 17
Figure 1.10. Flowchart of the bulk till sample used in pebble counts (Plakholm et al., 2020). 18
Figure 2.1. Glacial geomorphology of the region encompassing the study area (red box) (Dulfer et al., 2023) 21
Figure 2.2. Surficial geology maps in the surrounding area. 22
Figure 2.3. Main study area with the ArcticDEM tile used in this study. Location of drumlin sections and outcrop sites are also represented. 27
Figure 2.4. Rose diagram of the erosional ice flow indicators listed in Table 3.1. 28
Figure 2.5. Outcrop-scale ice flow indicators showing the westward iceflow (260-270 deg.). The photo is taken facing west at site 1. 29
Figure 2.6. Outcrop site 1. A) Outcrop-scale ice flow indicators with stoss-lee relationships establishing the southern flow as the oldest phase (185 deg.). The photo is taken facing south. B) Outcrop-scale ice flow indicators establishing the northwest ice flow phase (322 deg.). The photo is taken facing south. C) Outcrop-scale ice flow indicators establishing the southwestern ice flow phase

(220 to 226 deg.) including striations, grooves and chattermarks. D) The general view of the stoss-lee relationship between the younger (southwest) and lower (south) surfaces. The photo is taken facing south. 30
Figure 2.7. Outcrop site 2. A) Outcrop-scale ice flow indicators showing the south ice flow (190 deg.). B) Outcrop-scale ice flow indicators showing the southwest ice flow (222 deg.). 31
Figure 2.8. ArcticDEM elevation grid (2m resolution) of study area with ice flow parallel lineations from Dulfer et al. (2023). 33
Figure 2.9. ArcticDEM hillshade (2m resolution) west of Birch Lake and geomorphological mapping of ice flow parallel lineations (Dulfer et al., 2023). 34
Figure 2.10. ArcticDEM hillshade (2m resolution) south of Birch Lake and geomorphological mapping of ice flow parallel lineations (Dulfer et al., 2023)..... 34
Figure 2.11. (a) Elevation from the ArcticDEM (2m resolution) south of Birch Lake and (b) geomorphological mapping of subglacial ribs (Dulfer et al., 2023)..... 36
Figure 2.12. a) ArcticDEM east of Birch Lake and (b) geomorphological mapping of ice flow parallel lineations with overprinted and irregular till ridges. 37
Figure 3.1. Cut view of drumlin section 1. The photo is taken facing west. 42
Figure 3.2. A close-up view of the till..... 46
Figure 3.3. Stratigraphic log for drumlin section 1 and its four clast fabrics. Kamb density contours have been added to the stereonets. 47
Figure 3.4. Stratigraphic log for drumlin section 2 and its three clast fabrics. Kamb density contours have been added to the stereonets. 48
Figure 3.5. Stratigraphic log for drumlin section 3 and its four clast fabrics. Kamb density contours have been added to the stereonets. 49
Figure 3.6. Fabric shape of all samples. 50
Figure 3.7. Grain size distribution of drumlin section 1..... 51
Figure 3.8. Grain size distribution of drumlin section 2..... 52
Figure 3.9. Grain size distribution of drumlin section 3..... 53
Figure 3.10. A) Distribution of Canadian Shield clasts across the drumlin sections 1 to 3; B) Distribution of WCSB clasts across the same drumlin sections..... 54
Figure 3.11. Pebble counts results of drumlin section 1..... 55
Figure 3.12. Pebble counts results of drumlin section 2..... 56

Figure 3.13. Pebble counts results of drumlin section 3. 57
Figure 3.14. General texture of all samples in terms of their proportions of gravel, sand, and mud (silt and clay). Red points are the section samples and black points are the surficial samples. 58
Figure 3.15. Grain size results of the surficial samples. 59
Figure 3.16. Clast lithology counts map of the study area. Ice flows are noted at the top right corner. The relationship between lithology and geological formation are listed in Table 3.2 60
Figure 3.17. Summary of ice flows and till stratigraphy in the study area. A) Oldest south ice flow. B) Second oldest west ice flow. C) Second youngest southwest ice flow. D) Youngest northwest ice flow. 64

List of Tables

Table 1.1. Information about the drumlin sections. 14
Table 2.1. Measurements of ice-flow indicators at two sites. 27
Table 2.2. Basic metrics of the drumlins. 32
Table 3.1. Classification of grain size. 43
Table 3.2. Lithology groups for pebble counts. 45

Chapter 1
Introduction

1.1 Research Problem

During the late Wisconsinan glaciation, the Laurentide Ice Sheet (LIS) waxed and waned over most of Canada reaching its greatest extent and volume at about 21 ka BP (Dyke & Prest, 1987; Dyke et al. 2002; Dalton et al., 2020; Dalton et al., 2022). The last glaciation is the most well-understood of Quaternary glaciations, although large uncertainties persist due to rare stratigraphic records being preserved, especially regarding pre-Last Glacial Maximum (LGM) events (e.g., Dalton et al. 2022). Our understanding of previous glaciations is more limited, but there is compelling evidence that the glaciations of the Quaternary have had a major impact on landscape evolution and the nature and distribution of surficial sediments in Canada.

Considerable effort has been put in reconstructing the last glaciation, with a focus on the geometry of the LIS ice margins and of their retreat pattern and chronology (e.g., Dyke & Prest 1987; Dyke et al. 2003; Dalton et al. 2020). To understand the long-term evolution of the LIS during a glaciation, a reconstruction of ice flow phases including the dynamics of ice streams, ice divide positions and migration phases, and related ice flow shifts are also necessary (Parent et al., 1995; Veillette et al., 1999; Clark et al., 2000; McMartin & Henderson, 2004). While most of these studies focus on specific regions of the LIS and rely heavily on the landform record, some include the stratigraphic record and data useful for glacial sediment transport analysis (e.g., Gauthier et al., 2019). Nonetheless, glacial history remains poorly constrained in many regions covered by the LIS. New research is thus needed to more completely integrate evidence from erosional and depositional records.

The integration of till stratigraphic and sedimentologic studies with landform-based ice flow analysis helps advance our understanding of subglacial processes and glacial history (e.g., Hodder et al., 2016), including those related to subglacial landform generation such as drumlins (e.g., Ó Cofaigh et al., 2013; Evans et al., 2015; Benediktsson et al., 2016; Menzies et al., 2016), especially those containing one or more till sheets (cf. Stokes et al., 2013). Few drumlin studies include till provenance analysis and those that do typically involve sparse data and limited provenance indicators (e.g., Sookhan et al., 2021). There is thus a potential to improve our understanding of the stratigraphy of drumlins and provenance of till in drumlin fields to better establish the relationships with glacial history, subglacial sediment transport, and drumlin forming processes.

Studying till sedimentary processes from preserved clues in the till to reconstruct or interpret the processes responsible for their deposition is helpful to understand the configuration of the LIS and related ice-flow dynamics problems. This type of research is needed to better understand the long-term behavior of ice sheets, their response to internal and external forces, and how ice sheets change landscapes and landforms during glaciations.

Research on subglacial landforms and sediments is also important for certain applications such as mineral exploration. Mineral exploration commonly uses glacial sediments to trace indicator minerals and geochemical pathfinder elements back to their buried bedrock sources (McClenaghan & Paulen, 2018). However, certain mechanisms which might have significant influences on the design of till sampling and the interpretation of till compositional data, require improvement. Recent research near Lac De Gras in Northwest Territories shows the influence of ice flow shifts and local bedrock topography on three-dimensional till dispersal patterns (Kelley et al., 2019; Stirling, 2022). Stirling (2022) also documented the potential net effect of ice flow shifts and drumlinization on surficial till compositional patterns. It is thus important to expand this type of research to other drumlin fields to better document these effects and assess implications for till provenance studies in the context of ice sheet research, as well as for applications in mineral exploration and environmental protection.

1.2 Study Area

A few criteria were considered to select the study area for this research. First, the area must include a subglacial bed with a drumlin field. The study area also needed to be accessible and with a potential for till sections either along drumlin flanks or across drumlins. In addition, the bedrock geology needed to consist of sufficiently contrasting bedrock units extending approximately perpendicular to the long axis of drumlins. The latter criterion is particularly useful for till provenance analysis. The selected study area that meets all these criteria is in the Northwest Territories, more specifically west of Great Slave Lake (GSL) within National Topographic System (NTS) map 85K. This area represents a great opportunity to investigate tills and related sedimentary processes within a drumlin field due to the presence of road cuts extending across several drumlins along Highway 3, which are part of a drumlin field hereafter referred to as the Dessert Lake drumlin field (Figure 1.1).

The entire area is a flat area with average elevation at 209 meters and has many water bodies, including the west arm of GSL and Birch Lake, and several smaller lakes and streams.

The physiography of the area was influenced by lithology of the bedrock, glacial history, and glacial lake occurrences. Large stretches of spruce bog and fen with peat and low flora and mosses are indicative of extensive water ponding and a poor drainage pattern caused by low permeability sediments and the flat topography of the region (Lemmen, 1990). Weeds, white spruce, and black spruce trees make up the thick mixed forest that dominates raised regions above organics.

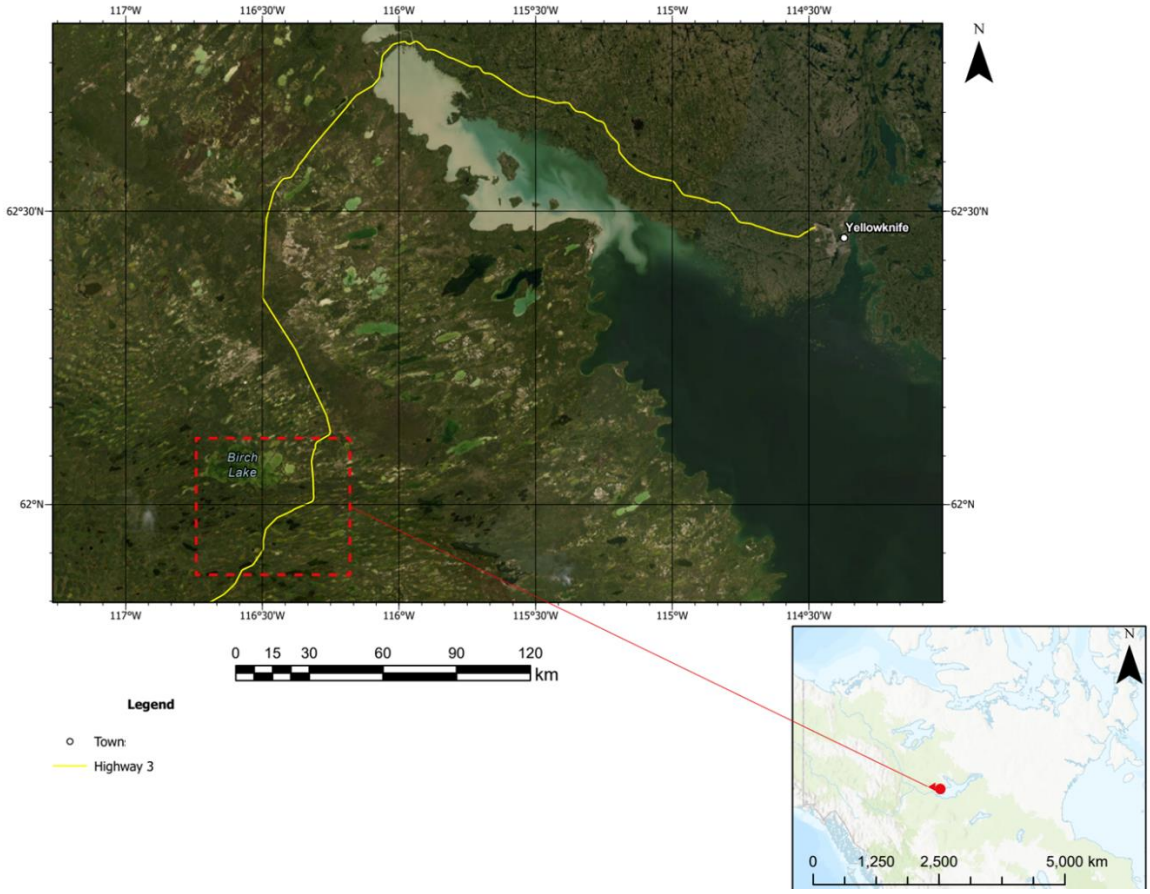


Figure 1.1. Map of the study area (outlined in red) from and its location in Canada (inset map). Background satellite image is from the World Imagery Basemap from ESRI. Inset map is from the World Topographic Map from ESRI.

1.3 Bedrock Geology

Numerous provenance investigations have been conducted across Canada by classifying glacial clasts into useful bedrock lithology categories and determining their relative proportions to get insights into sediment transport directions and distances from the different bedrock source regions (e.g., Hagedorn, 2022; Rice et al., 2024). Similarly, indicator minerals and geochemical pathfinder elements in till matrix are also commonly used to analyze till dispersal patterns from distinct bedrock sources (e.g., McMartin & Paulen, 2007; McClenaghan and Paulen, 2018; McClenaghan et al., 2023). Furthermore, because bedrock may consist of lithologies with a wide range of properties such as jointing and hardness, it is important to have a good knowledge of bedrock geology to understand its potential impact on glacial sediment supply and texture. Therefore, this section provides a summary of the regional bedrock geology of the study area, as well as of the known up-ice directions (to the east and northeast) based on recent studies in the region by Rice et al. (2013, 2019) and Hagedorn (2022).

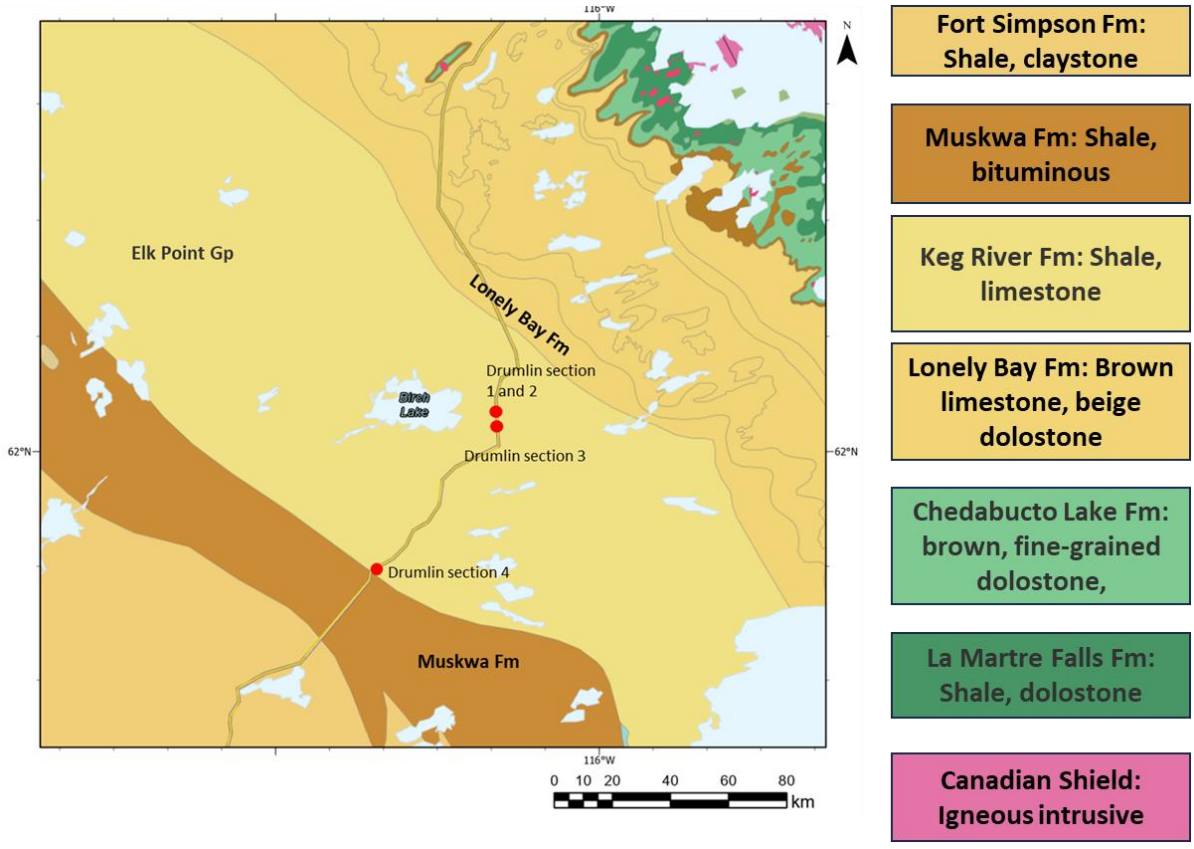


Figure 1.2. Bedrock domains around the study area (outlined in red) (Okulitch, 2006).

The basement rock is Canadian Shield rocks, which primarily composed of Precambrian rocks and are older than 541 million years. The main rock types are igneous intrusive, including felsic rocks like granite and mafic rocks like gabbro (Harrison et al., 2011). On top of the basement rocks lies the Western Canadian Sedimentary Basin (WCSB), a thick (350–600 m) gently sloping (1.9 m/km west) carbonate series that was formed throughout the Paleozoic (Rhodes et al., 1984). According to Okulitch (2006), Paleozoic middle Devonian makes up most of bedrock surface in the research area, which spans the time interval between 387.7 million and 382.7 million years ago. The bedrock of the study area is formed by bituminous shale and limestone of the Keg River Formation, Elk Point Group (Figure 1.2). Its lower bed consists of bituminous and fossiliferous marlstone; its upper bed is made of very fine-grained, dark brown and grey limestone. The bedrock geology up-ice of the study area belongs to Lonely Bay Formation, which mainly consists of brown limestone and thinly bedded beige dolostone (Okulitch, 2006). Another geological formation southwest of the study area is Muskwa Formation from Horn River Group, which mainly contains bituminous shale (Okulitch, 2006).

1.4 Surficial Geology

The surficial geology of the region has been mapped at various scales using different techniques. The most recent map that covers the entire study area was made using remote predictive mapping techniques (Kerr et al., 2016), which is essentially based on remote sensing data with limited field observations. This is a relatively fast way of producing surficial maps, but it can lead to lower resolution and greater uncertainty on the nature and origin of surficial sediments. Nevertheless, it provides useful information about the regional surficial geology.

Research by Craig (1965) and Lemmen (1990), and more recently by Hagedorn (2022) provide evidence for till stratigraphy and associated ice flow shifts in the region. First Craig et al. (1965) documented till sheets and evidence for two paleo-ice flow directions in the area, i.e., a younger flow to the northwest and an older flow to southwest. The southwest flow was indeed interpreted at the time to be the youngest based on its predominant landform footprint on the landscape. However, the most recent research by Hagedorn (2022) documented a clockwise ice flow shift in their study area, thus putting the southwest flow phase as older than the northwest flow phase. This is based on a detailed till stratigraphic study and outcrop-scale ice flow indicators along the Mackenzie River, in the vicinity of Fort Providence, and further to the south around Hay River and part of the Cameron

Hills (Figure 1.3). Results of the provenance analysis of the tills by Hagedorn (2022) are consistent with the clockwise shift suggesting a good correspondence between the erosional and depositional records: i.e., the oldest till contains clast fabric and compositional evidence consistent with southwest ice flow sediment transport (and northeast bedrock sources), whereas the younger tills seem to be mostly derived from bedrock sources that are more extensive to the east and southeast and also have clast fabrics indicative of paleo-ice flow to the west and northwest.

Further to the southeast, detailed studies (Rice et al., 2013; McClenaghan et al., 2018) at Pine Point (Figure 1.3) have documented four till units and an ice flow record that includes an old southwest phase (~230 deg.), followed by west northwestward phase (~300 deg.), and one single striation site suggests a subsequent ice flow to the north-northwest (~330 deg.). Finally, a late 'ice streaming' southwestward (~250 deg.) phase (Rice et al., 2013). Correlations with the tills and ice flow phases between Rice et al. (2013) and Hagedorn (2022) are not straightforward due to the possible local differences in glacial dynamics at similar times across this large region.

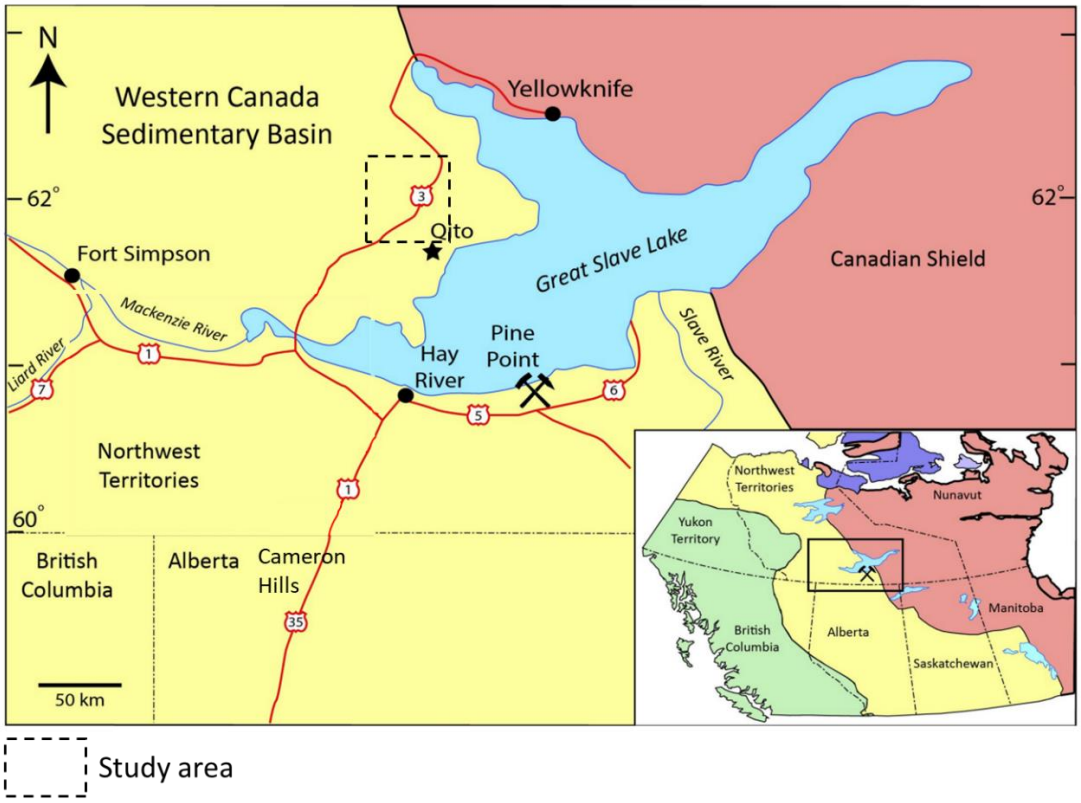


Figure 1.3. Location of Pine Point and Cameron Hills to the Canadian Shield (pink) and WCSB (yellow). Modified from Menzies et al. (2019).

There is extensive evidence that glacial lakes inundated the region upon the retreat of the ice margin. Lemmen et al. (1994) investigated the proglacial meltwater ponding and drainage along a substantial stretch of the western edge of LIS. Figure 1.4 displays the periods for the evolution of glacial lakes and ice reconstruction.

Ice had a significant impact on proglacial meltwater routing as the ice sheet retreated eastward since natural northeast drainage was blocked (Lemmen et al., 1994). New meltwater outlets were created by the continuing retreat to the east, and the landscape isostatically adjusted. A lobate ice sheet margin formed around terrain high points and glacial lakes formed at different elevations during deglaciation, the details of which have been refined after Lemmen (1990) by Hagedorn (2022).

Based on glacial lake reconstructions (Lemmen et al., 1994; Smith, 1994; Hagedorn, 2022), a large portion of the study area, the terrain below 240 m asl (modern day elevation), was inundated by Glacial Lake McConnell (GLM) during the extensive Mackenzie phase. During this phase, the GLM connected the basins of the Great Bear, Great Slave, and Athabasca lakes. Following this phase, relative lake levels dropped in the area due to glacial isostatic adjustment and ice margin retreat opening lower outlets. The drop is indicated in the study area by beach ridges and other evidence of shallow littoral and sublittoral processes, as well as by post-glacial eolian activity. One important implication of the events that followed ice margin retreat in the area is that the subglacial landscape and its surficial till were partly reworked to various degrees across the study area. For instance, reworking occurs through shoreline processes, surface winnowing, and eolian activites eroded some surficial sediments, created eolian deposits which cover some areas. Postglacial weathering and soil forming processes also affected surficial sediments to different extents depending on sediment and surface characteristics and elevation. This is something that needs to be considered in the analysis of surficial till, especially for its texture and composition.

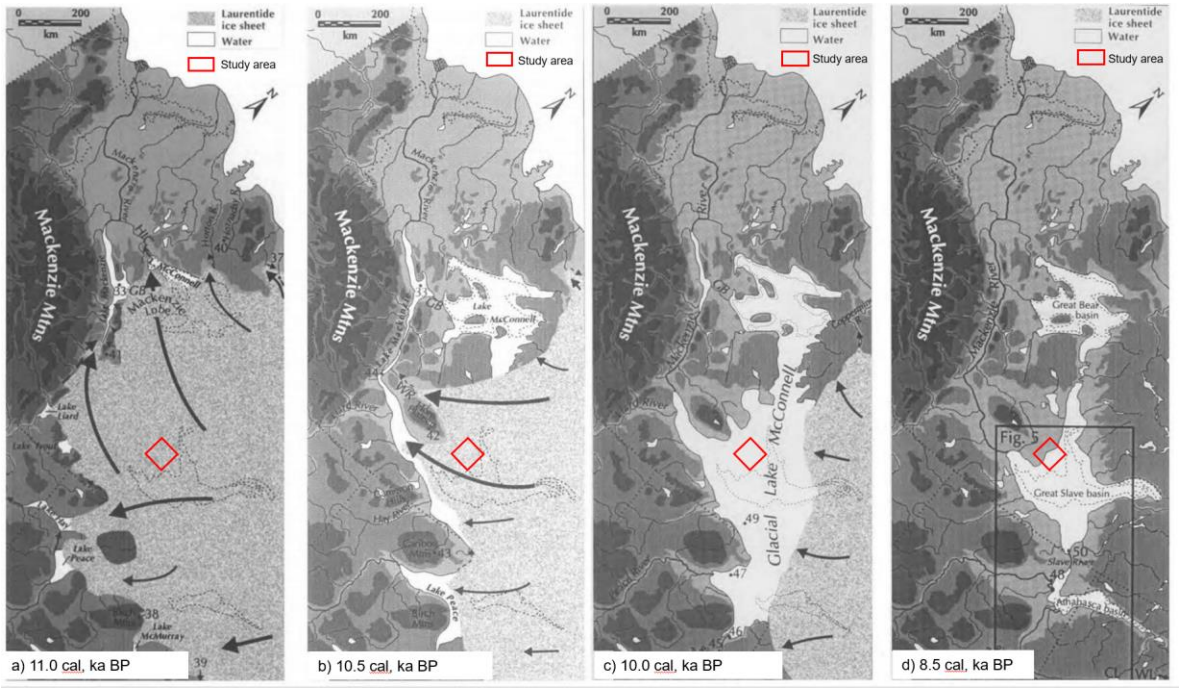


Figure 1.4. LIS flow lines, ice margins, and glacial lake extents at different time steps (from Lemmen et al., 1994). The study area is outlined in red.

1.5 Research Objectives

This M.Sc. research focuses on the glacial dynamics and subglacial sediment transport of the Dessert Lake drumlin field area within NTS map sheet 85K and part of 85 F. The specific objectives are as follow:

1) Reconstruct the ice flow history of the "Dessert Lake drumlin field", from the erosional and depositional records, and compare with findings from other studies in the region.
   a) Build a till stratigraphic framework.
2) Determine the mixed provenance of the coarse (pebble) fraction (bedrock source contributions) of the till units.
3) Explore implications of results on drumlin formation and evolution.

1.6 Methodology Overview

To achieve the thesis objectives, a combination of fieldwork, laboratory, and data analysis techniques were employed. The overarching approach involved formulating a comprehensive

understanding of ice-flow history, the composition of glacial sediments, and the provenance of till units (Figure 1.5).

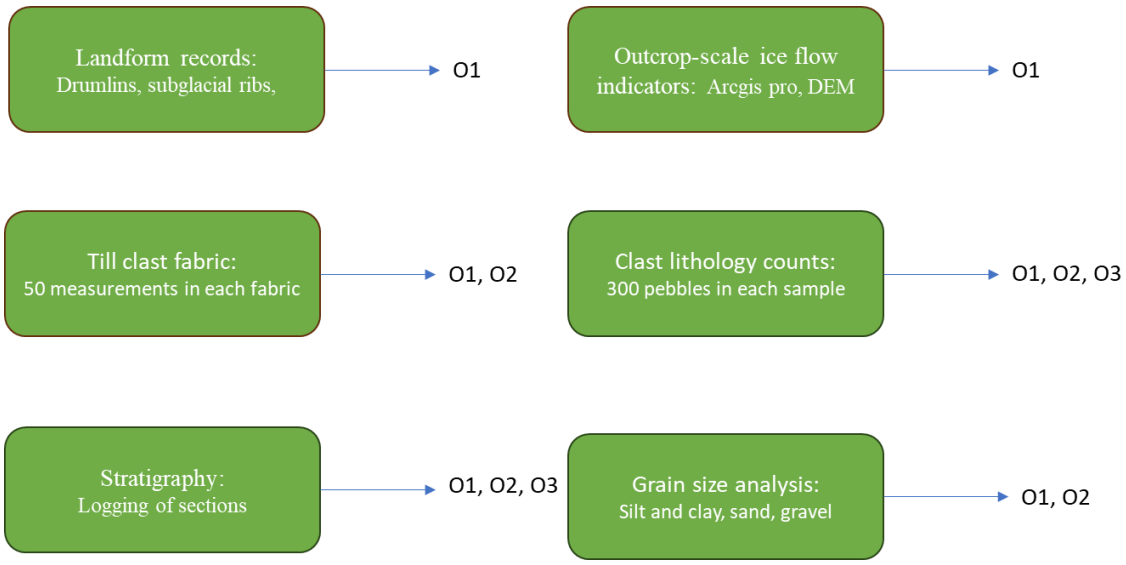


Figure 1.5. Methodology overview flowchart.

1.6.1 Field Work

The proposed research relies in large part on field observations and on the analysis of sediment samples that must be collected in the field. The research used data from samples collected by the Northwest Territories Geological Survey (NTGS) during the 2020 sampling program and supplemented with samples obtained in August 2021. In addition, striations and other outcrop-scale erosional indicators were measured at a few sites in 2021, and four stratigraphic sections were logged along Highway 3 to document the stratigraphy and sedimentology of drumlins, including till clast fabrics, and to obtain till samples along selected vertical profiles. This was completed with follow-up work in August 2022, during which we recollected samples at several sites for a more complete till clast fabric data.

1.6.1.1 Outcrop Ice Flow Indicators

As the glacier sole slides over bedrock outcrops, debris lodged at the base acts as an erosive, abrasive. As a result, bedrock outcrops are polished and striated, providing several clues of ice flow direction, and where striae cross-cutting and overprinting of earlier features are present, relative age relationships can also be determined (e.g., Parent et al., 1995; Veillette et al., 1999; Paulen et al., 2013). In addition, the sliding process on a hard bed may lead to quarrying of the lee-side of rock obstacles (e.g., Hallet, 1996; Iverson, 2012), and the resulting longitudinal asymmetric shapes provide another type of paleo-ice flow indicator.

Due to an extensive Quaternary sediment cover, bedrock outcrops are uncommon in the study area. Carbonate rock surfaces also tend to be weathered and have lost most of the glacial indicators. The shape of glacially sculped outcrops was studied to establish stoss-lee relationships, and the orientation and crosscutting of striations and other features (e.g., chattermarks) were analyzed and measured to reconstruct paleo-ice flow directions and their relative age following established methods (e.g., Parent et al., 1995; Veillette et al., 1999; Paulen et al., 2013).

1.6.1.2 Till Stratigraphic Section

Till stratigraphic sections were investigated by digging a series of steps using hand shovels and pickaxes on drumlin sections along Highway 3. Two main sections were created this way on one large drumlin, with one on the west side of the highway and one on the east side. The third section was also on the west side of the highway, but it is located in a different drumlin south of the first one. The fourth section was made on yet another drumlin further south, also along the highway. Figure 1.6 shows the location of the four sections. There were approximately 15 holes or steps dug into each section, and each hole was about 0.4 m in height (Figure 1.7). Therefore, the average height of till stratigraphic sections is about 5.5 m. In each hole, 8 to 15 clasts were selected, and the general shape (sphericity and roundness) of the clasts, sorting and compaction of the till were recorded to get initial field observations. This was to determine if the material had the characteristics of subglacial traction till as described in the literature (e.g., Benn & Evans, 2010). In addition, the color of the sediment was also recorded using the Munsell color system. Overall, the sediment in most holes is a matrix supported diamicton containing abundant faceted sub-angular clasts with polished and striated surfaces interpreted as a subglacial traction till. The latter is defined as “sediment deposited by a

glacier sole either sliding over and/or deforming its bed, the sediment having been released directly from the ice by pressure melting and/or liberated from the substrate and then disaggregated and completely or largely homogenized by “shearing” (Evans et al., 2006). The sediment within the studied drumlin sections is therefore suitable for a study of subglacial transport and depositional processes and glacial dynamics reconstructions.

Till stratigraphic logging can provide information about ice sheet depositional and erosional events. Delineation of the main units and their thickness were recorded. The height of the section is the maximum vertical stratigraphy investigated between the road and the top of the drumlin along the road outcrop (Table 1.1). Samples and clast fabrics were taken from different units for some observations. All sites were documented photographically.

In the simplest form, the stratigraphic log is a graph with a vertical axis for thickness and a horizontal axis for particle size. The vertical scale varies according to the level of detail and the project objectives. Therefore, it can be modified to match the goal of the project, the time allotted, and the variety and thickness of the beds (Anderton, 1985). The material type is represented by standard symbols.

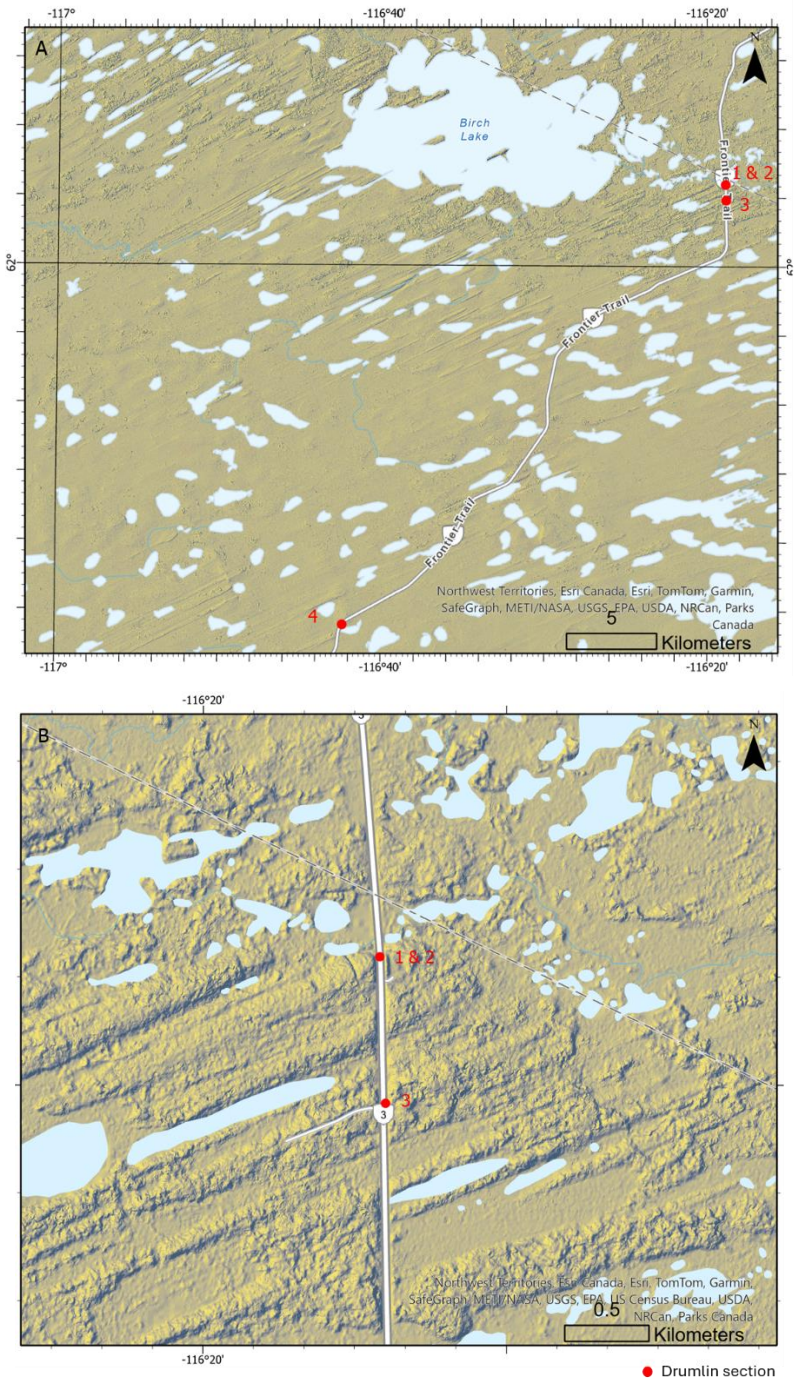


Figure 1.6. A) Location of drumlin sections. B) Specific positions of section 1 to 3 in the drumlin. Hillshade model is based on the Arctic DEM (2 m) obtained from the Polar Geospatial Centre (https://www.pgc.umn.edu/data/arcticdem/). The water bodies layer was obtained from the Geospatial Extraction tool (https://maps.canada.ca/czs/index-en.html).

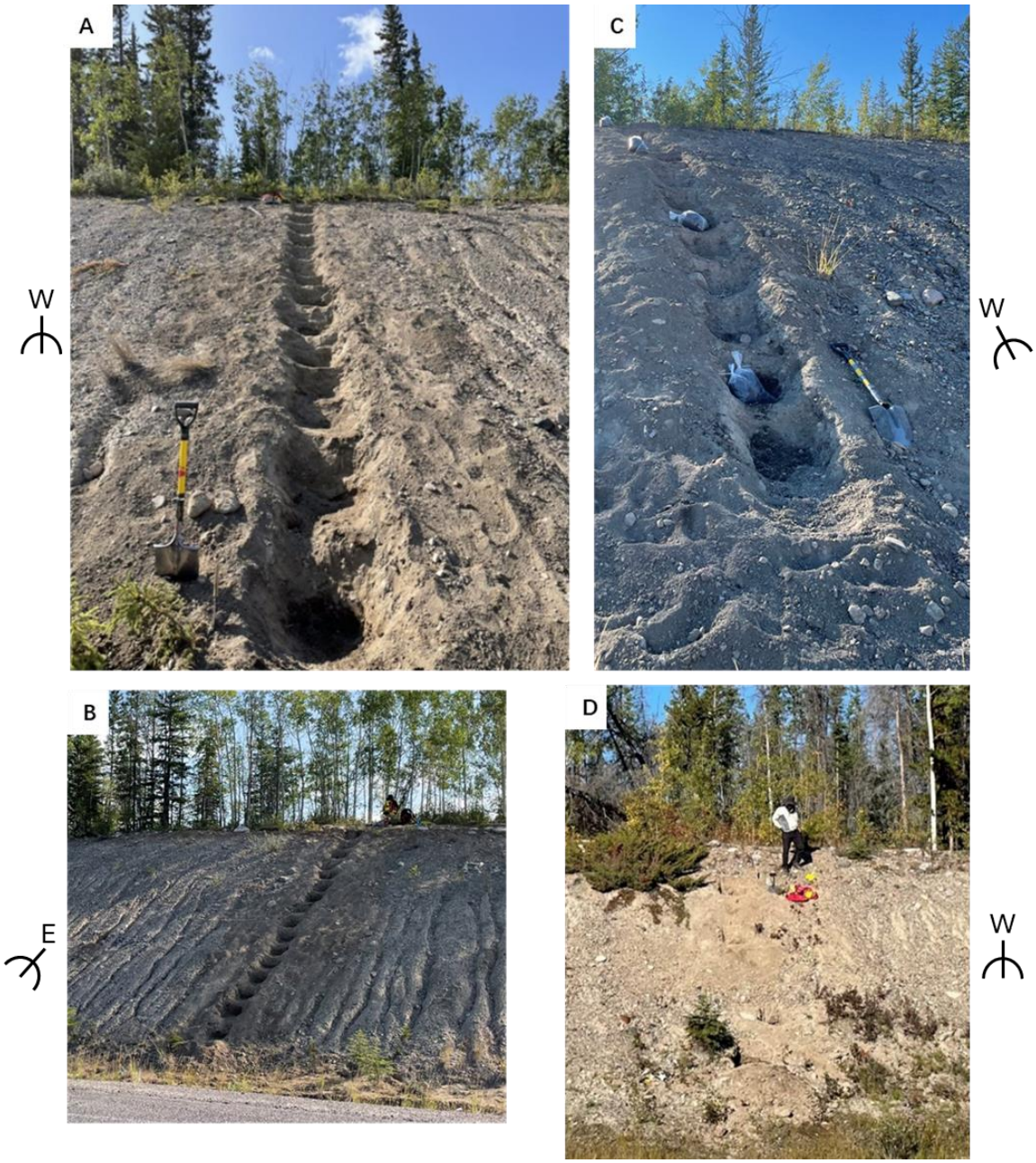


Figure 1.7. General view of the Stratigraphic section 1 to 4. A) Section 1: west of Hwy 3; B) Section 2: east of Hwy 3; C) Section 3: west of Hwy 3; D) Section 4: west of Hwy 3.

Table 1.1. Information about the drumlin sections.

	Vertical height	Average slope angle	Longtitude	Latitude
Section 1	6m	27°	116˚18’50”W	62˚2’24”N
Section 2	5.8m	27°	116˚18’50”W	62˚2’24”N
Section 3	5.3m	27°	116˚18’50”W	116˚42’21”W
Section 4	5m		116˚42’21”W	61˚49’36”N

1.6.1.3 Till Clast Fabrics

Elongated clasts in subglacial traction till tend to align parallel with the direction of shear, which can provide useful information about the subglacial stress experienced by till formations (Benn, 2004). Till clast fabric measurements were done in three holes at each till stratigraphic section, with one near the top, one in the middle, and one at the bottom. After the till hole has been prepared with a clean surface devoid of slump and roots, the next step in the procedure is to locate a protruding clast and to partially excavate it by gently removing the matrix around the clast, without moving the clast. This is to further reveal the outline of the clast. If the clast is elongated, then the clast can be removed and replaced by a non-magnetic narrow pen or knitting needle in the same orientation. The average ratio of a-axis to b-axis is 1.7. The trend and plunge of the pen is then measured using a geological compass (Allmendinger et al., 2012). The length of both the a-axis and b-axis is also measured, this time using a ruler. To get an adequate sample population, 50 clasts were measured in each hole, which is a typical number for till clast fabrics (Benn, 2013). By displaying the data on rose diagrams and lower hemisphere stereonets, the overall shape of the clast fabrics can be analyzed visually.

In addition to the visual inspection of a fabric’s shape, other useful parameters can be calculated. For instance, normalized eigenvalues (S_1, S_2, S_3) and eigenvectors can be calculated from the 3X3 orientation tensor matrix (Allmendinger et al., 2012). For till fabrics, eigenvalues and eigenvectors provide information about the main orientation of clasts and the strength of the till fabric. Results are sometimes displayed on biplots and ternary diagrams (e.g., Benn, 1994; Hicock et al., 1996). Several programs exist to plot the data on rose diagrams and equal-area stereonets. For this research, till clast fabric data was analyzed using python scripts developed at the University of Waterloo and available

on GitHub (https://github.com/GlacialGeo /PythonCodes) that make use of several existing packages including Pandas, Numpy, Matplotlib, Ternary, and mplstereonet to create plots and analyze till clast fabric data.

It is important to note that not all fabrics are useful for indicating ice flow direction. Some fabrics are too isotropic for determining the direction. A minimum threshold of about 0.54 for S1 is commonly used for ice flow direction interpretation using clast fabrics (e.g., Hodder et al., 2016).

1.6.1.4 Till Sampling

Most surficial till samples were collected throughout NTS map sheet 85K with a few collected in 85F (https://natural-resources.canada.ca/earth-sciences/geography/topographic-information/maps/9765). Some sample sites were accessed by truck, and parking areas were found along Highway 3. A helicopter was used to get access to sites that were located too far from the road. Holes were dug using hand shovels at 50 to 100 cm until C-horizon was reached, which is less oxidized. To decrease the risk of metallic contamination, unpainted metal shovels were used to collect the samples, and they were thoroughly cleaned after digging at each sample site to avoid cross-contamination (Smith et al., 2019). Two sample bags were filled at each site. The first was a large plastic bag with about 10 kg of till, which was for heavy mineral lab analysis, as well as for pebble lithology counts and grain size analysis. The second was a small plastic bag comprised of about 3 kg of till for till matrix geochemical analysis. In this thesis, only the results from the large bags were used.

Sample locations by sampling survey year and sampling type are shown in Figure 1.8. There are 58 samples been sampled in 2020 and 79 samples being sampled in 2021.

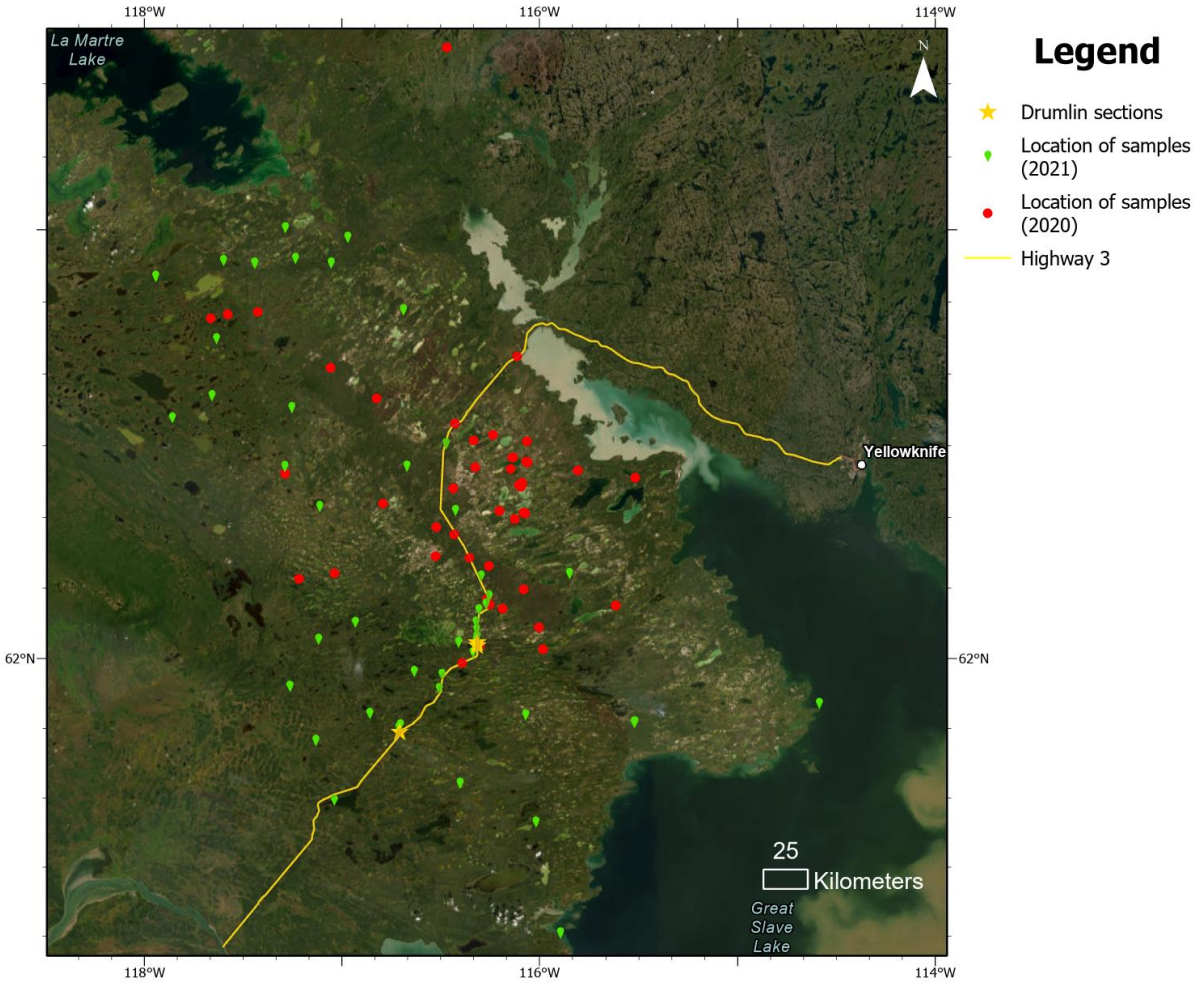


Figure 1.8. Location of sample sites in 2020 and 2021.

1.6.2 Laboratory Data Analysis

This section provides an overview of the laboratory procedures done at external commercial laboratories and at the University of Waterloo, as well as details regarding the methodology to prepare and analyze the data obtained from laboratory analyses.

1.6.2.1 Grain Size Analysis

A bulk sample split was obtained from all the large samples sent to Overburden Drilling Management (ODM) for indicator mineral analysis. The splits were sent to the University of

Waterloo for grain size analysis. Each dry sample is passed through the following stack of stainless-steel sieves according to mesh diameter: 8.00 mm, 4.00 mm, 2.00 mm, 1.00 mm, 0.500 mm, 0.250, 0.125 mm, and 0.063 mm. The material < 0.063 mm is then collected at the bottom in a stainless-steel pan. The sieving process is facilitated by using a Fritsch Analysette 3 Spartan shaker with a vibration amplitude of 2.0 mm for a duration of 15 minutes. Following that step, each sample fraction was weighted using an electronic scale with a 0.01g precision, bagged separately, and labelled with the sample number and size fraction (Figure 1.9).

The fraction less than 0.063 mm was then further analyzed using a laser diffractometer, a Fritsch Analysette 22 with a wet dispersion unit. The laser-based particle size distribution was obtained using Fraunhofer diffraction approximation (Jones, 1999). Only samples collected in the 2020 field season went through the laser diffractometer analysis.

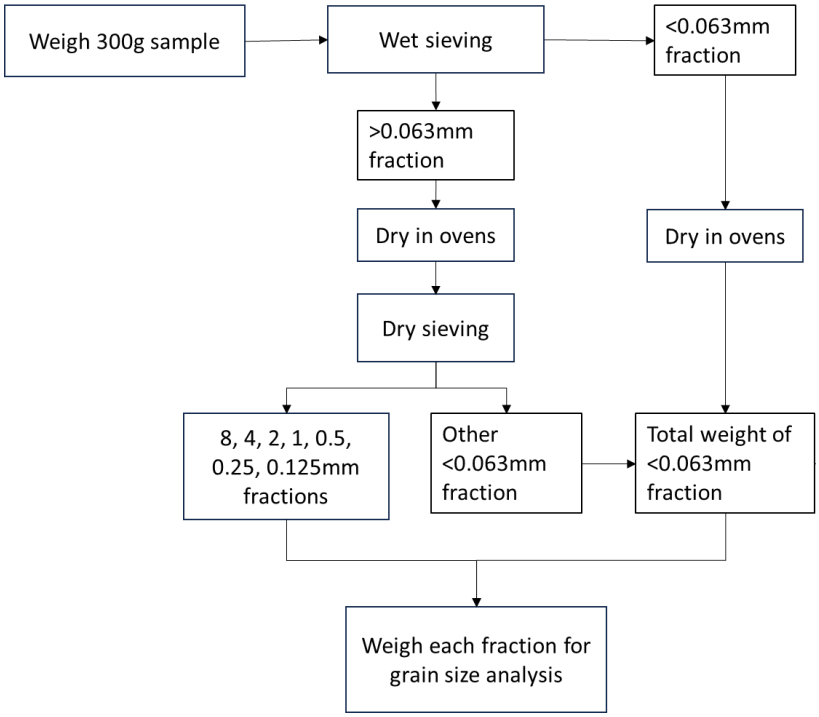


Figure 1.9. Workflow for grain size analysis.

1.6.2.2 Pebble Counts

The classification of till clasts by their lithology provides information about bedrock source regions, which helps understand the regional ice flow and sediment dispersal patterns (Plakholm et

al., 2019). Sometimes, insights into sediment transport distance can be obtained if a lithology has a unique bedrock source.

At ODM, bulk till samples were disaggregated and put through a 2.0 mm sieve following the wet sieving technique, which consists in passing sediment and water through a shaking sieve. To eliminate discoloration, the >2.0 mm size fraction was wet sieved again at 5.6 mm, with the 2.0 - 5.6 mm fraction being kept and the >5.6 mm fraction being washed with oxalic acid (Plakholm et al., 2020).

All pebble fractions of each sample were sent to the University of Waterloo. Each sample is examined to see if it has a minimum of 300 clasts over 5.6 mm size fraction. This is the selected fraction, which is large enough to facilitate the identification, yet small enough to have the needed number of clasts. The selected clasts were divided into two main categories and eight subcategories (Table 3.2), which is determined by the local bedrock geology and the various bedrock lithologies present in the surrounding region. The percentages obtained from the pebble count are subsequently employed to deduce the relative distribution of various bedrock sources incorporated within a given till sample.

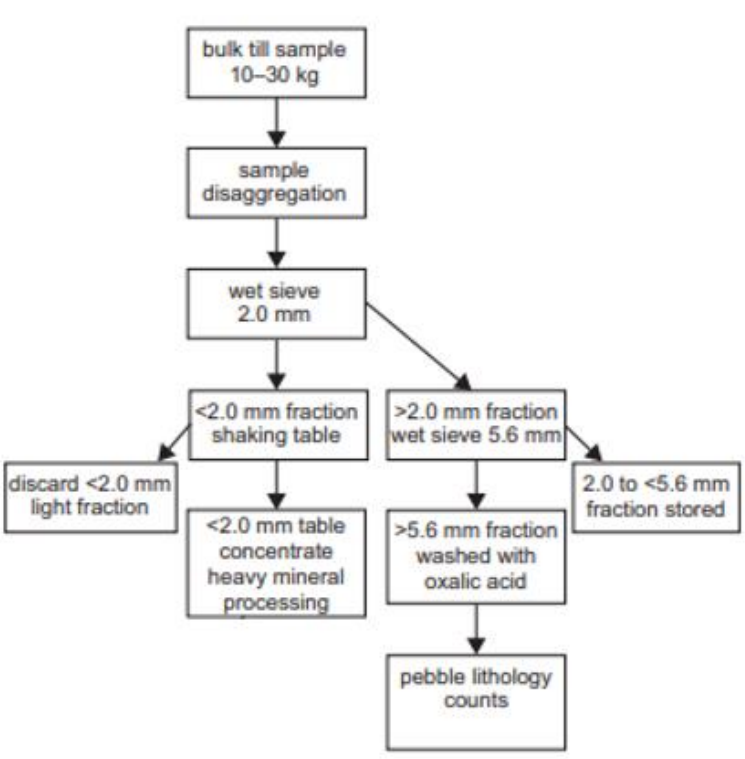


Figure 1.10. Flowchart of the bulk till sample used in pebble counts (Plakholm et al., 2020).

1.7 Thesis Structure

This thesis contains four parts: an introduction chapter, two research analysis chapters, and a conclusion chapter. The thesis research was undertaken as part of a project with NTGS and the University of Waterloo with Philippe Normandeau (NTGS) and supervision by Dr. Martin Ross.

The introductory chapter presents the scientific justification for the thesis, a concise overview of the geological contexts, primary research goals, and an outline of the methodologies employed. The rationale is elucidated by addressing gaps in knowledge and highlighting concerns by integrating findings from the geoscience literature pertaining to both the local vicinity and the designated study area.

Chapter two is the chapter of the subglacial landform analysis of the study area, which includes the analysis of outcrop-scale indicators like striations and landform-scale indicator including drumlins, MSGLs (mega-scale glacial lineations) and subglacial ribs. By illustrating both outcrop-scale erosional features and larger glacial landforms, it becomes feasible to reconstruct the dynamic history of ice flow during past glaciations. This chapter also provides valuable insights into the broader context of paleoclimatic and glacial changes.

Chapter three is the chapter of the till stratigraphy of the drumlin sections. The chapter includes the results of the grain size analysis, clast fabric analysis and clast lithology counts. By examining the till stratigraphy in conjunction with landform records, the understanding of past ice flow dynamics can be improved, thus helping to reconstruct the intricate history of glacial movements and the environmental conditions that influenced them.

Chapter four is the conclusion chapter which combines the results of landform analysis and till stratigraphy analysis, and reaches a more complete ice flow history of the study area.

Chapter 2 - An Analysis of Subglacial Landforms in the Birch Lake Area, West of Great Slave Lake (NTS 85K), Northwest Territories

2.1 Introduction

Glacial landform records encompass a variety of features, such as ribbed moraines, drumlins, and eskers. By carefully analyzing the orientation, size, and distribution of these landforms, several key insights into 'paleo-ice sheets' dynamics can be obtained (e.g., Stokes et al., 2015; Dulfer et al., 2023), which is critical to better understand subglacial processes, the long-term behavior of ice sheets, and past climate change (Clark et al., 2009). Drumlins, which are elongated hills aligned parallel to the direction of ice movement, are particularly useful to reconstruct paleo-ice flow phases. Ribbed moraines, a type of glacial or ice-sheet-formed till landform which form transverse to ice flow, are also commonly mapped and investigated as part of ice sheet reconstruction studies (Stokes et al., 2015). Other features like eskers, which are part of the record of the meltwater plumbing system of ice sheets provide key insights into the late-stage phases of ice sheet evolution (Stokes et al., 2015). On the meter to sub-meter scale, erosional features such as striations on glacially sculpted outcrops are also commonly used to reconstruct ice flow phases in an area (e.g., Rice et al., 2019). By examining both outcrop-scale erosional features and larger glacial landforms, it is possible to reconstruct the dynamic history of ice flow from past glaciations and gain insights into the broader regional context of paleoclimatic and glacial changes.

The goal of this chapter is to present an analysis of both outcrop-scale and landform-scale ice flow features and provide an interpretation of the significance of this record on the regional glacial dynamics reconstruction. It relates directly to thesis objective 1 (cf. Sect. 1.5), which is to reconstruct the ice flow history of the Dessert Lake drumlin field and to put it in the broader context of other regional studies.

2.2 Subglacial Landforms in the Study Area

Subglacial landforms are formed by the erosion, entrainment, transport and deposition of glacial material by ice and water through subglacial processes over time. The development of subglacial

landforms is influenced by various factors at the interface between the ice and the bed. The factors include the physical properties of the bed, such as composition, permeability and joints, as well as basal ice flow velocities, effective pressure, and other related properties (e.g., basal meltout) (Bingham et al., 2007).

As explained in Chapter 1, the study area was selected partly because of the occurrence of numerous drumlins and related elongated streamlined glacial landforms (e.g., MSGLs). Regional maps that include the study area show the distribution of the main landform types in and around the study area (Figure 2.1). In addition to drumlins and MSGLs, Dulfer et al. (2023) mapped several fields of larger landforms that they interpreted as "subglacial ribs", as well as raised shorelines. The surficial geology, including glacial landforms, have also been mapped as part of detailed mapping projects of a number of NTS map sheets surrounding the study area (Figure 2.2).

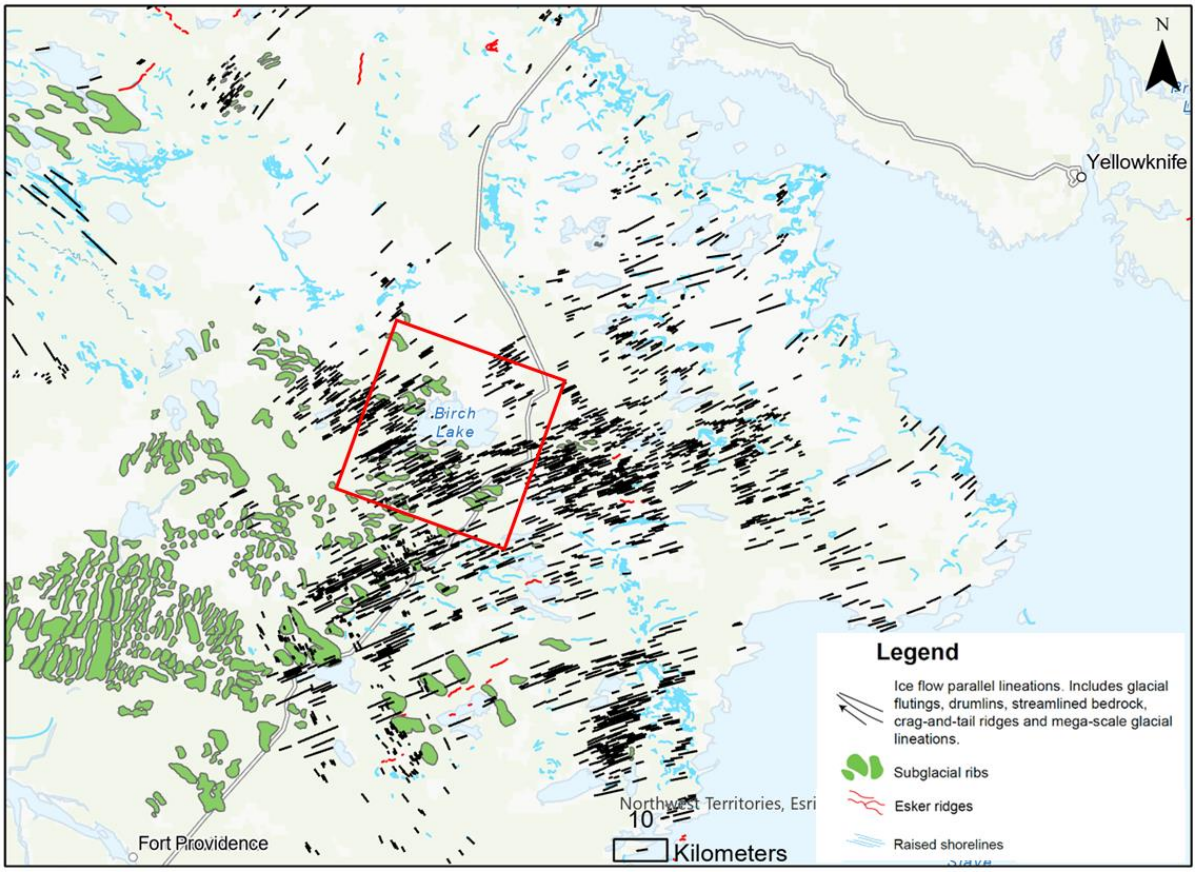


Figure 2.1. Glacial geomorphology of the region encompassing the study area (red box) (Dulfer et al., 2023).

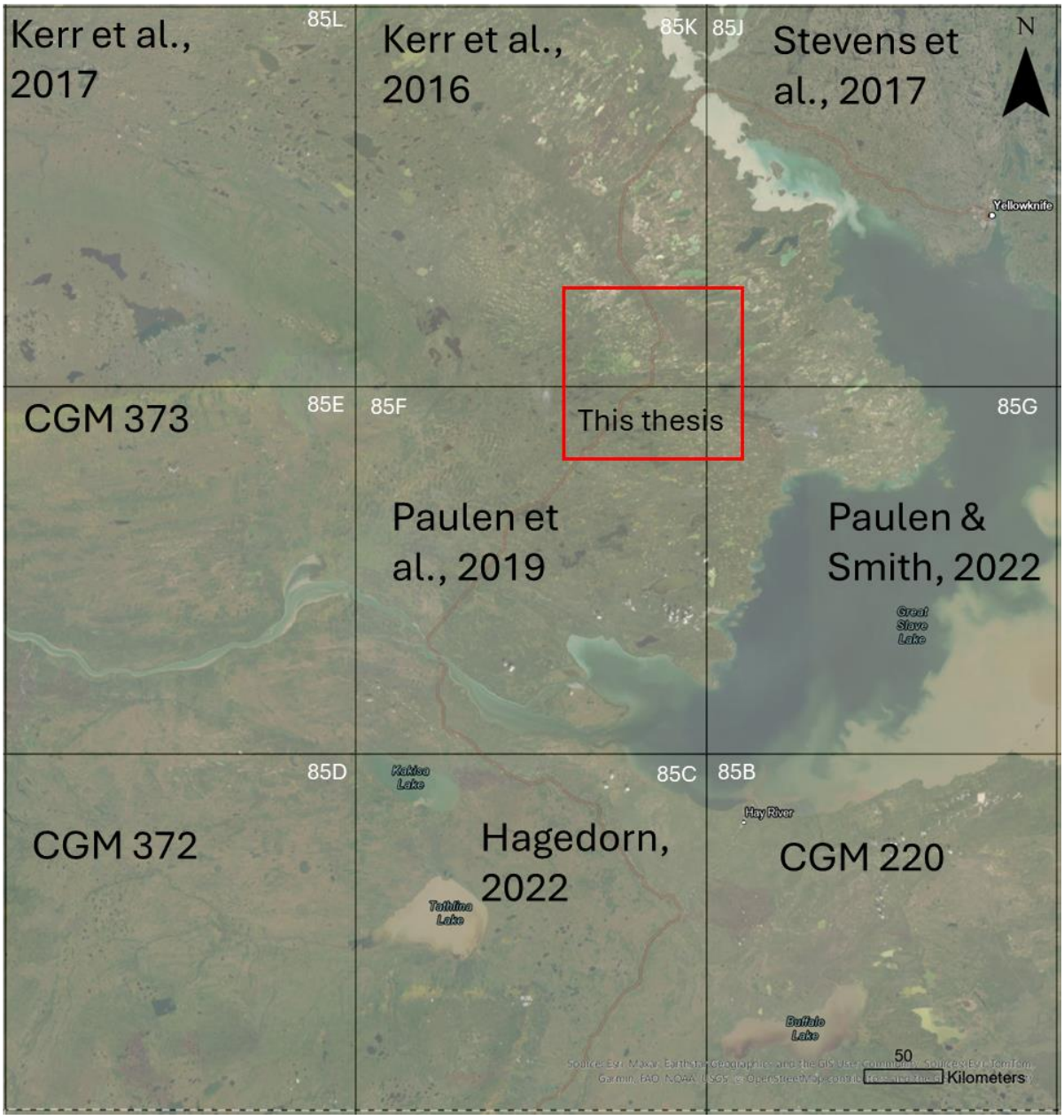


Figure 2.2. Surficial geology maps in the surrounding area.

2.2.1 Ice Flow Parallel Lineations

Ice flow parallel lineations refer to features on the landscape that were formed by the movement of ice in a consistent direction. These features mainly include drumlins (elongated hills or mounds)

and MSGLs (large-scale linear features on the bedrock). Indeed, these landforms encompass a range of ridges that were created either through deposition or erosion beneath the glacier. They extend lengthwise and align with the direction of ancient ice flow (King et al., 2009). Ice flow parallel lineations are typically found in fields or swarms, consisting of hundreds of lineations that share similar characteristics in terms of their shape, spacing, and orientation (Clark et al., 2018). However, drumlins and MSGLs are different morphologically. Most drumlins typically range in length from 250 to 1000 meters, with widths ranging between 120 and 300 meters. Their length-to-width ratios typically range from 1.7 to 4.1, indicating their elongated shape (Clark et al., 2009). Typically, MSGLs have lengths ranging from 6 to 70 kilometers, widths between 200 to 1300 meters, and spacings varying from 300 meters to 5 kilometers (Clark et al., 1993).

2.2.2 Subglacial Ribs

Subglacial ribs, also known as ribbed moraines, are ridges that form subglacially transverse to ice flow and cover extensive areas of the beds of former ice sheets. Subglacial ribs frequently occur in a wide range of scales and patterns, from extensive fields to isolated clusters, and are often characterized by their distinctive formation (Dunlop & Clark, 2006). While the size and shape of these subglacial ribs can vary significantly, ribs within the same field often exhibit a consistent and regular form (Dunlop & Clark, 2006). Subglacial ribs are believed to form from pre-existing sediments and are later preserved and/or partially reworked through shifting subglacial bed conditions (Trommelen et al., 2014).

Ribbed moraine ridges often undergo drumlinization and exhibit close spatial relationships with both drumlins and MSGLs (Dunlop & Clark, 2006). Spatial transitions occur between these landforms, which means ribbed moraines can be superimposed on glacial lineations and glacial lineations can be superimposed on ribbed moraines (Dunlop & Clark, 2006).

2.2.3 The Size and Shape Continuum of Subglacial Landforms

The drumlins mentioned above are not isolated occurrences but tend to cluster together in extensive fields containing hundreds to thousands of individual features. Examples of such fields include the Athabasca drumlin field in Alberta (Shaw et al., 2000), Canada, and the Peterborough

drumlin field in Ontario (Maclachlan & Eyles, 2013), Canada. Studies have examined the spatial patterns within these fields, revealing insights into their formation and evolution.

Subglacial bedforms, including drumlins, eskers, and moraines, are created by the interaction between glacial ice and the underlying bedrock or sediment. However, the debate continues about the relative contribution of erosion versus deposition in the formation of drumlins.

Ely et al. (2016) analyzed a large sample (close to 100k drumlins) of subglacial bedforms for their size and shape to test if they vary continuously or discretely across different types. The authors found that subglacial bedforms comprise a size and shape continuum across the various types, except for flutes (Ely et al., 2016). Especially, drumlins form a continuum of subglacial lineations while subglacial ribs can form a continuum of transverse subglacial bedforms. The continuum of theses landforms provides an argument to say that these bedforms may be generated by the same governing process. The study by Sookhan et al. (2021) largely supports this conclusion of a continuum across drumlins and MSGLs.

Stokes et al. (2016) reviewed all the published internal characteristics of ribbed bedforms, shedding light on their formation mechanisms. They concluded that the formation of these intermediate-sized bedforms is conjectural, but they may be related to wave-like instabilities in the coupled flow of ice and till, influenced by subglacial meltwater drainage and possibly glaciotectonism. These observations support the idea of a continuum of ribbed bedforms, suggesting a range of sizes and formations related to ice stream dynamics (Stokes et al., 2016).

Furthermore, the overprinting of these landforms by subsequent glacial advances, characterized by crosscutting and reshaping due to shifts in ice flow (Winkler, 2021), represents another key aspect of investigation in this research. Understanding the complex interactions between glacial processes and the resultant landforms is crucial for unraveling the geological history recorded in these subglacial features.

2.3 Methods

2.3.1 Outcrop-scale Ice Flow Indicators

Outcrop-scale ice-flow indicators, such as striations and grooves, play a crucial role in determining the direction of past ice flow. The primary method for using these indicators is to examine their orientation, since striations and grooves are typically aligned parallel to the direction of ice flow (McMartin & Paulen, 2007). In some cases, multiple sets of striations or grooves may be present, indicating different episodes of glaciation. The cross-cutting relationships between these features can be used to determine the sequence of ice flow events and understand changes in glacier dynamics over time (e.g., Parent et al., 1995; Veillette et al., 1999; Paulen et al., 2013).

Within the study area, the presence of bedrock outcrops is limited, and the signs of abrasion on the surface of carbonate rocks have largely disappeared due to weathering. Nevertheless, there are occurrences of harder igneous rocks of the Canadian Shield that are exposed in certain locations within and around the research area, which allowed, extensive outcrops displaying polished surfaces with abundant ice flow indicators to be examined at two specific sites (Figure 2.3).

A total of 15 measurements of striations were taken at 2 different outcrop sites and 6 different bedrock surfaces in the study area. To establish the correct direction of ice flow, the first step is to identify prominent striations on the outcrop. These striations form parallel lines due to the movement of glaciers or ice sheets. Next, identify the set of striations that are located on the highest surface of the outcrop and analyze the shape of the outcrop to determine the stoss and lee sides. Then, orient the compass so that its azimuth aligns with the direction of the striations that are pointing down the lee side of the outcrop. The azimuth thus provides the direction of paleo-ice flow for that feature. Then, look at any evidence of crosscutting striations and other ice flow indicators like crescentic scour marks. Determine if more than one ice flow direction is recorded on the outcrop. Repeat this process at multiple locations to confirm consistency and to account for any local variations. After these initial steps, examine the lee sides carefully to identify other polished and striated surfaces. This step may require digging into the lee-side till to expose the bedrock surface at the outcrop. These surfaces are important because they would be older as they would have been protected from the ice flow that generated the ones found on top of the outcrop. These strategies allow to document all the recorded ice flow phases on an irregular outcrop surface, which provide valuable insights into past glacial movements (e.g., Parent et al., 1995; Veillette et al., 1999).

2.3.2 Landform-scale Indicators

Most of the Northwest Territories of mainland Canada was covered by the LIS during the Last Glacial Maximum. The growing availability of high-resolution remote sensing data offers new prospects for mapping the glacial landforms and researching the glacial past of this distant region (Dulfer et al., 2023).

The primary dataset used in this study was the Arctic DEM Mosaic version 4.1 (https://www.pgc.umn.edu/data/arcticdem/). This high-resolution dataset, with a spatial resolution of 2 meters, provided detailed topographic information crucial for identifying landform-scale ice flow indicators accurately (Porter et al., 2018). The 2-meter spatial resolution files are distributed as 50 km × 50 km tiles, and one tile was used to generate a hillshade model with ArcGIS Pro. This process involved simulating the illumination of the terrain from a specified azimuth and altitude to produce shaded relief representations. The incident light azimuth is 0°, the altitude is 45° and the vertical exaggeration is 4 across the hillshade image. Hillshade models enhance the visualization of landform features and aid in the identification of ice flow indicators such as drumlins, subglacial ribs and raised shorelines.

The landforms mapped by Dulfer et al. (2023) as shape files were imported, serving as a reference for identifying different landforms.

Dulfer et al. (2023) provided a strong basis for the glacial geomorphology of the study area, however, due to the scale of their map, a detailed investigation and comparison was needed for this study. Therefore, the objective of this study related to glacial landform mapping includes enhancing Dulfer et al. (2023) map by improving the accuracy and detail by adjusting the direction of the lines overlying the drumlin long axis and refining boundaries of subglacial rib polygons, and adding features as needed. In the study area, there are totally 475 parallel lineations and 48 subglacial ribs, in which 441 parallel lineations and 44 subglacial ribs were plotted by Dulfer et al. (2023), and I added 34 parallel lineations and 4 subglacial ribs. In addition, basic metrics such as azimuth of line features were calculated in ArcGIS Pro to get information about ice flow directions indicated by the glacial landforms.

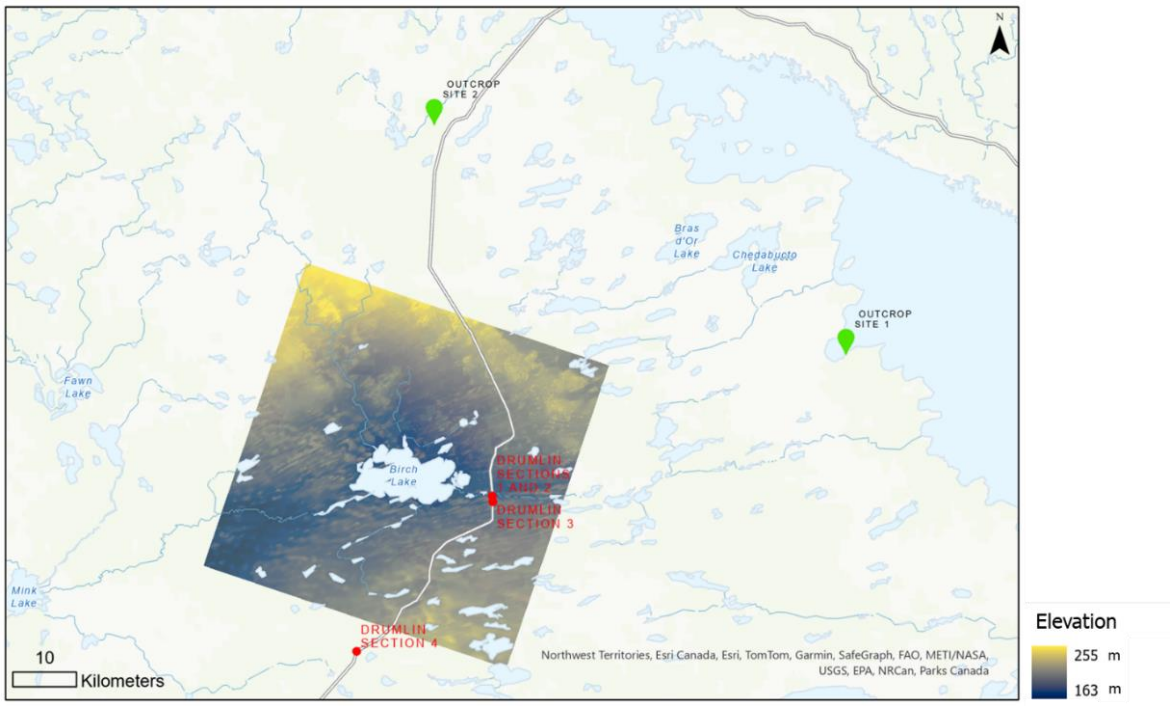


Figure 2.3. Main study area with the ArcticDEM tile used in this study. Location of drumlin sections and outcrop sites are also represented.

2.4 Results

2.4.1 Outcrop Scale Ice-flow Indicators

All the measurements of outcrop ice-flow indicators are summarized in Table 2.1. And there is a rose diagram that shows the relative age of the features (Figure 2.4).

Table 2.1. Measurements of ice-flow indicators at two sites.

Site name	Lat. Decimal deg.	Long Decimal deg.	Elevation M asl	Azimuth Deg.	Feature	Relative age 1 = oldest
Site 1	62.235	-115.2711	170	226	Striations	2
Site 1	62.235	-115.2711	160	219	Striations	2

Site 1	62.2347	-115.2711	170	217	Striations	2
Site 1	62.2347	-115.2711	170	220	Striations	2
Site 1	62.2347	-115.2714	170	185	Striations	1
Site 1	62.2353	-115.2708	150	229	Striations	2
Site 1	62.2353	-115.2708	160	322	Striations	4
Site 1	62.2353	-115.2714	160	186	Striations	1
Site 1	62.2353	-115.2714	160	263	Striations, grooves	3
Site 2	62.5497	-116.4844	300	222	Striations	2
Site 2	62.5497	-116.4844	310	230	Chattermarks	2
Site 2	62.5497	-116.4844	300	233	Chattermarks	2
Site 2	62.5497	-116.4844	310	205	Striations	1
Site 2	62.5497	-116.4844	300	217	Striations	2
Site 2	62.55	-116.4847	310	190	Striations	1

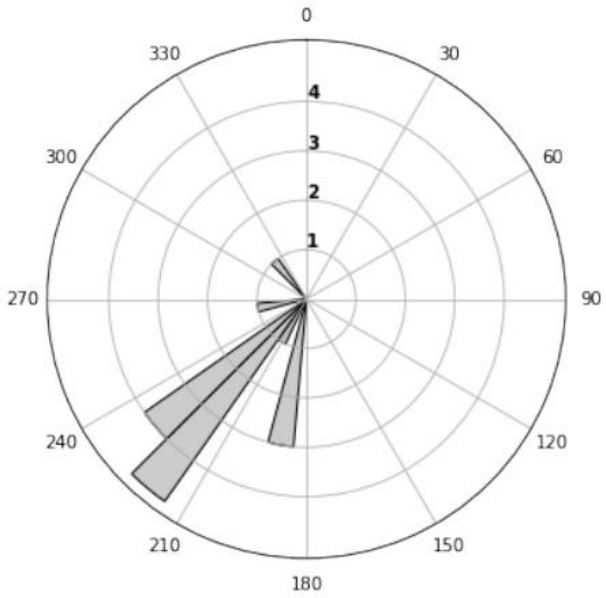


Figure 2.4. Rose diagram of the erosional ice flow indicators listed in Table 3.1.

The first site is located near the shore of GSL, and it consists of a prominent rock knob of igneous and metamorphic rocks. Most ice flow indicators found at the top (~170 m asl) of the outcrop indicate ice movement towards the southwest (Table 2.1). Evidence for an older southward ice flow phase was identified on two protected (lee side) surfaces. In addition, limited but clear evidence for a youngest flow towards the NW was also recognized at site 1. Finally, long striations towards 260-270 degrees were noted near the end of the survey, but the age relationship with the southwest flow could not be established with confidence (Figure 2.5). It was also noted that these westward striations were observed only at one place on the flank of the outcrop. There is thus a possibility for a local outcrop topographic effect, which makes the significance of this observation uncertain. Photos of the main observed features are shown on Figure 2.6.

The record at the second site (Site 2) is similar as it also indicates a clockwise shift from south-southwest to more southwest direction, although it lacks evidence for the westward and youngest northwest flows (Figure 2.7).

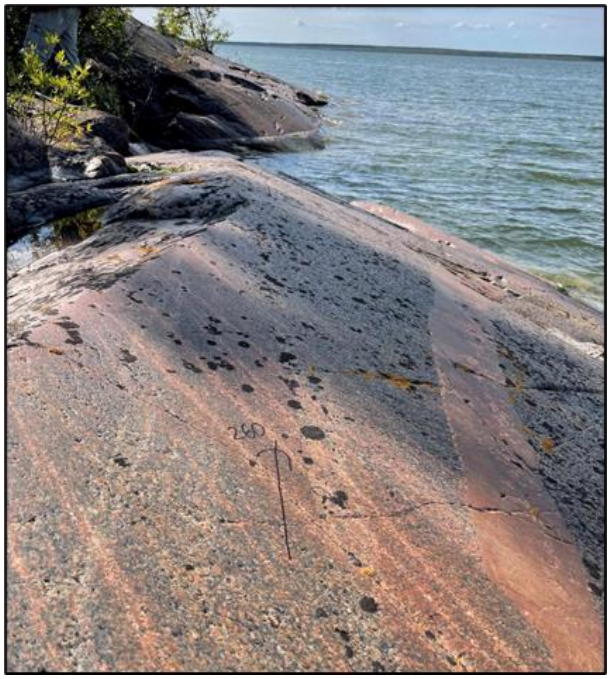


Figure 2.5. Outcrop-scale ice flow indicators showing the westward iceflow (260-270 deg.). The photo is taken facing west at site 1.

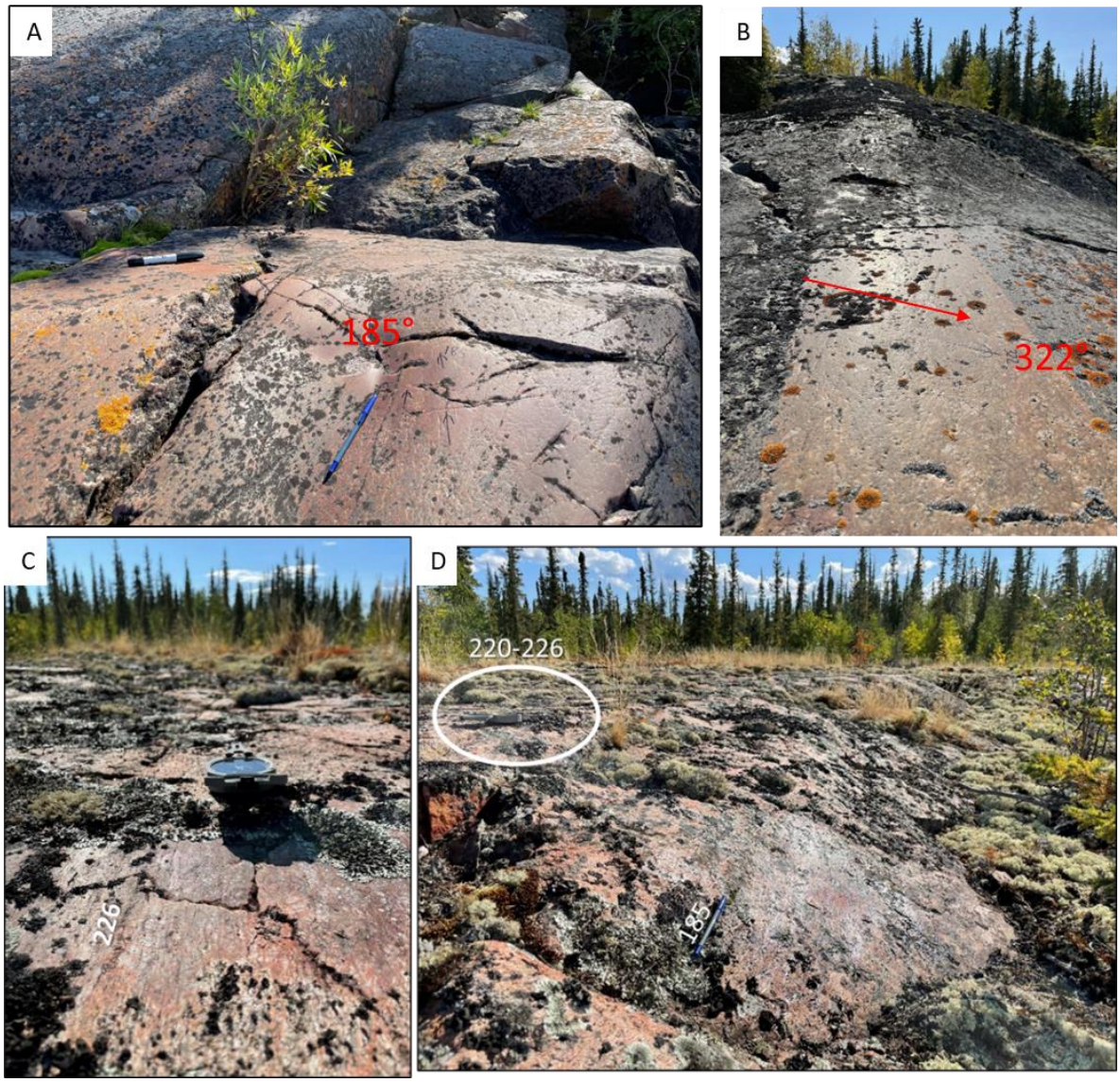


Figure 2.6. Outcrop site 1. A) Outcrop-scale ice flow indicators with stoss-lee relationships establishing the southern flow as the oldest phase (185 deg.). The photo is taken facing south. B) Outcrop-scale ice flow indicators establishing the northwest ice flow phase (322 deg.). The photo is taken facing south. C) Outcrop-scale ice flow indicators establishing the southwestern ice flow phase (220 to 226 deg.) including striations, grooves and chattermarks. D) The general view of the stoss-lee relationship between the younger (southwest) and lower (south) surfaces. The photo is taken facing south.

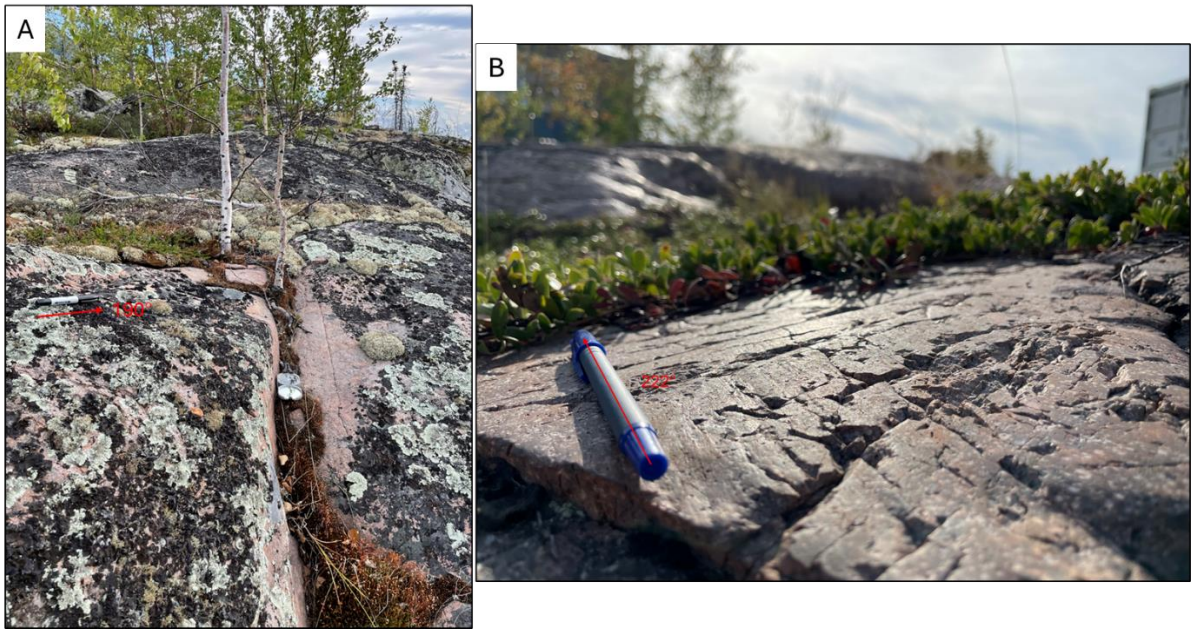


Figure 2.7. Outcrop site 2. A) Outcrop-scale ice flow indicators showing the south ice flow (190 deg.). B) Outcrop-scale ice flow indicators showing the southwest ice flow (222 deg.).

Overall, the ice flow indicators at the two bedrock outcrop sites provide evidence for a clockwise ice flow shift from south to southwest and, perhaps more restricted to the low topographic area of GSL, and a youngest northwest ice flow phase. In summary, the oldest ice flow phase was to the south-southwest (180 to 190 deg.), followed by ice flow phases towards the southwest direction (220 to 235 deg.) and, possibly also a more westward direction, although that one remains uncertain from the limited outcrop-scale observations. Finally, there is a late-stage phase to the northwest, which was spatially more restricted (320 to 325 deg.) as it was observed only at Site 1 along the shore of GSL.

2.4.2 Landform Record

The map of the study area clearly shows a diverse range of landforms which are good evidence for ice flow direction. Figure 2.3 shows the area of focus for the landform analysis using the ArcticDEM data (Porter et al. 2018). Streamlined elongated till ridges forming drumlins and MSGLs, wider and more irregular ridges aligned oblique or transverse to the drumlins, as well as eskers and raised shorelines occur across the landscape of the study area. Most features were identified and

mapped by Dulfer et al. (2023) in their regional mapping effort. The following sub-sections describe and analyze these features in more detail.

2.4.2.1 Drumlins and MSGLS

The mapped till lineations vary in length from tens of meters to about 5 km in length. Most of the mapped lineations are drumlins since their lengths are within 5 km, with the average length at 1.97km (.). The longest of these lineations exhibit dimensions characteristic of mega-scale glacial lineations, which have elongation ratios exceeding 10:1 and can range in length over 5 kilometers (Figure 2.8). The mapped ice flow parallel lineations typically cluster into distinct swarms characterized by similar size, spacing, and orientation (Dulfer et al., 2023). These swarms can collectively create convergent and divergent patterns across the landscape.

Figure 2.9 shows several drumlins west of Birch Lake, and all of them are indicative of southwest ice flow within a narrow range of directions from 227 degrees to 244 degrees, with an average of 237 degrees. Similarly, abundant drumlins occur south of Birch Lake, and they indicate southwest ice flow directions ranging from 234 degrees to 250 degrees, with an average of 242 degrees (Figure 2.10).

Table 2.2. Basic metrics of the drumlins.

Number of drumlins	443
Average length of drumlins	1.97 km
Average azimuth of drumlins	242.87 degrees

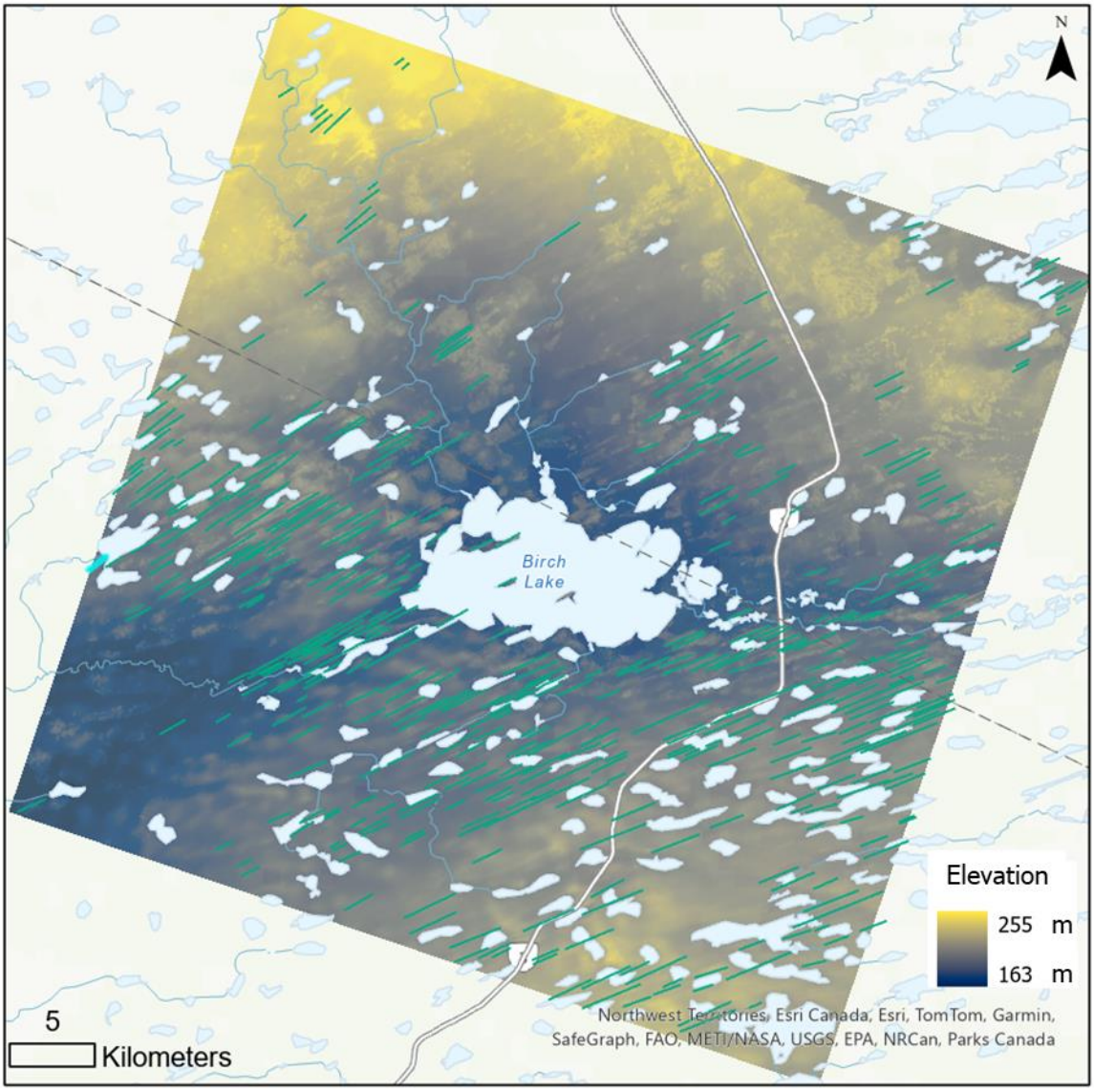


Figure 2.8. ArcticDEM elevation grid (2m resolution) of study area with ice flow parallel lineations from Dulfer et al. (2023).

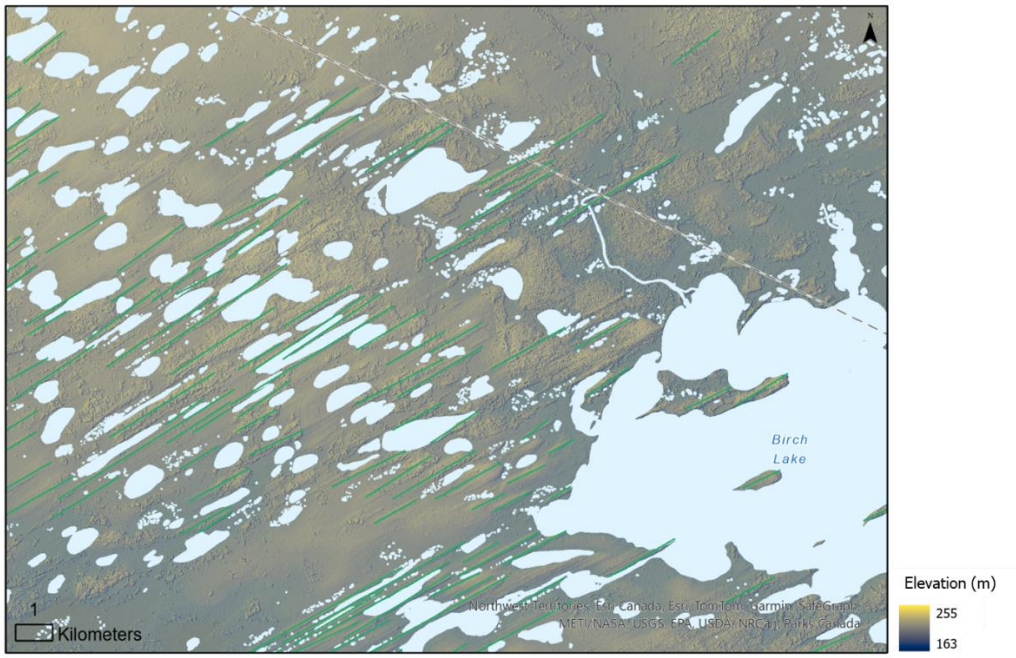


Figure 2.9. ArcticDEM hillshade (2m resolution) west of Birch Lake and geomorphological mapping of ice flow parallel lineations (Dulfer et al., 2023).

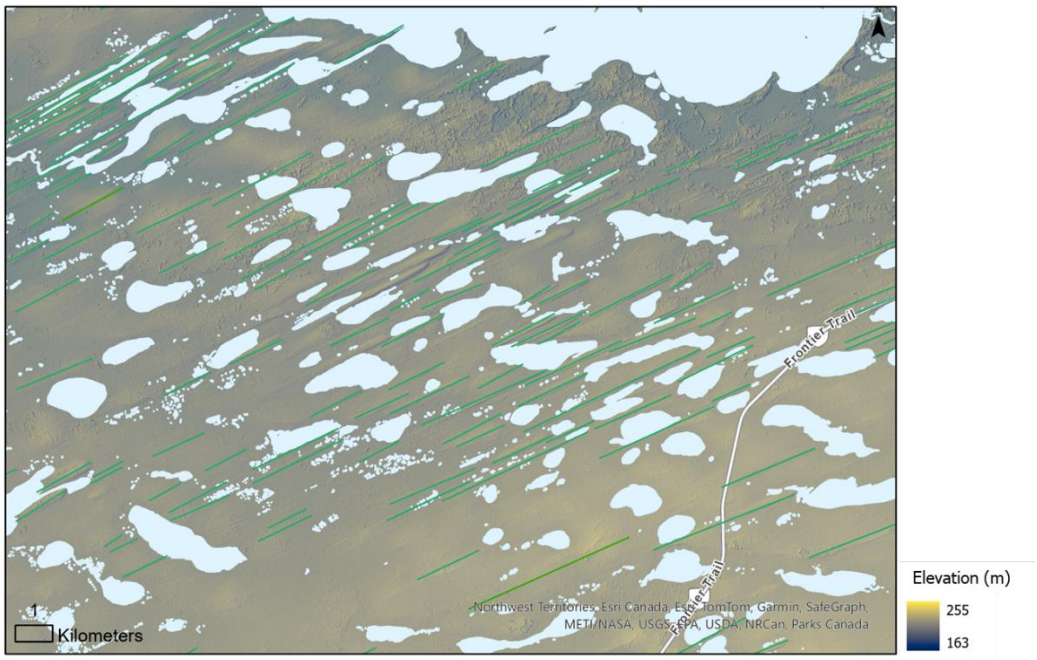


Figure 2.10. ArcticDEM hillshade (2m resolution) south of Birch Lake and geomorphological mapping of ice flow parallel lineations (Dulfer et al., 2023).

2.4.2.2 Other Elongated and More Irregular Ridges

Dulfer et al. (2023) also mapped wider and more irregular landforms that they interpreted to be subglacial ribs that formed oblique or transverse to ice flow. Within the focus area shown on Figure 2.8, there are 44 of them. The features exhibit a range of lengths, varying from 0.1 km to 10 km, and display diverse shapes (Dulfer et al., 2023). However, the ones within the same swarm typically maintain a consistent size and morphology. Several subglacial ribs form a cluster around the area south of Birch Lake, and most of them are either east-west oriented or slightly SE-NW, with some showing evidence of overprinting by the SW drumlins (Figure 2.11). This would indicate that these features formed prior to the drumlins.

The area east of Birch Lake also contains numerous drumlins indicative of SW-trending ice flow, as well as a few 'subglacial ribs' from Dulfer et al. (2013) (Figure 2.12). Some of these ridges were not identified and mapped as subglacial ribs by Dulfer et al. (2023), but the occurrence of east-west elongated and irregular ridges is clear in that area (Figure 2.12). Interestingly, just east of Birch Lake, a series of four of these E-W oriented ridges are also clearly overprinted by smaller and younger drumlins (Figure 2.12). Here, I argue that these features could be older drumlins that were partially re-shaped by later ice flow phases. In this scenario, these E-W features would provide evidence for an old westward ice flow phase in this area. This challenges the subglacial rib and transverse-to-flow interpretation of Dulfer et al. (2023), at least for some of these elongated and more irregular and overprinted till ridges. However, only one set of striations indicative of westward ice flow (.) was documented at Site 1 (cf. Sect. 2.4.1) and its relative chronology, although uncertain, could be younger than the features described here, which are older than the SW drumlins. It is possible that the westward flow recorded by these irregular elongated ridges was spatially restricted to the low-lying area aligned with Birch Lake and would thus not have left a record at the outcrop sites further to the north (Figure 2.3). It is also possible that the indicators of this flow were missed at the outcrops due to the size of the outcrops and the limited time available to investigate them. It is important to note that a westward flow was also documented by Hagedorn (2022) to the south, but placed after the southwest flow in the relative chronology of that area. The detailed study of till sheets from within the drumlins along Highway 3 will serve as a test of this hypothesis of a westward flow in the area and provide some independent insights into its relative chronology (cf. Chapter 3). The alternate interpretation would be that these west-trending irregular ridges represent relict rib moraines related to the older southward ice flow phase identified in the outcrop-scale record (cf. Sect. 2.4.1).

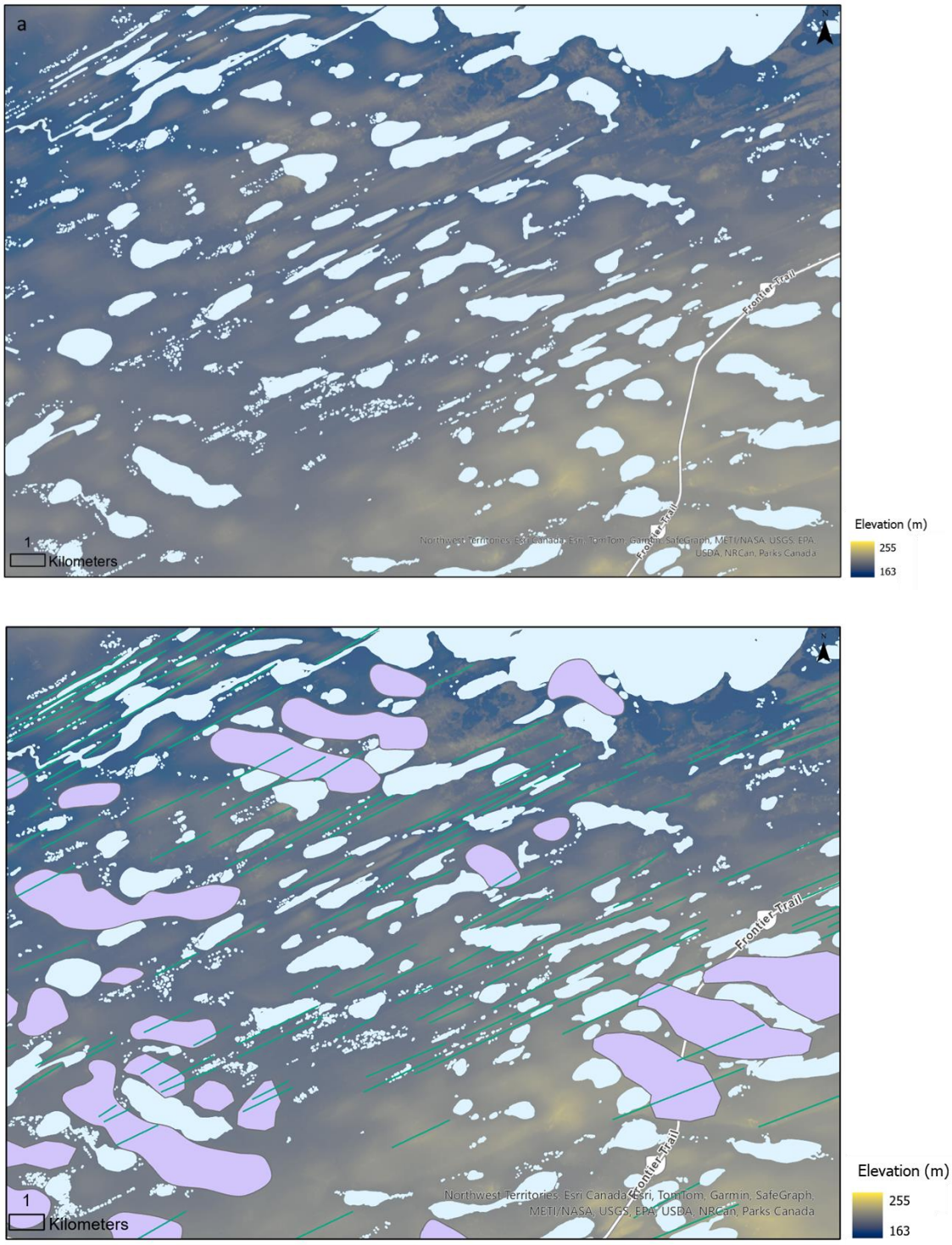


Figure 2.11. (a) Elevation from the ArcticDEM (2m resolution) south of Birch Lake and (b) geomorphological mapping of subglacial ribs (Dulfer et al., 2023).

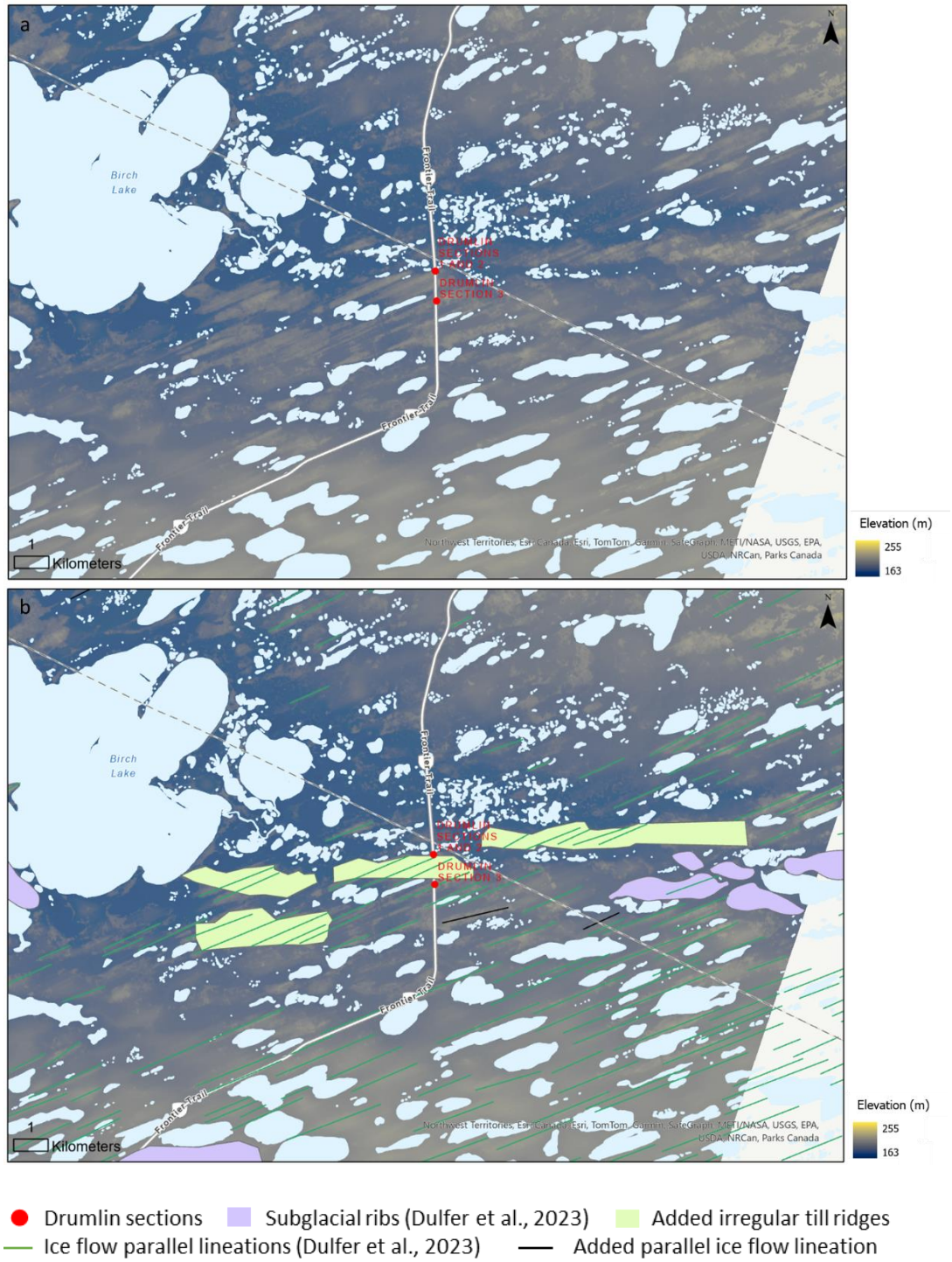


Figure 2.12. a) ArcticDEM east of Birch Lake and (b) geomorphological mapping of ice flow parallel lineations with overprinted and irregular till ridges.

2.5 Discussion

In this section, the outcrop-scale ice flow indicators and glacial landform records are used to recognize different ice flows in the study area in relative chronology order.

2.5.1 Southward (180-190 deg.) Ice Flow

The oldest ice-flow phase in the study region is indicated by the oldest striations discovered at the outcrop site 1 and 2 (Figure 2.3), which are found with stoss-lee relationships (Figure 2.6). The south ice flow is the oldest because it is at the leeside of the outcrop and its bedrock surface is protected from the ice flow that generated on top of the outcrop. However, because of the limited study area of landform records, no landforms indicating south ice flow.

2.5.2 Westward (260-270 deg.) Ice Flow

Evidence of westward ice flow was also found at outcrop site 1, where striations and grooves indicate ice flow directions at 260 to 270 degrees (Figure 2.5.). As mentioned previously, there is uncertainty about this because of the limited evidence and its position on the flank of the outcrop. However, westward-trending landforms also occur east of Birch Lake (Figure 2.12). These landforms are clearly overprinted by the smaller southwest-trending drumlins, which indicates that a westward ice flow phase preceded the younger southwest flow phase.

Glacial lineations trending westward are present along the southwestern border of the study area and extend into the lowlands to the west (Bednarski, 2008). In addition, some westward striations were found at southwest Northwest Territories and south of GSL, suggesting westward ice-flow trajectories (Paulen et al., 2011). The striations are observed at the abandoned Pine Point mine, which indicates that any mineralized debris from the Pine Point deposits was transported westward, north of the Cameron Hills (Paulen et al., 2011).

2.5.3 Southwest (220-235 deg.) Ice Flow

The striations at outcrop sites 1 and 2 suggest one or more ice flows towards the southwest direction from 220 to 230 degrees (Figure 2.6). In addition, some chattermarks were also found at site 2. Chattermarks are crescent-shaped fractures created by friction of sliding ice onto bedrock. They

typically occur as a series or track of nested fractures with their concave side pointing in the down-ice direction (Rea, 2007; Benn & Evans 2010). They also tend to decrease in size in the down-ice direction. Due to these characteristics, they are useful indicators of past glacial movement and can provide valuable insights into the direction and force of the glacial motion. At site 2, they indicate ice flow towards 230 and 235 degrees.

In the landform record, the study area exhibits a diverse array of ice flow parallel lineations, indicating various subglacial depositional and erosional environments. This diversity encompasses features such as drumlins, and mega-scale glacial lineations (MSGLs). These features align with fields indicative of a southwest ice flow phase. The pattern that the southwest oriented drumlins are superimposed on larger E-W oriented ridges suggests the westward ice flow phase is older than the southwest flow phase which produced the drumlins.

There is also evidence of southwestward flow in the region surrounding the study area. Streamlined landforms including glacial flutings and moraines around Trout Lake, which is situated to the southwest of the study area, also exhibit a southwestward ice flow direction (Bednarski, 2008).

2.5.4 Northwest (320 to 325 deg.) Ice Flow

The outcrop-scale ice-flow indicators pointing to the northwest are the youngest features within the study area, suggesting a relatively recent occurrence of this directional flow. The striations at outcrop site 1 show an ice flow direction at 320-325 degrees (Figure 2.6). However, the impact of the northwestward flow on the landscape was probably restricted, primarily due to the limited ability of a thin lobe to cause substantial erosion and sediment entrainment.

2.6 Conclusion

In conclusion, the combination of outcrop-scale ice flow indicators and glacial landform records is a critical step towards a comprehensive analysis of ice flow phases in an area. Outcrop-scale indicators such as striations and grooves offer detailed, localized evidence of past glacial movement, providing precise information about flow direction at specific locations. Meanwhile, landform records encompass larger-scale features shaped by glacial processes, offering broader insights into regional patterns of ice flow.

Specifically, outcrop ice-flow indicators were found at two sites, and provide clear evidence for different ice flow phases. Striations suggest an older phase characterized by southward ice flow. Most features are, however, indicative of southwest ice flow. There is also limited evidence for a westward phase, but it is uncertain due to possible local topographic deflection effect like the shape of bedrock. Its relative age is also uncertain. There is also a youngest phase towards the northwest that is recorded only along the shore of GSL. From the landform record, this NW phase does not appear to have affected the central area around Birch Lake and its drumlin field. These sequential ice flow directions provide valuable insights into the complex history of glacial movements over time in the study area.

As for the landform records, specifically, the map area displays a diverse range of ice flow parallel lineations, suggesting different subglacial depositional and erosional environments. This variety includes features such as drumlins and MSGLs. These features parallel fields indicative of a SW ice flow phase. Drumlins, especially smaller ones are frequently superimposed onto longer and wider ridges oriented obliquely (E-W) relative to the drumlins. The diverse orientations of all these till ridges and their crosscutting relationships can serve as indicators of the fluctuation in ice flow directions over time. These overprinted features suggest that a westward ice flow phase preceded the SW flow phase that produced the drumlins. If this interpretation is correct, it means that the two records, the outcrop-scale erosional record and the landform record, are not fully consistent. The former provides evidence for a relatively simple clockwise shift of ice flow directions (from south to southwest, and northwest), whereas the landform analysis suggests a counterclockwise shift from west to southwest. Additional information is thus needed to resolve this puzzle, and this is what the till stratigraphy analysis of Chapter 3 will try to achieve.

Chapter 3 - An Analysis of Till Stratigraphy in the Birch Lake Area, West of Great Slave Lake (NTS 85K), Northwest Territories

3.1 Introduction

Till stratigraphy plays a crucial role in comprehending temporal changes in ice sheet erosive and depositional conditions over time (Menzies et al., 2019). By examining the superposition of different till stratigraphic units, researchers can gain insights into the sequence of till sheets and their bedrock (up-ice) provenance, allowing them to reconstruct ice flow phases and subglacial conditions based on the sedimentary record and then compare with the landform and outcrop-scale records for an integrated analysis. This enables the reconstruction of ice flow phases and helps in understanding how ice sheets have influenced the landscape over time. Stratigraphic sections are exposed primarily along Highway 3 in the study area (Figure 1.6).

The direction of the paleo-ice flow at the time of drumlin formation can be determined by the orientation of the long axis of the drumlin. However, the subglacial till in drumlins can be several meters thick, and part of the till might not be related to the ice flow phase that generated the drumlins (Hodder et al., 2016; Stirling, 2022). Additionally, the formation of drumlins is also affected by erosional processes (Eyles et al., 2016). As a result, till from different stratigraphic positions could be exposed at the surface, thus complicating the provenance analysis of surficial till in drumlin fields (Stirling, 2022). In this situation, landform record cannot be the sole criterion to reconstruct the glacial history of drumlin fields.

The goal of this chapter is to present a comprehensive analysis of the complexities involved in interpreting till stratigraphy within drumlin fields, with a focus on analyzing the ice flow phases and understanding past glacial dynamics. Clast fabrics and composition of till are the main methods used to reconstruct the ice flow history in the study area in combination with outcrop-scale ice flow indicators and subglacial landforms in Chapter 2.

3.2 Methodology

Stratigraphic log is created by drawing the thicknesses of sediment layers found along a vertical line through a drumlin. The main methods used in the till stratigraphy analysis are particle size

analysis, till clast fabrics and clast lithology counts. The grain size of sediment at each elevation is indicated using a scale from clay to gravel. Sediment layers are filled in with standard patterns or textures based on the rock type. Clast fabrics indicate ice flow direction at different levels of the log. The results are combined to provide a comprehensive and organized representation of the observed geological layers and their characteristics.

In addition, stratigraphic logging is the description of stratigraphic sections, detailed information regarding major units was recorded, including their sedimentological characteristics such as sorting, color, compaction, and thickness (Evans & Benn, 2004). Sites were systematically documented through photography, capturing visual records of the stratigraphic sections. The whole drumlin cut is shown on Figure 3.1, and the close-up view showing the steps on the section is on Figure 1.7.



Figure 3.1. Cut view of drumlin section 1. The photo is taken facing west.

3.2.1 Grain Size Analysis

The subglacial traction till consists of particles of a wide grain size range including boulders, cobbles, gravel, sand, silt, and clay. Particle size is the diameter of individual grains within the sediment, which serves as a fundamental descriptive measure for sediments in various environments (Das, 2016). In the case of glacial sediments, grain size analysis is essential to examine the patterns

and trends in surface processes associated with dynamic conditions of sediment transportation and deposition (Das, 2016). It is challenging, and not necessarily realistic, to produce grain size curves that include boulders in the till. However, by analyzing the grain size distribution of the till matrix, we can gain insights into the specific physical characteristics of till sheets and perhaps also on subglacial sedimentary processes or the link to bedrock sources.

Different grain size scales have been developed for geosciences and engineering. In sedimentology, one of the most commonly used is the Udden-Wentworth scale. In this study, grain sizes are subdivided into three categories, namely gravel, sand, silt and clay, which are further subdivided into fine, medium, and coarse. Gravel includes particles over 2 mm, sand includes particles from 0.063 mm to 2 mm and, finally, silt and clay include particles less than 0.063 mm. Table 3.1 presents the portion of the Wentworth scale used in this study. It includes the logarithmic (phi) scale introduced by Krumbein (1938), which is useful to present grain size data in units of equal intervals and for calculations.

Table 3.1. Classification of grain size.

Category	Sub-category	Size	Phi
Gravel	Mediem	>8mm	<-3.0
	Fine	4-8mm	-3.0 ~ -2.0
	Very fine	2-4mm	-2.0 ~ -1.0
Sand	Very Coarse	1-2mm	-1.0 ~ 0.0
	Coarse	0.5-1mm	0.0~1.0
	Medium	0.25-0.5mm	1.0~2.0
	Fine	0.125-0.25mm	2.0~3.0
	Very fine	0.063-0.125mm	3.0~4.0
Silt/Clay	Silt/Clay	<0.063mm	>4.0

In this research, a total of 104 samples were prepared, sieved, and subsequently analyzed to determine their particle size distribution (Figure 1.9). Among them, there are 56 samples from 2020 and 48 samples from 2021. This includes all the samples from 2020 and most of the samples from 2021. Specifically, 20 samples from the drumlin sections are all analyzed.

3.2.2 Clast Fabrics

Particles found in sedimentary deposits with a platy or elongated shape commonly exhibit a certain level of directional alignment. Platy particles typically align themselves in planes that closely

mirror the bedding surfaces of the deposits (Boggs, 2006), whereas elongated particles exhibit a tendency to orient with their long axes pointing in a similar direction. The alignment of these particles is a consequence of transport and deposition processes, specifically influenced by flow velocities and other conditions at the deposition site (Boggs, 2006). In the case of subglacial traction till, the orientation of elongated clasts can be a valuable indicator of the direction of shear stress, which is commonly interpreted as reflecting the paleo-ice flow direction (Benn, 2013).

A Python script was used for the till fabric analysis to generate equal-area stereonets and obtain results such as eigenvalues and eigenvectors. The code "Till Fabric Analysis Demo – Copy 1" is accessible online (https://github.com/GlacialGeo/PythonCodes). The stereonets facilitate the visualization of the clast fabrics and aid in the identification of potential ice flow directions based on the 3D orientation of clasts. Eigenvalues and eigenvectors are the factors determining the strength and orientation of the fabric. The eigenvalues were normalized to the sample size, in which S1 is higher than S2 and S2 is higher than S3, and they add up to 1. Clast fabrics can exhibit variations when shear plane is inclined (Iverson, 2017) or particle size are different (Carr & Ross, 2003). Therefore, clast fabrics are ideally used in combination with other ice flow indicators, such as landform records, for a more comprehensive analysis.

Fifty clasts were measured in selected stairs to obtain a sufficient sample population, which is a common practice for till clast fabrics (Benn, 2013). Specially, in drumlin section 3, only 46 measurements at the bottom of the section and 47 measurements in the middle of the section were plotted on the equal-area stereonets, because the measurements with plunge over 60 degrees are removed. Clasts that are less steeply plunging are considered to be more accurate paleo-ice flow indicators. Since fabrics were measured to get paleo-ice flow directions rather than fabric modality to interpret internal processes, a few steeply plunging clasts measurements were not used. This approach has been recently adopted by other researchers (e.g. Hodder et al., 2024)

3.2.3 Clast Lithology Counts

Clast lithology counts on subglacial till serve as a crucial tool in deciphering the bedrock sources of the till deposit. Comparing the lithology of clasts with known bedrock formations in the region allows for the identification of similarities, thereby indicating potential bedrock sources (Menzies et al., 2023). Additionally, the presence of unique lithologies or indicator minerals within the clasts can offer clues about distant bedrock formations or geological environments (Rice et al., 2024). Mapping

the distribution of clast lithologies within the till deposit further aids in tracing the pathways of glacial ice movement and inferring the locations of bedrock sources based on the direction and distance of ice flow.

Hagedorn (2022) used pebble lithology as part of a provenance analysis just south of the study area, used four broad lithological groups that were then further classified into 15 sub-categories. According to the regional bedrock geology map (Okulitch, 2006), the bedrock geology of the study area is similar to that of Hagedorn's research area. Specifically, it consists mostly of shales, carbonates, and evaporites. However, there are important lateral facies transitions across the region, which means that some differences are to be expected. For instance, according to the geological map of Okulitch (2006), black bituminous shales are more abundant in this study area than in the south, across the Mackenzie River. Therefore, the lithology groups used in this study differ to some extent (Table 3.2).

During the laboratory work, 300 clasts over 5.6mm from each sample bag are selected to do pebble counts. If there are fewer than 300 clasts over 5.6 mm in the sample bag, then all clasts larger than 5.6mm are used to do pebble counts. There are 24 section samples and 33 surficial samples chosen to do pebble counts, and the specific experimental procedure is shown in section 1.6.2 (Figure 1.10).

Table 3.2. Lithology groups for pebble counts.

Canadian shield	**WCSB (Paleozoic)**
Felsic intrusive	Dark grey dolostone (Chedabucto Lake formation)
Mafic intrusive	Red dolostone (La Martre Falls formation)
Quartzite	Shale (Muskwa formation)
	Dark siltstone
	Siliciclastic rock (Keg River formation)
	Brown limestone (Lonely Bay formation)

3.3 Results

3.3.1 Results of Drumlin Sections

3.3.1.1 Till Stratigraphy

The road cuts along the highway reveal the internal nature of the drumlins. Overall, the sediment is poorly sorted, massive matrix-supported diamicton. The clasts are dominantly sub-angular and polished, and some exhibit striations (Figure 3.2). The sediment is interpreted as a subglacial traction till because of its wide range of particle sizes and irregular stratigraphic structures. In each section, three or four sets of till fabric data were recorded separately at the top, middle and bottom of the drumlin sections. The results of grain size analysis are also shown in the stratigraphic columns. This integrated data can be particularly useful for reconstructing ice flow phases and determining the sources of the till.



Figure 3.2. A close-up view of the till.

Specific to drumlin section 1, a total of 14 holes were created. The sample at section 21-PXN-031 at the bottom of the section (13th hole) gives a strong clast fabric (S1=0.72) with spread unimodal distribution showing southwestward ice flow (214 deg.). One clast fabric done at sample 21-PXN-029 in the middle of section 1 (9th hole) shows moderate clast fabric (S1=0.65) with spread bimodal distribution and suggests a southwestward ice flow (237 deg.). Another clast fabric done at site 21-PXN-027 is in the middle of section 1 (6th hole), which also shows moderate clast fabric

(S1=0.67) with spread bimodal shape and suggests a southwestward ice flow (240 deg.). 21-PXN-025 has a moderate clast fabric (S1=0.67) with spread bimodal shape on the upper till (2nd hole), which gives a southwestward ice flow direction (246 deg.). Generally, from the bottom to the top, the ice flow has changed from south-southwest to west-southwest (Figure 3.3).

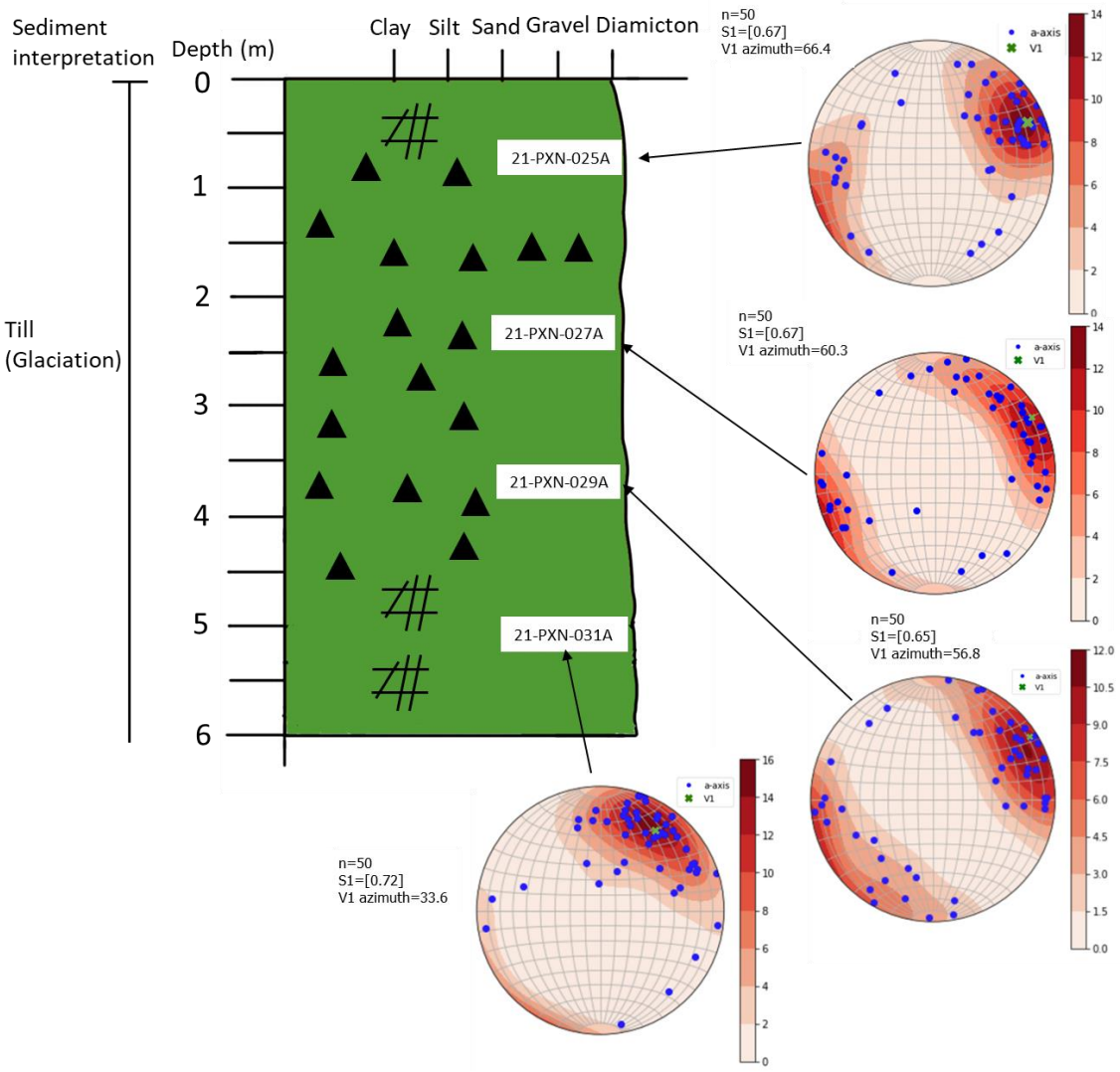


Figure 3.3. Stratigraphic log for drumlin section 1 and its four clast fabrics. Kamb density contours have been added to the stereonets.

Drumlin section 2 is just across the highway from section 1. The clast fabric at site 21-PXN-040 at the bottom of the section (15th hole) shows a moderate clast fabric (S_1=0.67) with spread bimodal modality showing southwestward ice flow (233 deg.). Another fabric was done at site 21-PXN-035 in

the middle of section 2 (6th hole), which also shows moderate clast fabric (S_1=0.65) with spread bimodal modality and suggests a west-southwestward ice flow (254 deg.). 21-PXN-033 suggests a moderate clast fabric (S_1=0.68) with spread bimodal modality on the upper till (2nd hole), which gives a west-southwestward ice flow direction (260 deg.). Compared with the results from section 1, section 2 also suggests a southwestward ice flow but closer to the west.

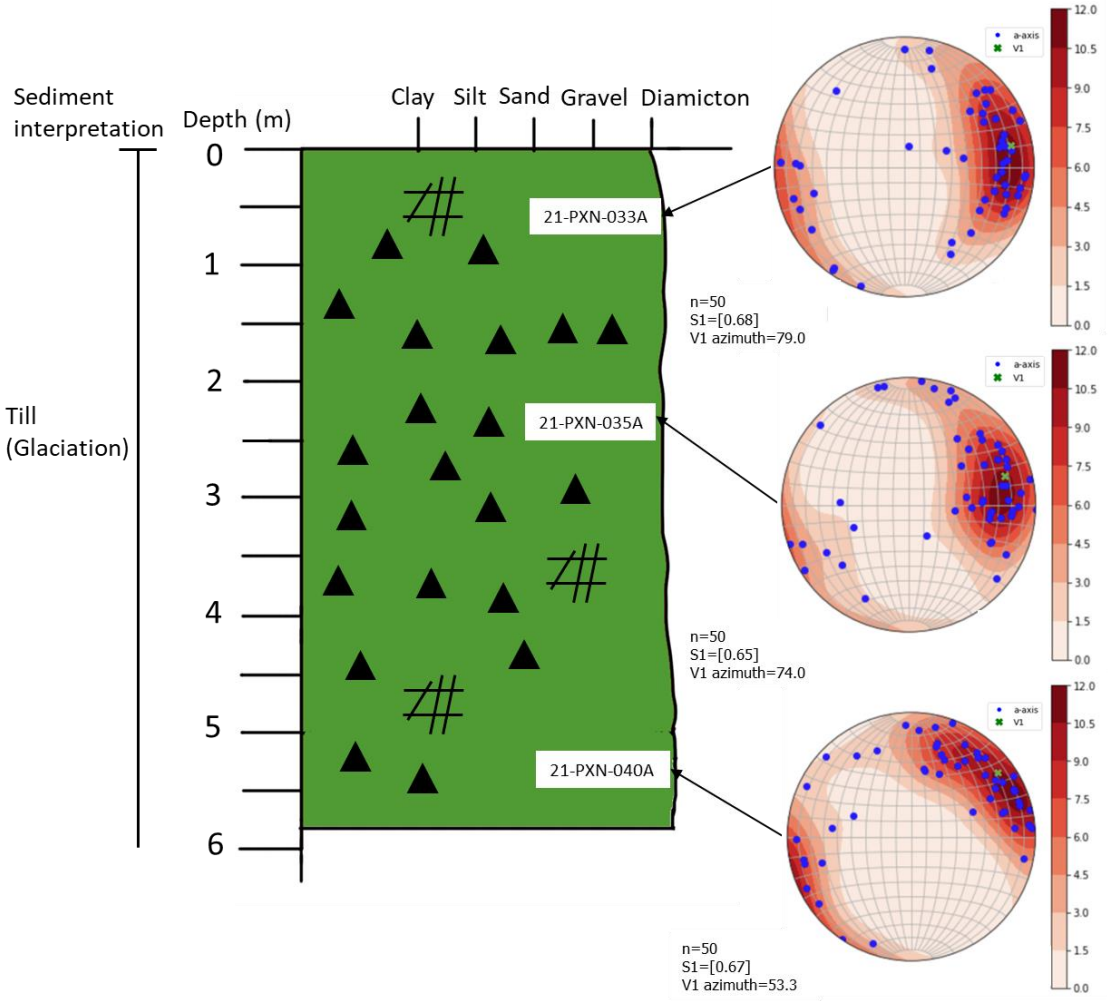


Figure 3.4. Stratigraphic log for drumlin section 2 and its three clast fabrics. Kamb density contours have been added to the stereonets.

Drumlin section 3 is on the west side of the highway and south of section 1 and 2. The upper part (1m from top) is characterized by gravelly sand, and sand is fine to medium. While the middle and lower sediment (1m to 5m) is poorly-sorted, massive matrix-supported diamicton interpreted as

subglacial traction till. The clast fabric at section 21-WL-004 on the lower till (16th hole) shows a moderate fabric (S_1=0.62) with spread bimodal modality showing south-southwestward ice flow (191 deg.). Another fabric was done at site 21-WL-003 in the middle of section 3 (12th hole), which shows moderate clast fabric (S_1=0.60) with spread bimodal modality and suggests a southwestward ice flow (207 deg.). 21-WL-001 suggests a strong clast fabric (S_1=0.71) with spread unimodal modality on the upper till (4th hole), which gives a southwestward ice flow direction (232 deg.). In general, from bottom to top of the section, ice flow has changed from nearly south to southwest. Another fabric was done in the middle of this section (8th hole) at site 21-WL-002, but it is a weaker till fabric (S_1=0.54) with higher isotropy and lower elongation, so it is less reliable for paleo-ice flow.

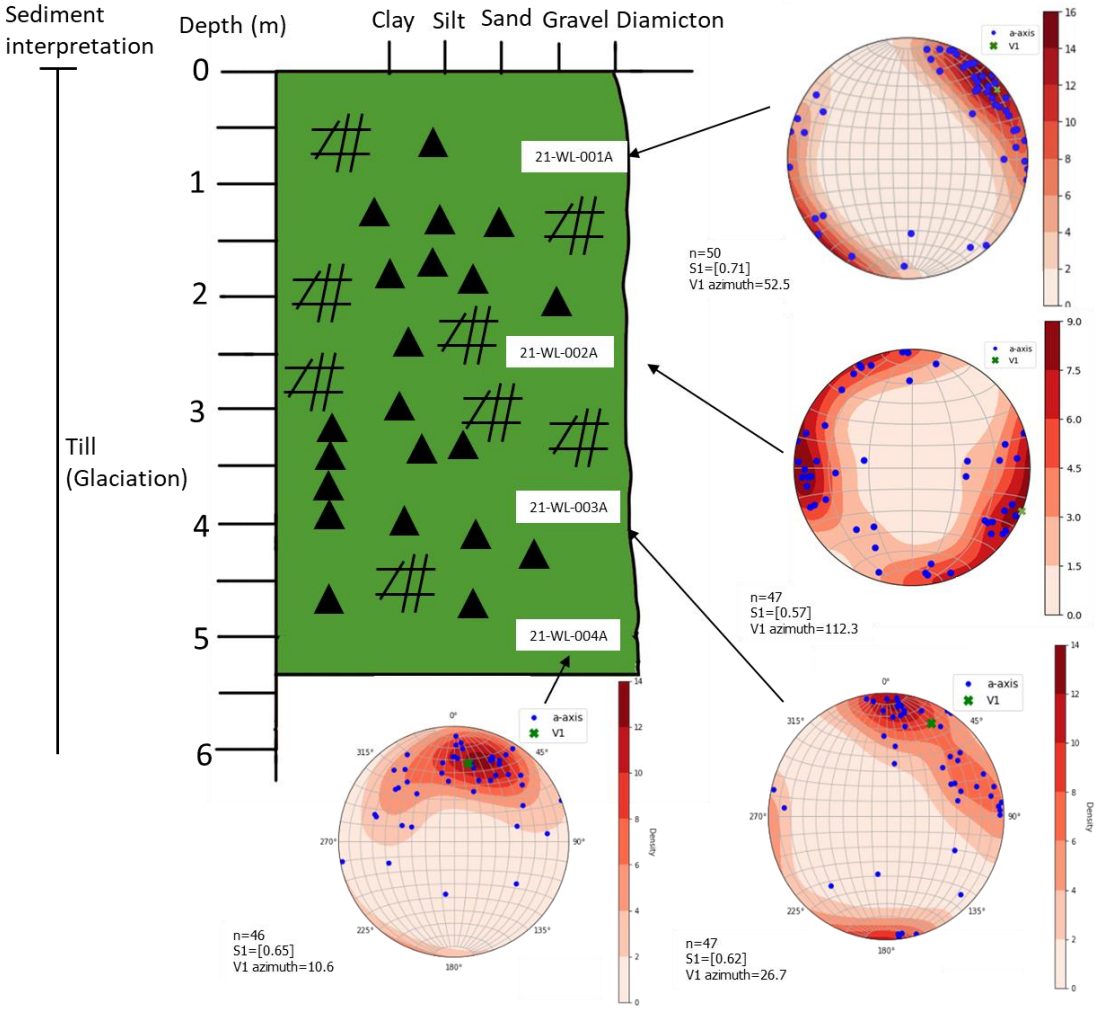


Figure 3.5. Stratigraphic log for drumlin section 3 and its four clast fabrics. Kamb density contours have been added to the stereonets.

Unfortunately, the only two fabric analysis done in section 4 at site 21-PXN-064 and 21-PXN-065 both result in weak till fabric (S_1=0.54 and 0.52). Therefore, drumlin section 4 is unreliable for paleo-ice flow direction and the data is presented only in Appendix B.

As for the fabric shape, different fabrics from all sections are close to the corner of cluster so they tend to be more cluster-like. As Figure 3.6 shows, all fabrics exhibit low isotropy and high elongation. They are all moderate to strong fabric so they can be useful to interpret paleo-ice flow direction. Moderate fabric has eigenvalue S1 between 0.6 to 0.7, with spread bimodal modality. Strong fabric has eigenvalue S1>0.7 and spread unimodal modality.

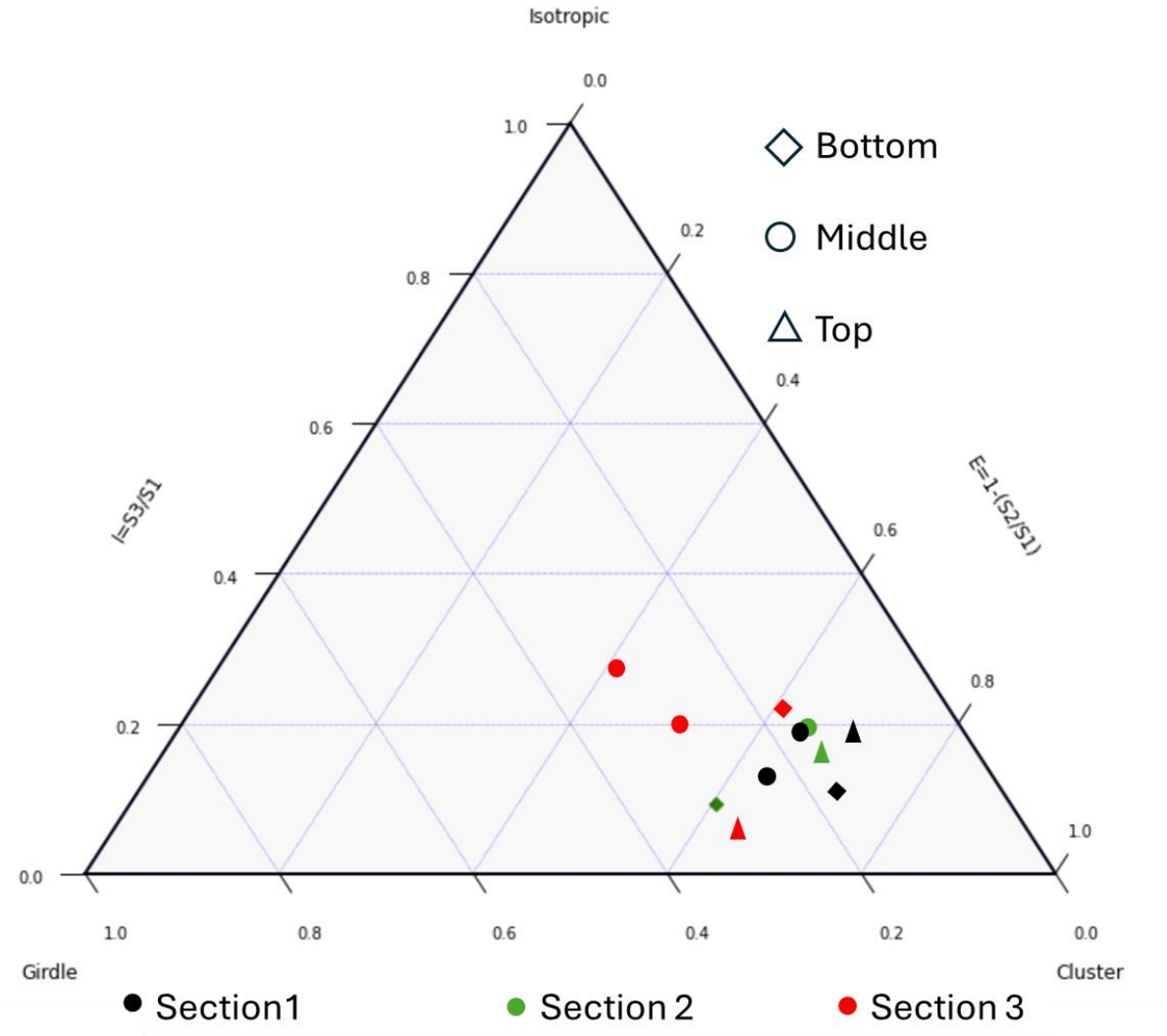


Figure 3.6. Fabric shape of all samples.

3.3.1.2 Grain Size in Drumlin Sections

Different types of distributions in grain size can be observed in different samples. In drumlin sections, the most common grain size distribution is clast-poor and mud-rich, which are described as till in the database. However, at the top of the drumlin sections, sand is the dominant component, which takes up over 60 wt. percent of all particles. When it comes to the bottom of the drumlin section, the portion of silt and clay becomes higher, which means there are more fine particles. Gravel is always the rarest grain size, which maintains 5 to 15 wt. percent of all particles.

For example, in drumlin section 1, sample 21-PXN-025B at the top has dominant sand portion, so it can be described as sandy diamicton (Figure 3.7). Other samples have a mixture of unsorted and unstratified sediment, including a range of particle sizes from clay to gravel, so they can be described as diamicton. However, in drumlin section 2, there are more sandy diamicton layers at the upper part of the till, from sample 21-PXN-033B to 21-PXN-036B (Figure 3.8). For drumlin section 3, it has a similar grain size distribution as section 1, with a sandy diamicton layer at the top (Figure 3.9).

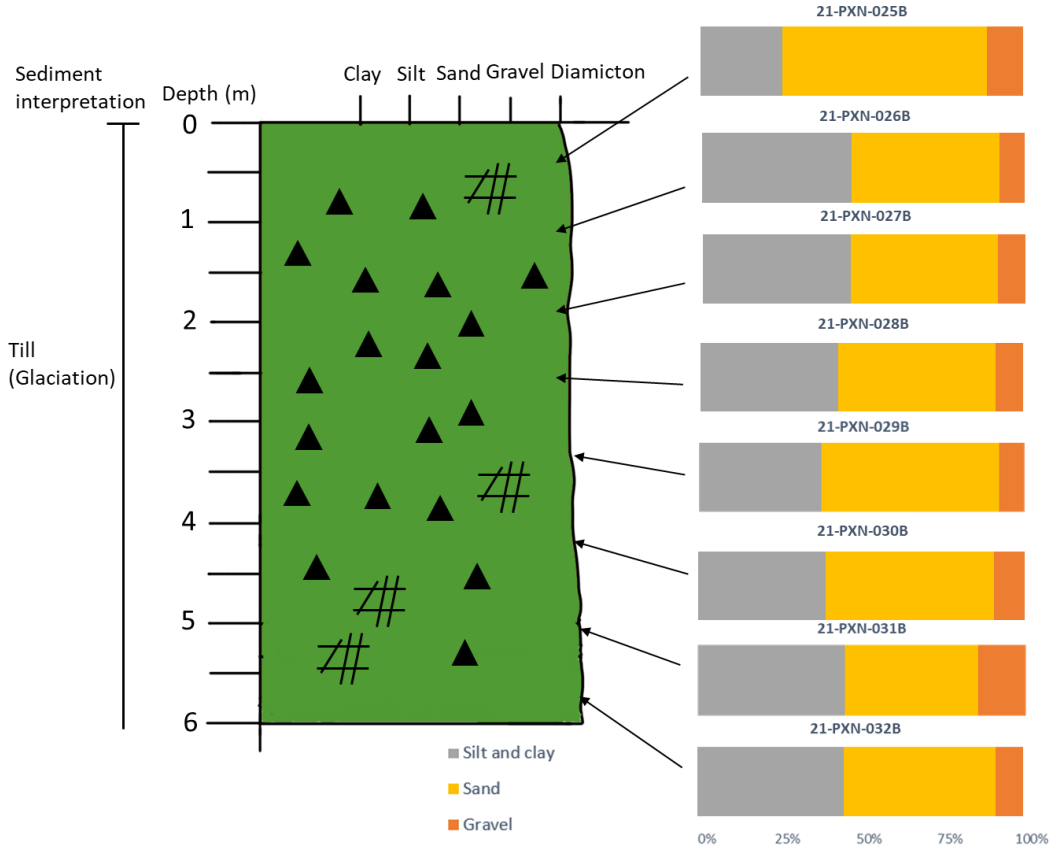


Figure 3.7. Grain size distribution of drumlin section 1.

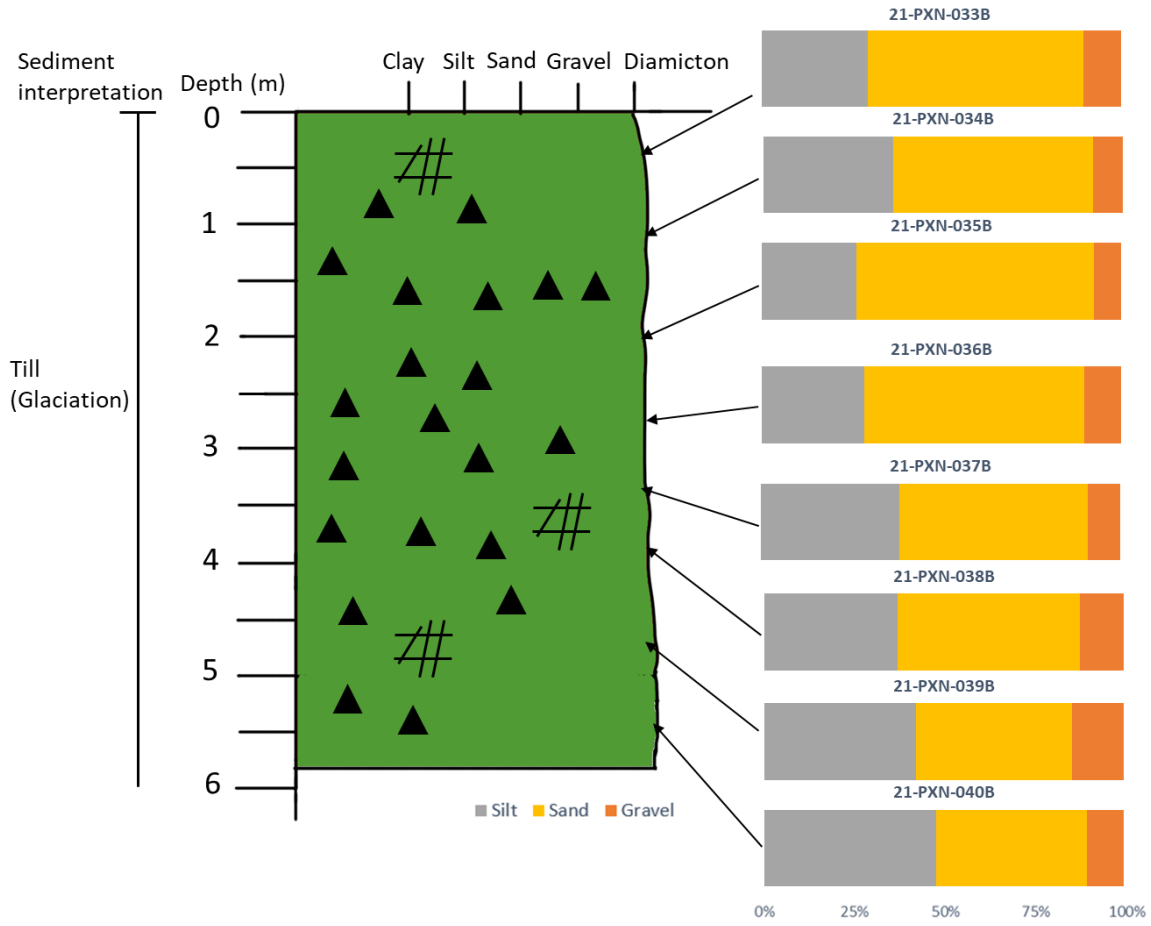


Figure 3.8. Grain size distribution of drumlin section 2.

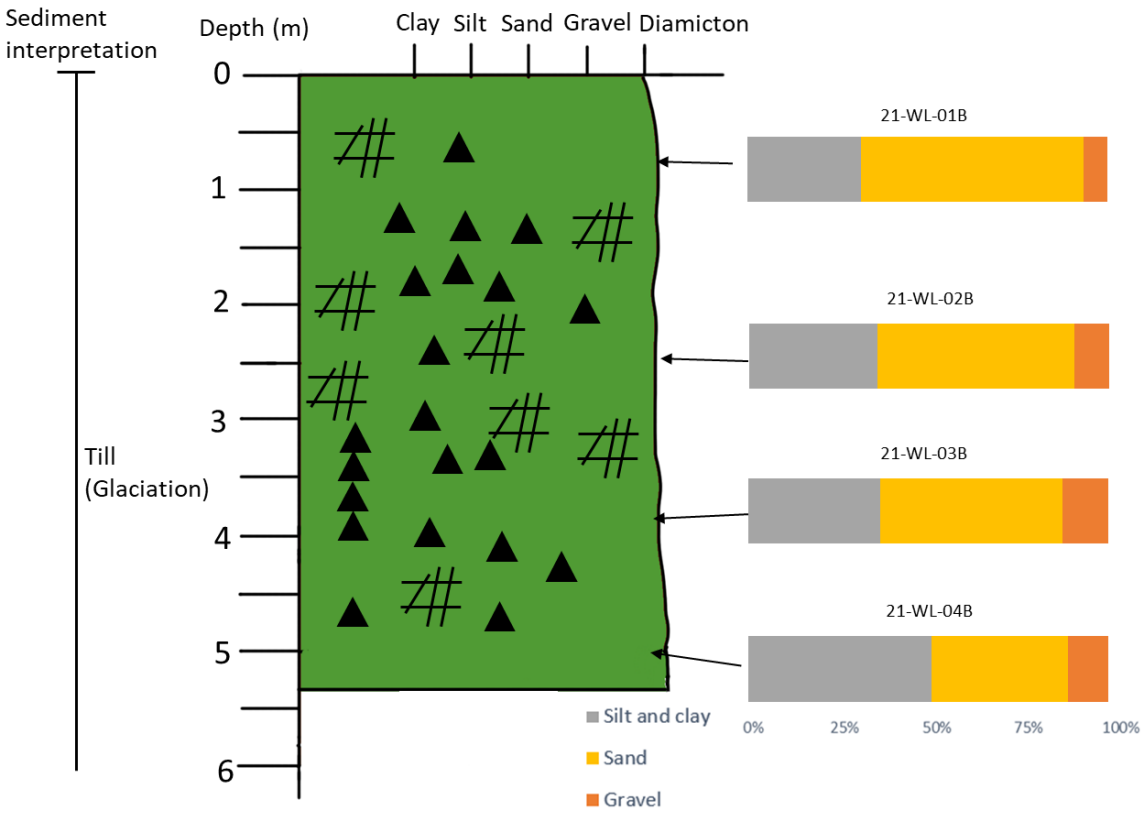


Figure 3.9. Grain size distribution of drumlin section 3.

3.3.1.3 Pebble Counts Results of Drumlin Sections

Figure 3.10 illustrates the disparity in clast lithology percentages among drumlin sections 1 through 3. The findings indicate that the till in section 1 exhibits a higher proportion of Canadian Shield clasts and a correspondingly lower proportion of clasts from WCSB compared to the till observed in the other two drumlin sections. It is noteworthy that section 1 and section 2 originate from the same drumlin, with section 1 situated closer to the middle of the drumlin and section 2 situated closer to the up-ice end of the drumlin. The cumulative percent of different components suggest that in all sections, there are more WCSB clasts than Canadian Shield clasts.

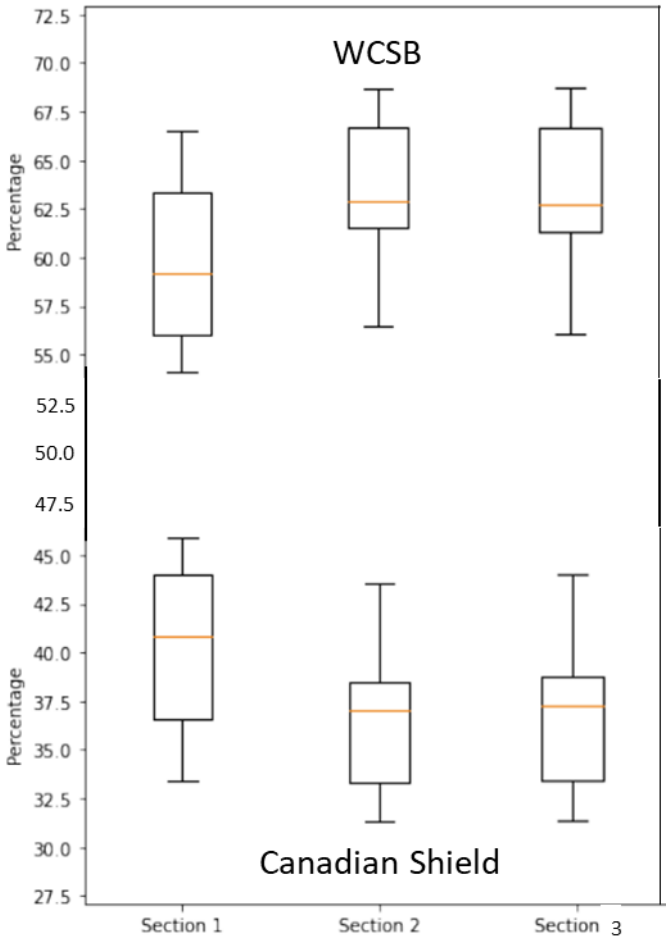


Figure 3.10. A) Distribution of Canadian Shield clasts across the drumlin sections 1 to 3; B) Distribution of WCSB clasts across the same drumlin sections.

Clast lithology counts indicate variations in composition between tills both in terms of spatial distribution and stratigraphy. Within the dataset, three distinct compositional groups were observed. First lithology group is from the pebble count results of drumlin sections, which is characterized by 30% to 45% Canadian Shield component , including felsic, mafic igneous rocks and quartz. Carbonate rocks also occupy 30% to 45% of the clasts. The remaining part is composed of siliciclastic rocks (10% to 15%), red dolostone (4% to 7%) and shale (3% to 13%). Among section 1 to 3, samples in the middle part are richer in Canadian Shield, while samples at the upper till tends to be richer in carbonate rocks (Figure 3.11 & Figure 3.12). Specially, sample 21-WL-04 at the bottom

of section 3 has a greater proportion of brown and beige carbonates and relative lower proportion of dark and grey limestone (Figure 3.13 & sample 21-WL-004 in Appendix C on p. 124).

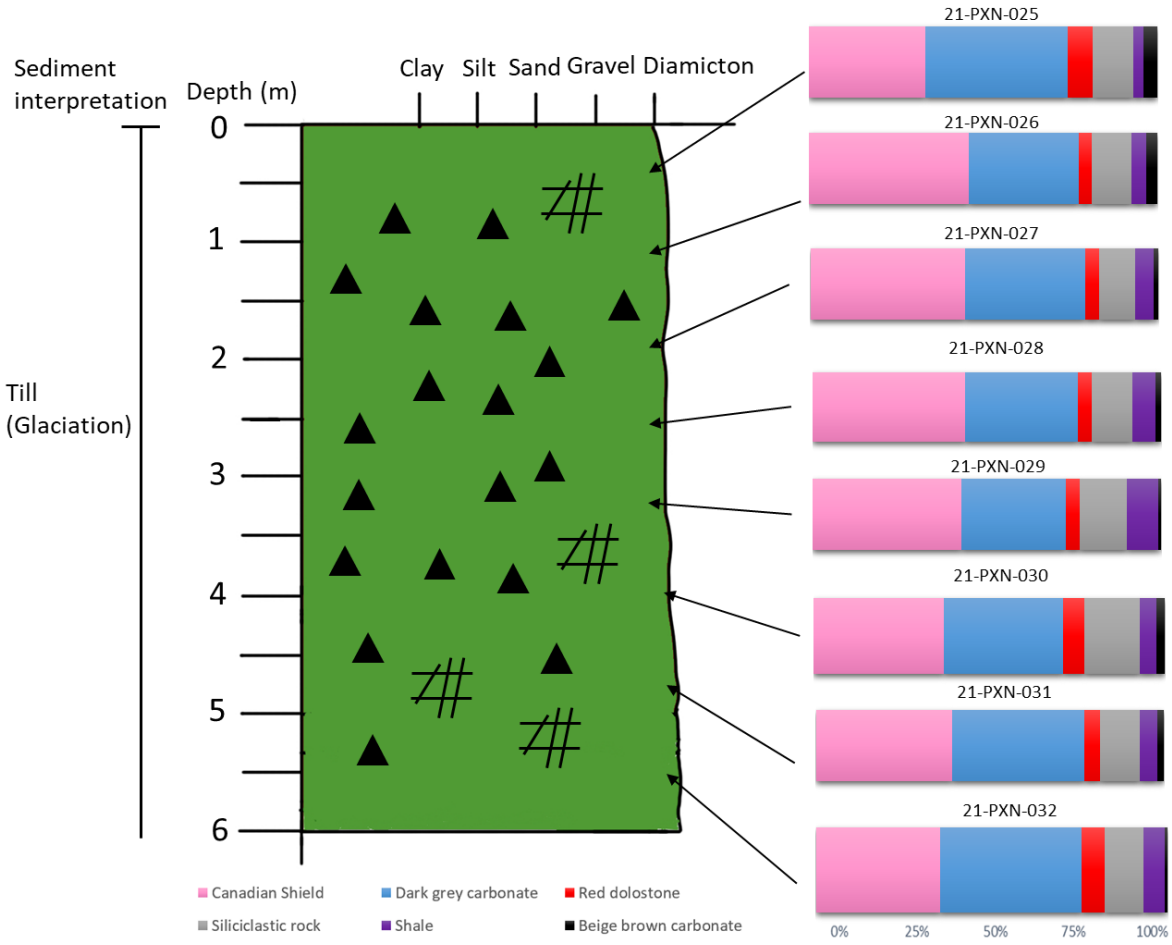


Figure 3.11. Pebble counts results of drumlin section 1.

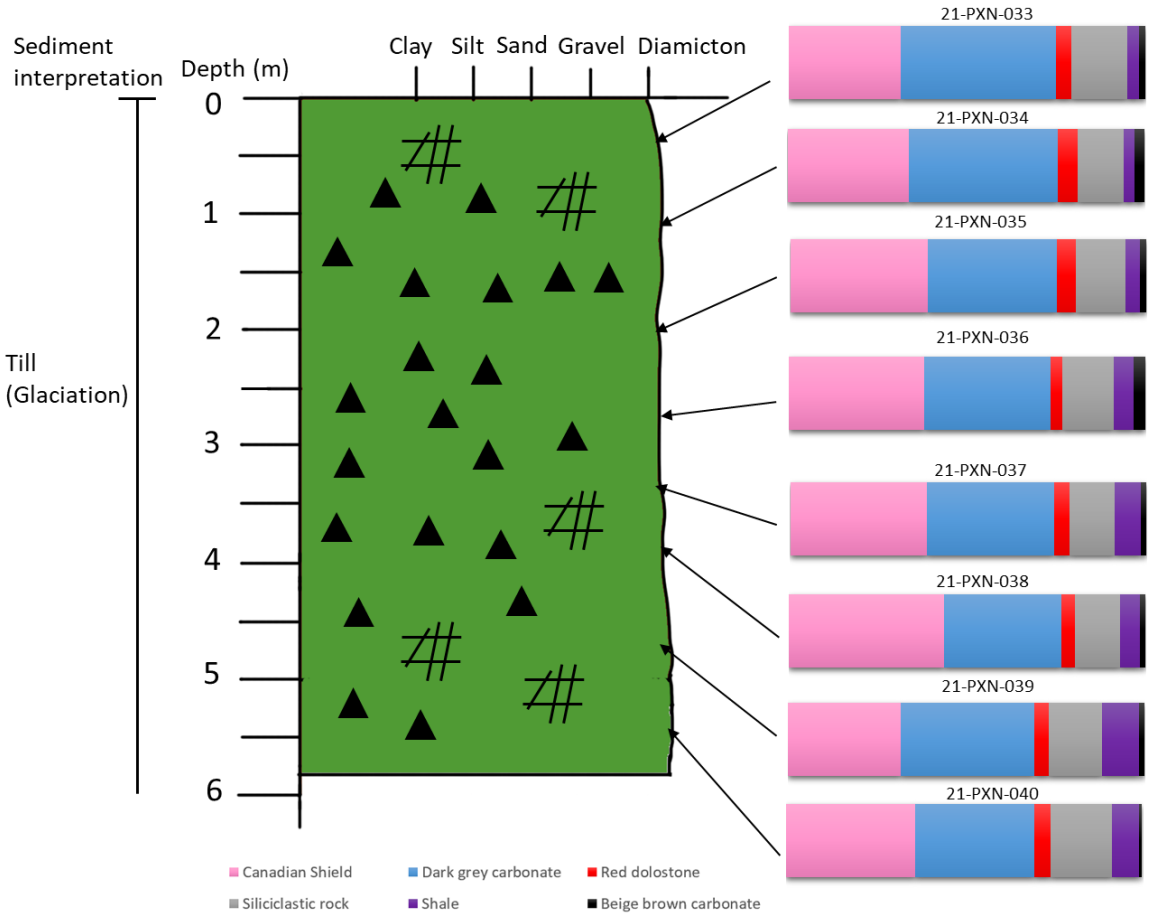


Figure 3.12. Pebble counts results of drumlin section 2.

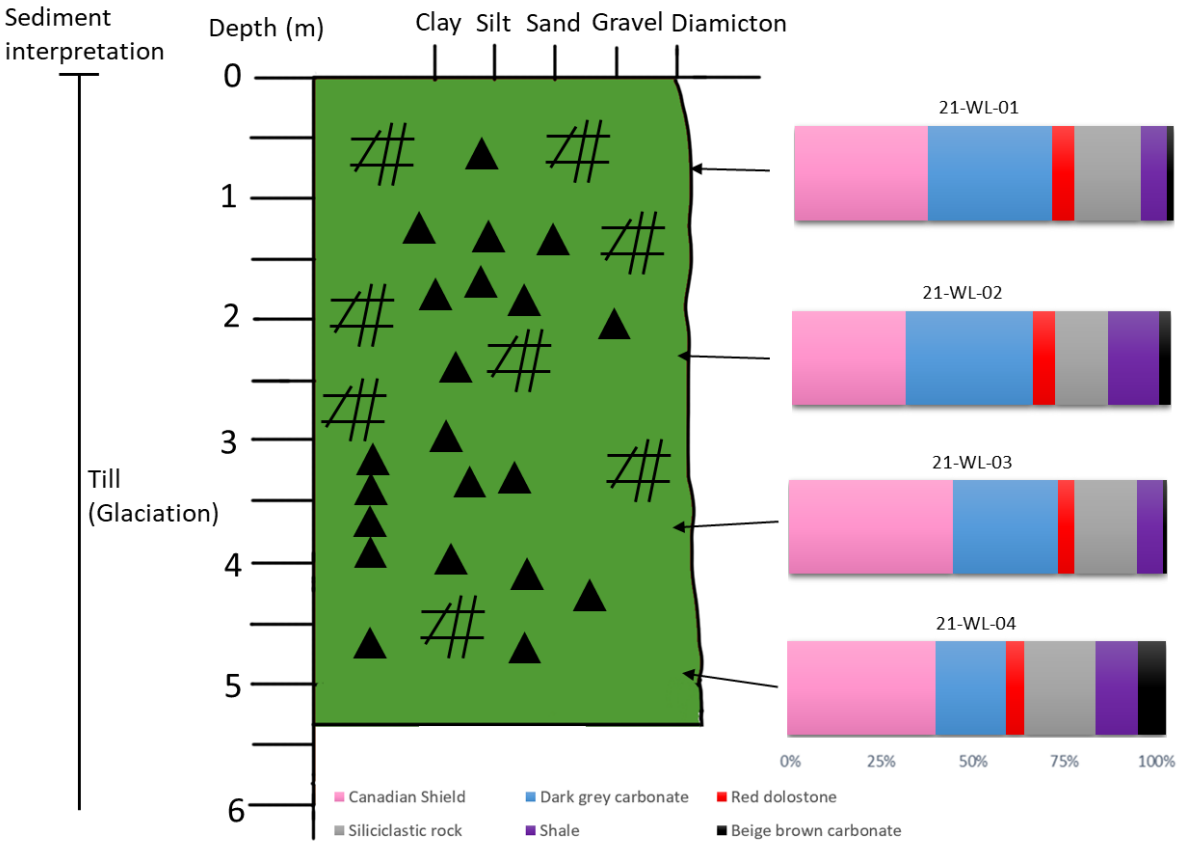


Figure 3.13. Pebble counts results of drumlin section 3.

3.3.2 Results of Surficial Samples

3.3.2.1 Grain Size of the Samples in the Study Area

Figure 3.14 provides an overview of the texture of the samples collected both in 2020 and 2021, which reveals the variability in sediment texture among the samples. The figure indicates that certain samples are predominantly composed of sand-sized particles, while a few samples exhibit a gravelly texture. Furthermore, there are samples that primarily contain silt and clay particles. However, most of the samples exhibit a poorly sorted mixture of grains ranging from mud-sized to gravel-sized particles. These samples are commonly referred to as 'till' in the database, reflecting their unsorted nature and heterogeneous composition. The red points are samples from three drumlin sections, and they are clustered together in a similar silty-sandy range, with very little gravel.

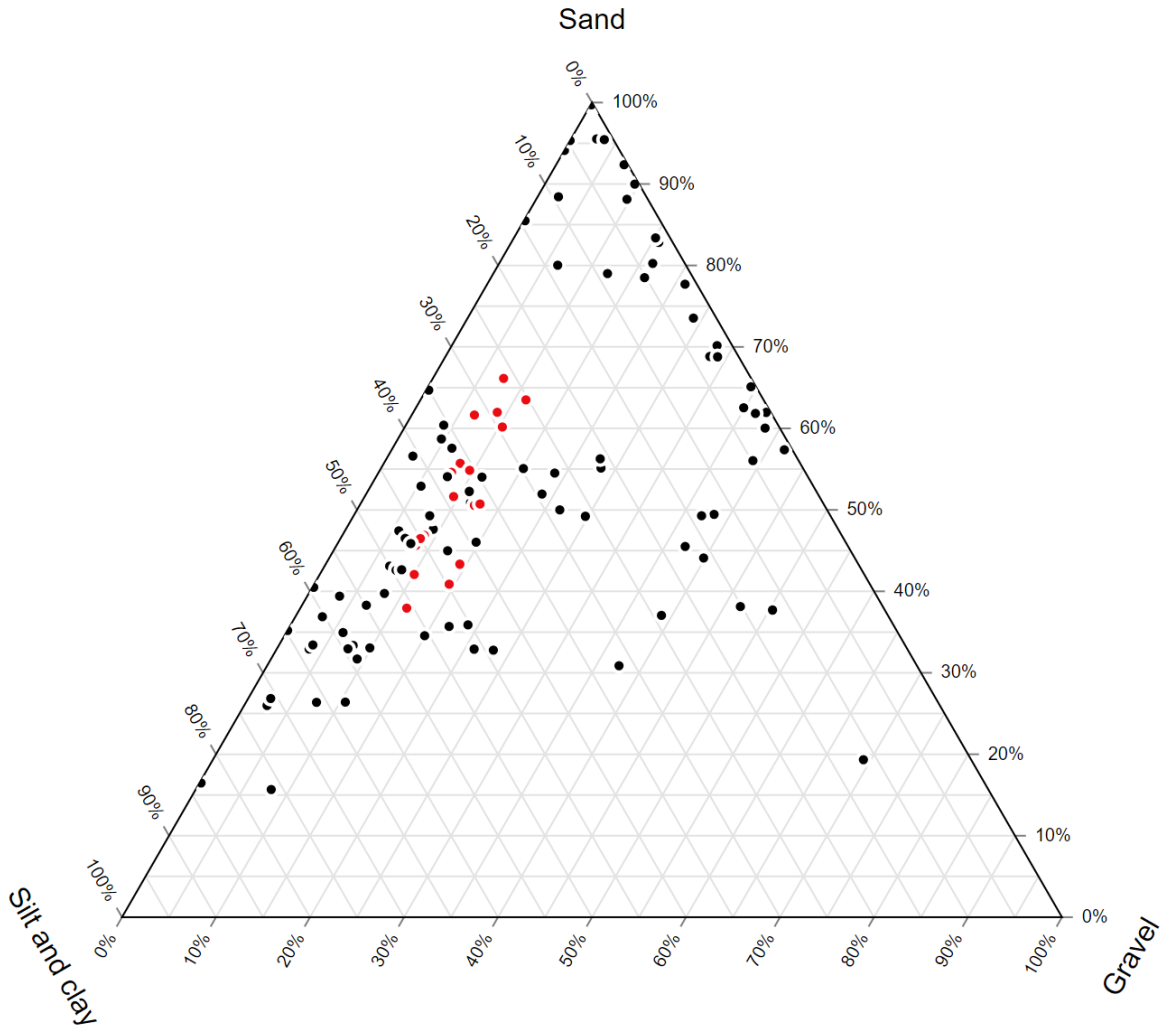


Figure 3.14. General texture of all samples in terms of their proportions of gravel, sand, and mud (silt and clay). Red points are the section samples and black points are the surficial samples.

Figure 3.15 is a map showing the grain size distribution of the samples around the drumlin sections, which are also the samples that have undergone clast lithology counts. The samples closer to the drumlin sections tend to have more fine particles, and some of them like 21-PXN-017A are abundant in silt and clay. In addition, some samples have very few fine particles (silt and clay) and are abundant in sand, which are similar to the samples at the top of drumlin sections. For example, 21-PXN-024A has very few silt and clay.

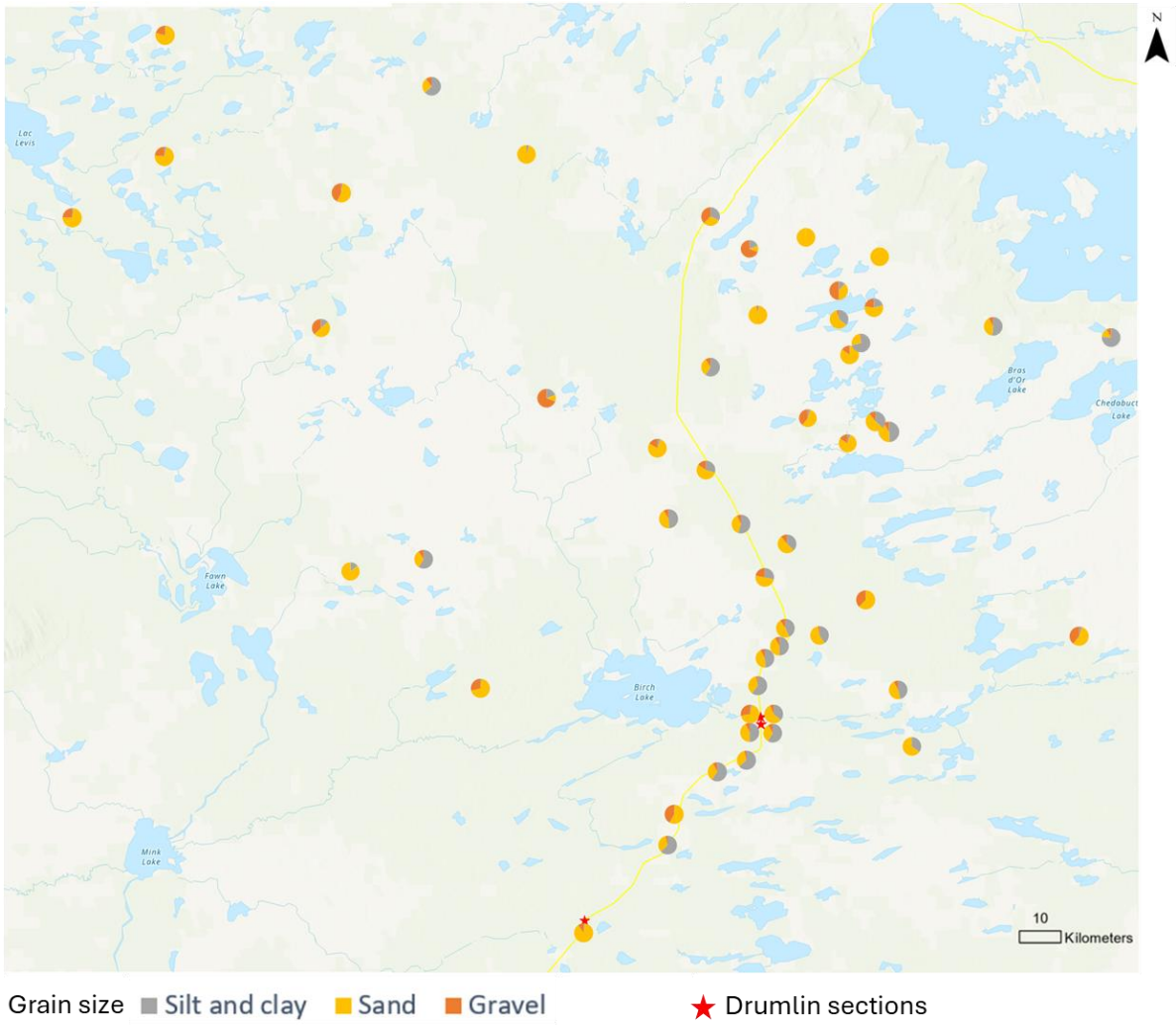


Figure 3.15. Grain size results of the surficial samples.

3.3.2.2 Clast Lithology Counts in the Surficial Till

The map of clast lithology counts shows the location of samples that have been analyzed, and they are irregularly distributed around the drumlin sections. The results suggest that most samples are mainly composed of Canadian Shield (felsic, mafic and quartz), carbonate and siliciclastic rocks (sandstone, siltstone, mudstone). Small amounts of shale, red dolostone and dark siltstone are present in each sample.

Most samples that have been counted for lithology are located over the Keg River Formation, including all samples from the drumlin sections. It mainly consists of bituminous and fossiliferous marlstone, very fine-grained, dark brown and grey limestone. Some pebble counts samples are from Lonely Bay Formation, which is made of brown limestone and thinly bedded beige dolostone. One sample southwest of the study area is from the Muskwa Formation from Horn River Group, which mainly contains bituminous shale.

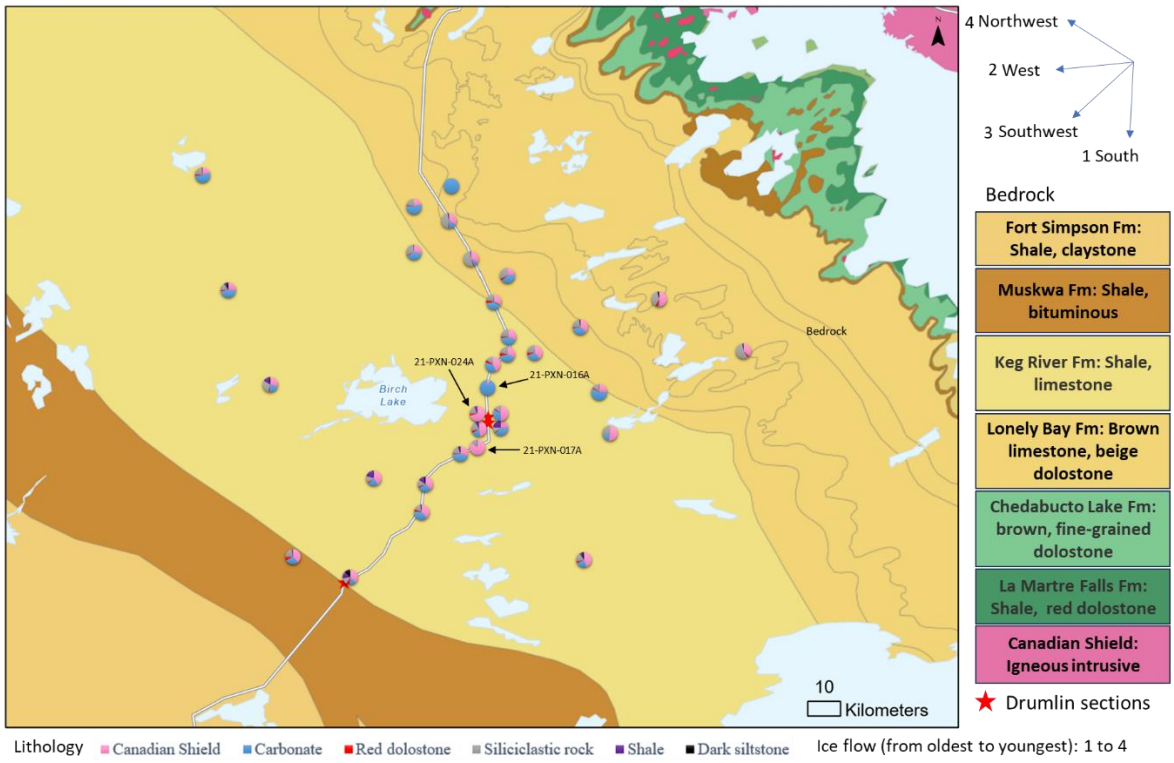


Figure 3.16. Clast lithology counts map of the study area. Ice flows are noted at the top right corner. The relationship between lithology and geological formation are listed in Table 3.2.

Site 21-PXN-024 has an unusual proportion of clast lithologies (Figure 3.16). It contains 70% Canadian Shield, 17% siliciclastic rocks. Notably, there is no carbonate in this sample. The sample was taken on the flat surface from the top of the drumlin, not actually on section 1. Another sample in this area is 21-PXN-017, which has even more Canadian shield (86%) and 11% siliciclastic rocks. Site 21-PXN-016 (Figure 3.16) is characterized by the predominance of carbonate rocks, which account for more than 95% of the composition. The remaining small portion is 5% Canadian Shield.

Shale clasts are absent in this sample. The location of this site is north of section 1 and 2, close to the highway.

3.4 Discussion - Paleo-ice Flow Reconstruction

In this section, the results and evidence are used to reconstruct the paleo-ice flow phases in the study area in relative chronology order starting with the oldest. The implications of the findings on subglacial sediment provenance and drumlin formation and evolution are then discussed.

3.4.1 Southward (180-190 deg.) Ice Flow Phase

The fabric at site 21-WL-004 near the base of drumlin section 3 provides supporting evidence for a southward ice flow to 180-190 degrees (Figure 3.5). Because it is located in a lower stratigraphic position, this depositional evidence for a southward ice flow is correlated to the erosional indicators thus representing altogether one 'oldest' southward ice flow phase.

The till at the base of section 3, with a south-trending clast fabric, contains a greater proportion of brown, beige, buff color carbonates relative to grey carbonates than the other samples (see clast count photos in Appendix C, sample 21-WL-004 is on p. 124). A detailed separation of grey carbonates versus brown limestone and beige dolostones were done with samples from section 1 to section 3, and the results suggest sample 21-WL-004 has the largest proportion of brown and beige carbonates, which would be consistent with the fabric indicative of southward ice flow, or a northern bedrock provenance. Figure 1.6 shows the location of section 3 relative to the bedrock geology. There, we can see that the Lonely Bay Formation extends north-south along Highway 3 just a few kilometers to the north of section 3. The Lonely Bay Formation is dominated by brown limestone and beige dolostones (Okulitch, 2006), and the formation also occurs to the northeast and east, but the bedrock beds extend more perpendicular relative to the younger ice flow phases to the west and southwest (discussed below). It is therefore hypothesized that the longer north-south extent of the formation north of section 3 would have been more favorably eroded and incorporated into the till during the southward ice flow phase.

3.4.2 Westward (260-270 deg.) Ice Flow Phase

The stratigraphic sections offer valuable insights into westward ice flow movement within the study area. One clast fabric measured at the top of section 2 (21-PXN-033) distinctly indicates a westward ice flow direction at 260 degrees (Figure 3.4). This result is challenging to explain given the upper stratigraphic position of the fabric and the southwest orientation of the drumlin. All the other fabrics completed in that drumlin (sections 1 and 2) are all indicative of southwest ice flow. One possibility is that the up-ice end of the drumlin (section 2) contains a different till sequence than further into the middle of the drumlin such as at section 1. The other possibility is that the top fabric at section 2 was affected by a local shearing process at the up-ice end of the drumlin that deviated the clasts from the general southwest direction making it unsuitable for paleo-ice flow. Shallow clast fabrics around drumlins have shown patterns consistent with the shape of the landform, i.e., divergent at the stoss end, parallel in the middle (Schomacker et al., 2006), and convergent at the lee end of the landform (Krüger & Thomsen, 1984). This perhaps is the simplest and most likely explanation in this case for a shallow till clast fabric that is oblique to the drumlin long axis.

3.4.3 Southwest (215-245 deg.) Ice Flow Phase

The stratigraphic sections offer corroborative evidence that the southwestward flow movement produced a few meters of till in the study area. For example, three till fabric in drumlin section 1, the fabric in the middle of section 2 (21-PXN-035) and the fabric at the top of section 3 (21-WL-001) all suggest a southwestward ice flow from 215 to 245 degrees (Figure 3.4 & Figure 3.5). It means that the southwest ice flow phase is the dominant ice flow in the study area.

The results of clast lithology counts also suggest a northwestern bedrock source. 30% to 45 % percent of clasts in drumlin sections are Canadian shield clasts, which are from the northeastern bedrock sources. Additionally, the source of red dolostone is La Matre Falls formation, and the source of dark grey carbonate is Chedabucto Lake formation. They are both geological formations northeast of the study area.

The southwestern ice flow phase also played a crucial role in shaping the landscape and influencing dispersal of indicator minerals at the Pine Point Mississippi Valley-type (MVT) Pb-Zn deposit (McClenaghan et al., 2018; Rice et al., 2019).

3.4.4 Northwest (320 to 325 deg.) Ice Flow Phase

As the ice sheet thinning progressed during deglaciation with the ice margin retreating towards the east, the channeling effects of the Mackenzie River Valley and other surrounding topographic low areas became increasingly important (Lemmen et al., 1994). The channeling effect persisted, causing the flow to rotate further clockwise toward the northwest, especially near what is now the western shore of GSL. This northwestward direction represents the last phase of ice flow for a portion of the study area. This phase involved a distinct flow characterized by relatively thin ice, leading to limited erosion and sediment transport, particularly outside the confines of the Mackenzie River Valley (Lemmen et al., 1994). Within the study area, clear evidence of this phase is apparent only in the erosional features at Site 1, but there is more abundant evidence for a late-stage northwest flow just south of the study area (Hagedorn 2022).

The absence of till clast fabrics in the northwest direction is noteworthy, as it implies that the rotation of ice flow toward the northwest did not play a substantial role in sediment transport in the study area. This lack of evidence suggests that the prevailing forces influencing till formation were not primarily oriented in the northwest direction.

3.4.5 Integrated Evidence for Ice Flow History

The study provides key information about ice flow history, with evidence for four different ice flow phases. The evidence for the oldest south ice flow phase (1) is preserved at two outcrop sites, as well as in the fabric at the bottom of section 3 (Figure 3.17). The till at the base of section 3 also contains the highest proportion of clasts thought to be derived from the Lonely Bay Formation, which is consistent with a southward ice flow direction (i.e., northward provenance). Evidence for the westward ice flow phase (2) is preserved at the outcrop site along the shore of GSL, and in the E-W oriented drumlins (Figure 3.17). The southwest ice flow phase (3) is dominant in the study area, and the evidence includes striations at two outcrop sites, extensive southwesterly oriented drumlins and till clast fabrics (Figure 3.17). The counterclockwise shift from west to southwest is supported by the overprint relationship of southwesterly oriented drumlins on westerly oriented drumlins around the drumlin sections. Finally, there is evidence at the outcrop site along the shore of western GSL for a late northwestward flow phase (4) (Figure 3.17). Hagedorn (2022) also documented this northwest ice flow phase.

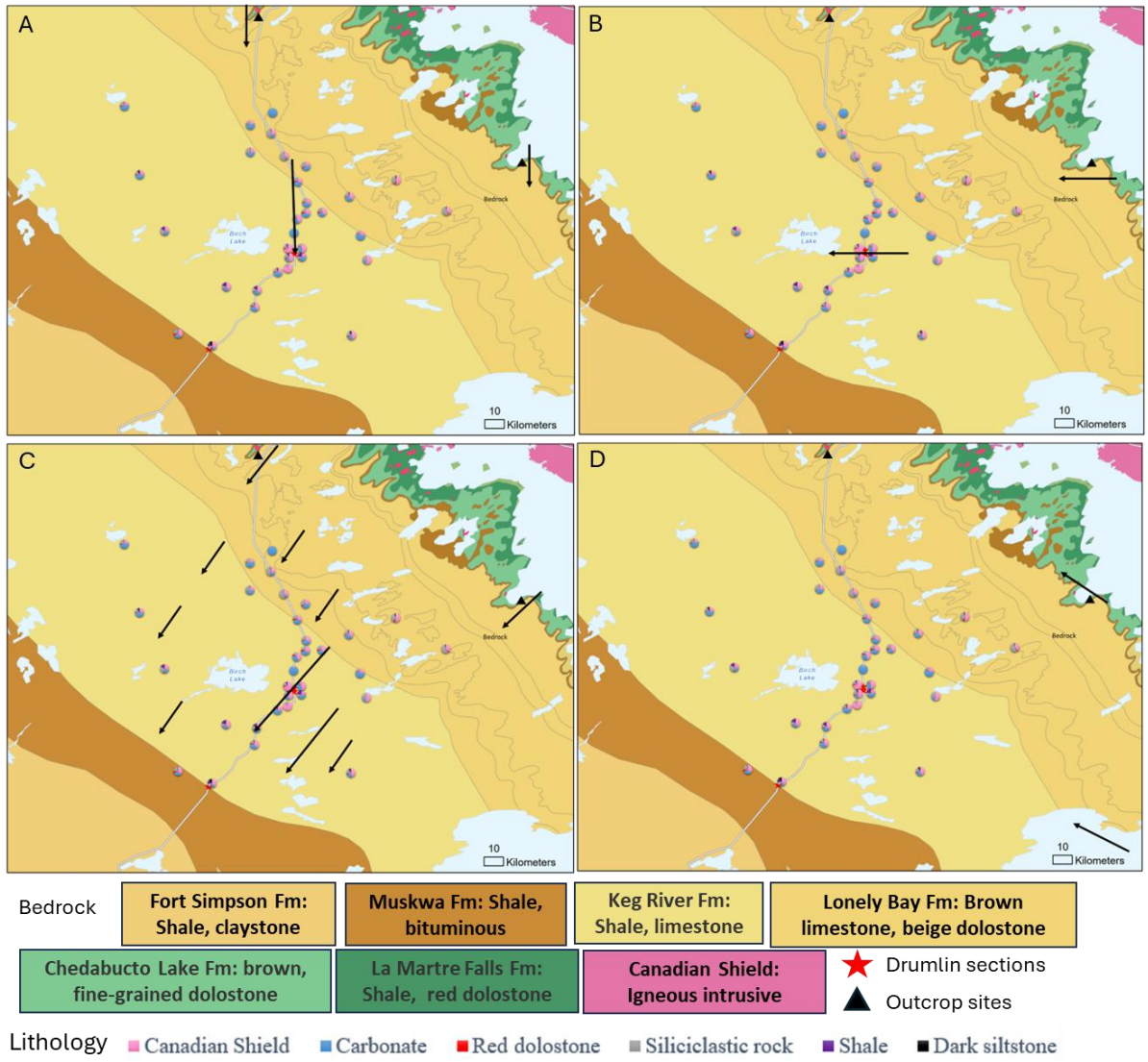


Figure 3.17. Summary of ice flows and till stratigraphy in the study area. A) Oldest south ice flow. B) Second oldest west ice flow. C) Second youngest southwest ice flow. D) Youngest northwest ice flow.

3.5 Conclusion

Four distinct ice-flow phases of the LIS are evident in the study area of western GSL. These phases are preserved in the outcrop-scale erosional record, in the form of subglacial streamlined landforms, and are also recorded in the depositional record, specifically in the till stratigraphic record

within accessible drumlins. The sequence of ice flows suggests 1) an initial south (180 to 190 deg.) flow phase, succeeded by a clockwise shift to 2) westward (260 to 270 deg.) flow, and subsequently to 3) a slight shift to southwestward (215 to 245 deg.). Finally, there is 4) a late northwestward (320 to 325 deg.) flow. The evidence for both the westward and the northwestward flows are limited and could thus have been spatially restricted flow phases not recorded everywhere in the study area. The southwestward ice flow phase is the most dominant of all in the different records investigated in this study.

The drumlin section type in the study is a mainly-till drumlin (Stokes et al., 2013). Grain size analysis suggests that the grains in drumlins are not well-sorted, with a mixture of particles like silt, clay, sand and gravel. The sediments are called as till because of their varied and heterogeneous composition. The till drumlin has an irregular surface and lacks distinct layers. This is because the sediments that make up these features have been subjected to intense deformation and mixing as a result of the glacier's traction and erosive forces. Therefore, the sediment can be called as subglacial traction till.

Chapter 4 Conclusion

4.1 Thesis Contribution

The research investigated the subglacial landform and sedimentary records of the last glaciation in a drumlin field located west of GSL, Northwest Territories. This area offers a great opportunity to study tills and associated sedimentary processes within a drumlin field. The presence of road cuts across several drumlins along Highway 3 provides access to these features, which are part of a drumlin field referred to as the Dessert Lake drumlin field. This region was covered by the LIS during the last glaciation (Dalton et al., 2020). While the general understanding of the glacial history has been established, several uncertainties and knowledge gaps were also identified prior to this research.

The nature and provenance of sediment within the drumlins were unknown and this has implications for the regional glacial history and source of indicator minerals (for mineral exploration). Studying the till from drumlin sections was an opportunity to contribute to drumlin research. Are drumlins in the study area mostly made up of till? Are they stratified? Was the till deposited during the same southwestward flow phase as the one that created the drumlin field or is there evidence for multiple ice flow phases and a longer glacial history in the till record? Are the ice flow phases similar to the ones documented further south by Hagedorn (2022) or there is a different record in the study area?

The research can answer the questions above. The drumlins in the study area are made up mostly of till. Variations in till fabric and composition were identified, but no major stratification was recognized. Based on these variations, the till is interpreted to have been deposited during at least three different ice flow phases, including an older south ice flow phase, an intermediate west ice flow phase and a final southwest flow phase. Hagedorn (2022) documented a clockwise ice flow shift from southwest to west, and finally to northwest just south of the study area in this research. The south ice flow phase is only documented in this study. Both studies documented a west ice flow phase, a southwest ice flow phase and a northwest ice flow phase, but their relative chronology differs somewhat. Instead of a single continuous clockwise shift, this research shows evidence for a counterclockwise shift from west to southwest. The difference in ice flow history can be due to a fragmentary record whereby the glacial history is not fully preserved in any of the study areas leading to incorrect correlations. For instance, it is possible that the evidence of westward ice flow in both

study areas is not from the same ice flow phase, which could explain the discrepancy in their relative chronology with the southwest phase.

Evidence for ice flow shifts have been presented from the erosional outcrop-scale record, the subglacial landform record, as well as from the till stratigraphy record from within the drumlins. The oldest ice flow phase was to the south and south-southwest. This southward ice flow phase is documented in the area for the first time. This phase was followed by a clockwise shift. There is limited evidence for westward ice flow phase, which could have been spatially confined to some areas. The best evidence for it is a series of E-W landforms east of Birch Lake that are overprinted by younger southwest drumlins. The drumlins indicate widespread southwestward flow. Till fabrics provide evidence that the southwest flow phase was not just erosional. A proportion of the till within the drumlins contain evidence for deposition during the southwest flow phase. This may have important implications for our understanding of the origin and formation of drumlins. It shows that drumlins are not just erosional, but also result from complex erosional and depositional process interactions (e.g., Stokes et al., 2013). Erosion helps to create a rough bedrock surface and transport sediment, while deposition builds up the drumlin cores and flanks. The specific balance of these processes can vary depending on factors such as ice thickness, velocity, and basal conditions.

Lemmen (1990) suggested that till composition reflected the lithology of the underlying bedrock geology. In this study, evidence has been presented for a more complex depositional record. While some of the surficial till samples show a dominantly local provenance, like shale and limestone from Keg River Formation, there is surficial till with a more distal signature such as more abundant Canadian Shield derived clasts. In addition, there is evidence for more than one till sheet. Most notably is the occurrence of the lower till at section 3 that has a characteristic pebble composition with abundant brown carbonates. This composition is consistent with the lower fabric indicating southward flow because the Lonely Bay Formation extends to the north more than in the other directions and it is characteristically composed of brown limestone and beige dolostones. There is evidence from the pebble lithology counts for till compositional variability across the surface. Finally, the grain size analyses provided evidence for variable textures, most likely due to surface winnowing by glacial lake processes during deglaciation. Glacial lakes can trap sediment transported by rivers and glaciers, leading to sedimentation within the lake and potentially affecting its depth and volume over time. In the context of till analysis across a subglacial bed that has been inundated by a glacial lake with evolving lake levels and shoreline positions, it is critical to get grain size data to get insights

into the degree of reworking of the surficial till as this has implications for the interpretation of the till and of its compositional signature.

4.2 Potential Implications of This Research and Recommendation for Future Research

Mineral exploration frequently uses glacial sediments to trace indicator minerals and geochemical pathfinder elements back to their concealed bedrock sources (McClenaghan & Paulen, 2018). Subglacial till is routinely sampled at the surface in mineral exploration to trace indicator minerals back to a buried bedrock source up regional ice flow. In drumlin fields, however, till is sometimes several meters thick, and some of it may be unrelated to the ice flow phase that created the drumlins. In addition, erosional processes play a role in the formation of drumlins. As a result, till from different stratigraphic positions could be exposed at the surface, thus complicating the provenance analysis of surficial till. Overall, the till in the study area appears to be stratified and the erosional processes related to drumlin formation may have exposed more than one till sheet, possibly with contrasting provenance, across the surface as well as at depth within the drumlin cores.

The research results tell a more complex glacial history than the single ice flow direction of the drumlins. In this context, it is likely that surficial till samples in the Dessert Lake drumlin field, and perhaps in other similar settings, will include till with different glacial transport pathways and bedrock source regions. It is thus critical for applications like mineral exploration to determine if the till in lower stratigraphic positions occurs at the surface of the drumlin field.

Another implication of this research is that the south ice flow implies an ice divide north of GSL. suggesting an early ice dome or divide position that does not correspond to the static central position of the Keewatin dome usually depicted in ice sheet reconstructions of the LGM and early deglaciation (e.g., Margold et al., 2018). However, other researchers have presented reconstructions involving a more mobile Keewatin dome (e.g. McMartin & Henderson, 2004; Hodder et al., 2016). Notably, previous work in the Lac de Gras region (Kelley et al., 2019) has revealed an old southwest flow phase, although there are no specific time constraints associated with this flow phase other than it being the oldest recorded, it could fit within the broader context of the mobile Keewatin ice divide hypothesis and ice divide position located somewhere north or northeast of GSL. Furthermore,

attempts at reconstructing pre-LGM ice sheet configuration also involves important changes in the growth and position of the Keewatin dome (e.g., Stokes et al., 2012; Dalton et al., 2022), but large uncertainties remain. Although research presented herein is consistent with that general idea of a mobile Keewatin dome and large scale ice sheet reconfigurations throughout the last glaciation, more research is needed to determine the positions of ice divides and timing of ice sheet configuration changes in the northwestern sector of the LIS and elsewhere.

The research presented in this thesis used multiple lines of evidence to reconstruct the glacial dynamics of the study area. Despite using a multi-faceted approach, several aspects were left out of the scope of the research and could be addressed in future work. The finest fraction of the till could be further analyzed using laser diffractometry, for example. Knowing the silt-to-clay ratio could be useful to refine the interpretation of the till, but also to better analyze and interpret the matrix composition. Data about indicator minerals and till matrix geochemistry were available, but they were not analyzed as part of this thesis. It would be useful in future work to analysis these other datasets in details as they could complement the clast lithology work of this thesis and add to the body of research on glacial dynamics and till provenance in the region.

References

Allmendinger, R. W., Cardozo, N., & Fisher, D. M. (2011). *Structural Geology Algorithms: Vectors & Tensors* (1st ed.). Cambridge University Press.

Anderton. (1985). Clastic facies models and facies analysis. *Geological Society Special Publication, 18*(1), 31–47. https://doi.org/10.1144/GSL.SP.1985.018.01.03

Bednarski, J. M. (2008). Landform assemblages produced by the Laurentide ice sheet in northeastern British Columbia and adjacent Northwest Territories; constraints on glacial lakes and patterns of ice retreat. *Canadian Journal of Earth Sciences, 45*(5), 593–610. https://doi.org/10.1139/E07-053

Benediktsson, Í. Ö., Jónsson, S. A., Schomacker, A., Johnson, M. D., Ingólfsson, Ó., Zoet, L., Iverson, N. R., & Stötter, J. (2016). Progressive formation of modern drumlins at Múlajökull, Iceland: stratigraphical and morphological evidence. *Boreas*, *45*(4), 567–583. https://doi.org/10.1111/bor.12195

Benn, D. (1994). Fabric shape and the interpretation of sedimentary fabric data. *Journal of Sedimentary Research, 64*(4a), 910–915. https://doi.org/10.1306/D4267F05-2B26-11D7-8648000102C1865D

Benn, D. I. (2004). Macrofabric. In D. J. Evans & D. I. Benn (Eds.), *A practical guide to the study of glacial sediments*. Hodder Education.

Benn, D. I., & Evans, D. J. A. (2010). *Glaciers and glaciations*. Hodder Arnold Publication.

Benn, D. I. (2013). GLACIAL LANDFORMS, SEDIMENTS | Till fabric analysis. In S. A. Elias & C. J. Mock (Eds.), *Encyclopedia of Quaternary Science* (2nd ed., pp. 76–80). Elsevier. https://doi.org/10.1016/B978-0-444-53643-3.00087-X

Bingham, R. G., Siegert, M. J., Young, D. A., & Blankenship, D. D. (2007). Organized flow from the South Pole to the Filchner-Ronne ice shelf: An assessment of balance velocities in interior East Antarctica using radio echo sounding data. *Journal of Geophysical Research: Earth Surface, 112*(F3). https://doi.org/10.1029/2006JF000556

Boggs, S. (2006). *Principles of sedimentology and stratigraphy* (4th ed.). Pearson Prentice Hall.

Carr, S. J., & Rose, J. (2003). Till fabric patterns and significance: Particle response to subglacial stress. *Quaternary Science Reviews*, *22*(14), 1415–1426. https://doi.org/10.1016/S0277-3791(03)00125-2

Clark, C. D. (1993). Mega-scale glacial lineations and cross-cutting ice-flow landforms. *Earth Surface Processes and Landforms*, *18*(1), 1–29. https://doi.org/10.1002/esp.3290180102

Clark, C. D., Knight, J. K., & T. Gray, J. (2000). Geomorphological reconstruction of the Labrador Sector of the Laurentide Ice Sheet. *Quaternary Science Reviews*, *19*(13), 1343–1366. https://doi.org/10.1016/S0277-3791(99)00098-0

Clark, C. D., Hughes, A. L. C., Greenwood, S. L., Spagnolo, M., & Ng, F. S. L. (2009). Size and shape characteristics of drumlins, derived from a large sample, and associated scaling laws. *Quaternary Science Reviews*, *28*(7), 677–692. https://doi.org/10.1016/j.quascirev.2008.08.035

Clark, C. D., Ely, J. C., Spagnolo, M., Hahn, U., Hughes, A. L. C., & Stokes, C. R. (2018). Spatial organization of drumlins. *Earth Surface Processes and Landforms*, *43*(2), 499–513. https://doi.org/10.1002/esp.4192

Craig, B. G. (1965). *Glacial Lake Mcconnell, and the Surficial Geology of Parts of Slave River and Redstone River Map-Areas, District of Mackenzie.*

Dalton, A. S., Margold, M., Stokes, C. R., Tarasov, L., Dyke, A. S., Adams, R. S., Allard, S., Arends, H. E., Atkinson, N., Attig, J. W., Barnett, P. J., Barnett, R. L., Batterson, M., Bernatchez, P., Borns, H. W., Breckenridge, A., Briner, J. P., Brouard, E., Campbell, J. E., … Wright, H. E. (2020). An updated radiocarbon-based ice margin chronology for the last deglaciation of the North American Ice Sheet Complex. *Quaternary Science Reviews*, *234*, 106223-. https://doi.org/10.1016/j.quascirev.2020.106223

Dalton, A. S., Stokes, C. R., & Batchelor, C. L. (2022). Evolution of the Laurentide and Innuitian ice sheets prior to the Last Glacial Maximum (115 ka to 25 ka). *Earth-Science Reviews*, *224*, 103875-. https://doi.org/10.1016/j.earscirev.2021.103875

Das, G.K. (2016). Sediment Grain Size. In: Kennish, M.J. (eds) *Encyclopedia of Estuaries*. Encyclopedia of Earth Sciences Series. Springer, Dordrecht. https://doi.org/10.1007/978-94-017-8801-4_148

Dunlop, P., & Clark, C. D. (2006). The morphological characteristics of ribbed moraine. *Quaternary Science Reviews, 25*(13), 1668–1691. https://doi.org/10.1016/j.quascirev.2006.01.002

Dulfer, H. E., Stoker, B. J., Margold, M., & Stokes, C. R. (2023). Glacial geomorphology of the northwest Laurentide Ice Sheet on the northern Interior Plains and western Canadian Shield, Canada. *Journal of Maps, 19*(1), 2181714. https://doi.org/10.1080/17445647.2023.2181714

Dyke, A. S., & Prest, V. K. (1987). Late Wisconsinan and Holocene history of the Laurentide Ice Sheet. *Géographie Physique et Quaternaire, 41*(2), 237–263. https://doi.org/10.7202/032681ar

Dyke, A. S., Andrews, J. T., Clark, P. U., England, J. H., Miller, G. H., Shaw, J., & Veillette, J. J. (2002). The Laurentide and Innuitian ice sheets during the Last Glacial Maximum. *Quaternary Science Reviews*, *21*(1), 9–31. https://doi.org/10.1016/S0277-3791(01)00095-6

Dyke, A. S., Moore, A. J. & Robertson, L. (2003). Deglaciation of North America. *Geological Survey of Canada, Open File*, 1574. https://doi.org/10.4095/214399

Ely, J. C., Clark, C. D., Spagnolo, M., Stokes, C. R., Greenwood, S. L., Hughes, A. L. C., Dunlop, P., & Hess, D. (2016). Do subglacial bedforms comprise a size and shape continuum? *Geomorphology*, *257*, 108–119. https://doi.org/10.1016/j.geomorph.2016.01.001

Evans, D. J. A., and Benn, D.I. 2004. Facies description and the logging of sedimentary exposures. In *A Practical Guide to the Study of Glacial Sediments*. Edited by D.J.A. Evans and D.I. Benn. Hodder Education, London, Eng. pp. 11–52

Evans, D. J. A., Phillips, E. R., Hiemstra, J. F., & Auton, C. A. (2006). Subglacial till: Formation, sedimentary characteristics and classification. *Earth-Science Reviews*, *78*(1), 115–176. https://doi.org/10.1016/j.earscirev.2006.04.001

Evans, D. J. A., Roberts, D. H., & Cofaigh, C. Ó. (2015). Drumlin sedimentology in a hard-bed, lowland setting, Connemara, western Ireland: Implications for subglacial bedform generation in areas of sparse till cover. *Journal of Quaternary Science*, 30(6), 537–557. https://doi.org/10.1002/jqs.2801

Eyles, N., Putkinen, N., Sookhan, S., & Arbelaez-Moreno, L. (2016). Erosional origin of drumlins and megaridges. *Sedimentary Geology*, *338*, 2–23. https://doi.org/10.1016/j.sedgeo.2016.01.006

Gauthier, M. S., Hodder, T. J., Ross, M., Kelley, S. E., Rochester, A., & McCausland, P. (2019). The subglacial mosaic of the Laurentide Ice Sheet; a study of the interior region of southwestern Hudson Bay. *Quaternary Science Reviews*, *214*(Complete), 1–27. https://doi.org/10.1016/j.quascirev.2019.04.015

Geological Survey of Canada (2016). Surficial geology, Buffalo Lake, Northwest Territories, NTS 85-B. 2, Prelim., Surficial Data Model V.2.0 Conversion, *Geological Survey of Canada, Canadian Geoscience Map*, 220. https://doi.org/10.4095/298705

Geological Survey of Canada (2019). Reconnaissance surficial geology, Mills Lake, Northwest Territories, NTS 85-E. surficial data model v.2.3.14 conversion, *Geological Survey of Canada, Canadian Geoscience Map*, 373. https://doi.org/10.4095/311291

Geological Survey of Canada (2022). Surficial geology, Kakisa River, Northwest Territories, NTS 85-D. Surficial Data Model v.2.3.14 conversion, *Geological Survey of Canada, Canadian Geoscience Map*, 372. https://doi.org/10.4095/308493

Hagedorn. (2022). Paleo-Ice Sheet and Deglacial History of the Southwestern Great Slave Lake Area. University of Waterloo.

Hallet, B. (1996). Glacial quarrying: A simple theoretical model. *Annals of Glaciology*, *22*, 1–8. https://doi.org/10.3189/1996AoG22-1-1-8

Harrison, J. C., St-Onge, M. R., Petrov, O. V., Strelnikov, S. I., Lopatin, B. G., Wilson, F. H., Tella, S., Paul, D., Lynds, T. L., Shokalsky, S. P., Hults, C. K., Bergman, S., Jepsen, H. F. & Solli, A. (2011). Geological map of the Arctic. *Geological Survey of Canada, "A" Series Map*, 2159A. https://doi.org/10.4095/287868

Hicock, S. R., Goff, J. R., Lian, O. B., & Little, E. C. (1996). On the interpretation of subglacial till fabric. *Journal of Sedimentary Research, 66*(5), 928–934. https://doi.org/10.1306/D4268441-2B26-11D7-8648000102C1865D

Hodder, T. J., Ross, M., & Menzies, J. (2016). Sedimentary record of ice divide migration and ice streams in the Keewatin core region of the Laurentide Ice Sheet. *Sedimentary Geology*, *338*, 97–114. https://doi.org/10.1016/j.sedgeo.2016.01.001

Hodder, T. J., Gauthier, M., Ross, M., Kelley, S. E., Lian, O. B., Dalton, A., & Finkelstein, S. (2024). Unravelling the fragmented sediment-landform assemblage in an area of thick Quaternary

sediment, western Hudson Bay Lowland, Canada. *Canadian Journal of Earth Sciences*. https://doi.org/10.1139/cjes-2024-0018

Iverson, N. R. (2012). A theory of glacial quarrying for landscape evolution models. *Geology*, *40*(8), 679–682. https://doi.org/10.1130/G33079.1

Iverson, N. R. (2017). Determining glacier flow direction from till fabrics. *Geomorphology*, *299*, 124–130. https://doi.org/10.1016/j.geomorph.2017.10.005

Jones, A. R. (1999). Light scattering for particle characterization. *Progress in Energy and Combustion Science*, *25*(1), 1–53. https://doi.org/10.1016/S0360-1285(98)00017-3

Kelley, S. E., Ross, M., Elliott, B., & Normandeau, P. X. (2019). Effect of shifting ice flow and basal topography in shaping three-dimensional dispersal patterns, Lac de Gras region, Northwest Territories, Canada. *Journal of Geochemical Exploration*, *199*, 105–127. https://doi.org/10.1016/j.gexplo.2019.01.012

Kerr, D. E., Morse, P. D. & Wolfe, S. A. (2016). Reconnaissance surficial geology, Rae, Northwest Territories, NTS 85-K. prelim., *Geological Survey of Canada, Canadian Geoscience Map*, 290. https://doi.org/10.4095/298838

Kerr, D. E., Morse, P. D. & Wolfe, S. A. (2017). Reconnaissance surficial geology, Willow Lake, Northwest Territories, NTS 85-L. prelim., *Geological Survey of Canada, Canadian Geoscience Map*, 304. https://doi.org/10.4095/299468

King, E. C., Hindmarsh, R. C. A., & Stokes, C. R. (2009). Formation of mega-scale glacial lineations observed beneath a West Antarctic ice stream. *Nature Geoscience*, *2*(8), 585–588. https://doi.org/10.1038/ngeo581

Krüger, J., & Thomsen, H. H. (1984). Morphology, Stratigraphy, and Genesis of Small Drumlins in Front of the Glacier Mýrdalsjökull, South Iceland. *Journal of Glaciology*, *30*(104), 94–105. https://doi.org/10.3189/S0022143000008534

Krumbein, W. C. (1934). *Manual of sedimentary petrography.* Society of Economic Paleontologists and Mineralogists.

Lemmen, D. S. (1990). Surficial materials associated with glacial Lake McConnell, southern District of Mackenzie. *Geological Survey of Canada, Paper 90-1D*, 79–83.

Lemmen, D. S., Duk-Rodkin, A., & Bednarski, J. M. (1994). Late glacial drainage systems along the northwestern margin of the Laurentide Ice Sheet. *Quaternary Science Reviews, 13*(9–10), 805–828. https://doi.org/10.1016/0277-3791(94)90003-5

Maclachlan, J. C., & Eyles, C. H. (2013). Quantitative geomorphological analysis of drumlins in the Peterborough drumlin field, Ontario, Canada. *Geografiska Annaler: Series A, Physical Geography*, *95*(2), 125–144. https://doi.org/10.1111/geoa.12005

Margold, M., Stokes, C. R., & Clark, C. D. (2018). Reconciling records of ice streaming and ice margin retreat to produce a palaeogeographic reconstruction of the deglaciation of the Laurentide Ice Sheet. *Quaternary Science Reviews*, *189*, 1–30. https://doi.org/10.1016/j.quascirev.2018.03.013

McClenaghan, M. B., & Paulen, R. C. (2018). Application of till mineralogy and geochemistry to mineral exploration. In *Past glacial environments* (2nd ed., pp. 689–751). Elsevier.

McClenaghan, M. B., Paulen, R. C., & Oviatt, N. M. (2018). Geometry of indicator mineral and till geochemistry dispersal fans from the Pine Point Mississippi Valley-type Pb-Zn district, Northwest Territories, Canada. *Journal of Geochemical Exploration, 190*, 69–86. https://doi.org/10.1016/j.gexplo.2018.02.004

McClenaghan, M. B., Paulen, R. C., Smith, I. R., Rice, J. M., Plouffe, A., McMartin, I., Campbell, J. E., Lehtonen, M., Parsasadr, M., & Beckett-Brown, C. E. (2023). Review of till geochemistry and indicator mineral methods for mineral exploration in glaciated terrain. *Geochemistry: Exploration, Environment, Analysis*, *23*(4), geochem2023-013. https://doi.org/10.1144/geochem2023-013

McMartin, I., & Henderson, P. J. (2004). Evidence from Keewatin (Central Nunavut) for Paleo-Ice Divide Migration. *Géographie Physique et Quaternaire*, *58*(2–3), 163–186. https://doi.org/10.7202/013137ar

McMartin, I., & Paulen, R. C. (2007). *Application of till and stream sediment heavy mineral and geochemical methods to mineral exploration in western and northern Canada*. Geological Association of Canada.

Menzies, J., Hess, D. P., Rice, J. M., Wagner, K. G., & Ravier, E. (2016). A case study in the New York Drumlin Field, an investigation using microsedimentology, resulting in the refinement of a

theory of drumlin formation. *Sedimentary Geology*, *338*, 84–96. https://doi.org/10.1016/j.sedgeo.2016.01.017

Menzies, J., Paulen, R. C., Rice, J. M., McClenaghan, M. B., Oviatt, N. M., & Dhillon, N. (2019). Deformation 'boundary front' movements in subglacial tills—A microsedimentological perspective from till sequences near Pine Point, NWT, Canada. *The Depositional Record*, *5*(2), 230–246. https://doi.org/10.1002/dep2.73

Menzies, J., Paulen, R. C., Reitner, J. M., Gao, C., Hodder, T., & Ross, M. (2023). Subglacial tills: A process model based on microsedimentological clues. *Journal of Sedimentary Research*, *93*(10), 705–728. https://doi.org/10.2110/jsr.2022.017

Ó Cofaigh, C., Stokes, C. R., Lian, O. B., Clark, C. D., & Tulacyzk, S. (2013). Formation of mega-scale glacial lineations on the Dubawnt Lake Ice Stream bed: 2. Sedimentology and stratigraphy. *Quaternary Science Reviews*, *77*(Complete), 210–227. https://doi.org/10.1016/j.quascirev.2013.06.028

Okulitch, A. V. (2006). Phanerozoic bedrock geology, Slave River, District of Mackenzie, Northwest Territories. *Geological Survey of Canada, Open File 5282*.

Parent, M., Paradis, S. J., & Boisvert, É. (1995). Ice-flow patterns and glacial transport in the eastern Hudson Bay region: Implications for the late Quaternary dynamics of the Laurentide Ice Sheet. *Canadian Journal of Earth Sciences*, *32*(12), 2057–2070. https://doi.org/10.1139/e95-159

Paulen, R. C., Paradis, S., Plouffe, A., & Smith, I. R. (2011). Pb and S isotopic composition of indicator minerals in glacial sediments from NW Alberta, Canada: Implications for Zn-Pb base metal exploration. *Geochemistry: Exploration, Environment, Analysis*, *11*(4), 309–320. https://doi.org/10.1144/1467-7873/10-IM-032

Paulen, R. C., McClenaghan, M. B., & Hicken, A. K. (2013). Regional and local ice-flow history in the vicinity of the Izok Lake Zn-Cu-Pb-Ag deposit, Nunavut. *Canadian Journal of Earth Sciences*, *50*(12), 1209–1222. https://doi.org/10.1139/cjes-2013-0064

Paulen, R. C., Smith, I. R., and Day, S. J. A. (ed.), 2019. GEM-2 Southern Mackenzie Surficial activity 2018 report: surficial geology and heavy mineral studies in southern Northwest Territories; *Geological Survey of Canada, Open File 8477*, 70 p. https://doi.org/10.4095/313419

Paulen, R. C. & Smith, I. R. (2022). Surficial geology, Sulphur Bay, Western Great Slave Lake, Northwest Territories, NTS 85-G. *Geological Survey of Canada, Canadian Geoscience Map,* 443. https://doi.org/10.4095/330073

Plakholm, J. A., Paulen, R. C., Sapera, J. R., & Hagedorn, G. W. (2019). Pebble lithology counts from till samples collected in the southern Northwest Territories (2010-2017); in GEM-2 Southern Mackenzie Surficial Activity 2018 report: Surficial geology and heavy mineral studies in Southern Northwest Territories (R. C. Paulen, I. R. Smith, & S. J. A. Day, Eds.). *Geological Survey of Canada, Open File 8477,* 43–51. http://doi.org/10.4095/313426

Plakholm, J. A., Paulen, R. C., & Paré, D. (2020). Clast-lithology data for selected surficial samples from the Trout Lake and Kakisa Lake protected area strategy surveys, southwest Northwest Territories. *Geological Survey of Canada, Open File 8437*.

Porter, C., Morin, P., Howat, I., Noh, M.-J., Bates, B., Peterman, K., Keesey, S., Schlenk, M., Gardiner, J., Tomko, K., Willis, M., Kelleher, C., Cloutier, M., Husby, E., Foga, S., Nakamura, H., Platson, M., 24 Wethington Jr., M., Williamson, C., Bauer, G., Enos, J., Arnold, G., Kramer, W., Becker, P., Doshi, A., D'Souza, C., Cummens, P., Laurier, F., and Bojesen, M. (2018). Arcticdem.

Rea, B. (2007). GLACIAL LANDFORMS, EROSIONAL FEATURES | Micro to Macro Scale Forms. In S. A. Elias (Ed.), *Encyclopedia of Quaternary Science* (pp. 853–864). Elsevier. https://doi.org/10.1016/B0-44-452747-8/00097-1

Rhodes, D., Lantos, E. A., Lantos, J. A., Webb, R. J., & Owens, D. C. (1984). Pine Point orebodies and their relationship to the stratigraphy, structure, dolomitization, and karstification of the Middle Devonian barrier complex. *Economic Geology, 79,* 991–1055. https://doi.org/10.2113/gsecongeo.79.5.991

Rice, J. M., Paulen, R. C., Menzies, J., McClenaghan, M. B., & Oviatt, N. M. (2013). Glacial stratigraphy of the Pine Point Pb-Zn Mine Site, Northwest Territories. *Geological Survey of Canada, Current Research, 2013-5*, 1–14. https://doi.org/10.4095/292184

Rice, J. M., Paulen, R. C., Menzies, J., & McClenaghan, M. B. (2014). Micromorphological descriptions of till from pit K-62, Pine Point mining district, Northwest Territories. *Geological Survey of Canada, Open File 7526,* 30 p. https://doi.org/10.4095/293478

Rice, J. M., Menzies, J., Paulen, R. C., & McClenaghan, M. B. (2019). Microsedimentological evidence of vertical fluctuations in subglacial stress from the northwest sector of the Laurentide ice sheet, Northwest Territories, Canada. *Canadian Journal of Earth Sciences, 56*(4), 363–379. https://doi.org/10.1139/cjes-2018-0201

Rice, J. M., Ross, M., Paulen, R. C., Kelley, S. E., Briner, J. P., Neudorf, C. M., & Lian, O. B. (2019). Refining the ice flow chronology and subglacial dynamics across the migrating Labrador Divide of the Laurentide Ice Sheet with age constraints on deglaciation. *Journal of Quaternary Science, 34*(7), 519–535. https://doi.org/10.1002/jqs.3138

Rice, J. M., Ross, M., Campbell, H. E., Paulen, R. C., & McClenaghan, M. B. (2024). Net evolution of subglacial sediment transport in the Quebec–Labrador sector of the Laurentide Ice Sheet. *Canadian Journal of Earth Sciences, 61*(4), 524–542. https://doi.org/10.1139/cjes-2023-0050

Ross, M., 2022. Update Till Fabric Analysis Demo-Copy1.ipynb.

Schomacker, A., Krüger, J., & Kjær, K. H. (2006). Ice-cored drumlins at the surge-type glacier Brúarjökull, Iceland: A transitional-state landform. *Journal of Quaternary Science, 21*(1), 85–93. https://doi.org/10.1002/jqs.949

Shaw, J., Faragini, D. M., Kvill, D. R., & Rains, R. B. (2000). The Athabasca fluting field, Alberta, Canada: implications for the formation of large-scale fluting (erosional lineations). *Quaternary Science Reviews, 19*(10), 959–980. https://doi.org/10.1016/S0277-3791(99)00027-X

Smith, D. G. (1994). Glacial lake McConnell: Paleogeography, age, duration, and associated river deltas, mackenzie river basin, western Canada. *Quaternary Science Reviews, 13*(9–10), 829–843. https://doi.org/10.1016/0277-3791(94)90004-3

Smith, I. R., Paulen, R. C., Deblonde, C., Hagedorn, G. W., King, R. D., and Pyne, M. D., 2019. Surficial geology and drift isopach mapping; *in* GEM-2 Southern Mackenzie Surficial Activity 2018 report: Surficial Geology and Heavy Mineral Studies in Southern Northwest Territories, (eds.) R.C. Paulen, I.R. Smith and S.J.A. Day; *Geological Survey of Canada, Open File 8477*, p. 7-16. http://doi.org/10.4095/313421

Sookhan, S., Eyles, N., Bukhari, S., & Paulen, R. C. (2021). LiDAR-based quantitative assessment of drumlin to mega-scale glacial lineation continuums and flow of the paleo Seneca-Cayuga paleo-

ice stream. *Quaternary Science Reviews*, *263*(Complete). https://doi.org/10.1016/j.quascirev.2021.107003

Stevens, C. W., Kerr, D. E., Wolfe, S. A. & Eagles, S. (2017). Predictive surficial geology, Yellowknife and Hearne Lake, Northwest Territories, NTS 85-J and NTS 85-I. 2, prelim., *Geological Survey of Canada, Canadian Geoscience Map*, 200. https://doi.org/10.4095/299516

Stirling. (2022). Ice Flow Shift, Drumlin, and Bedrock Topography Effects on Glacial Dispersal from Kimberlites in the Lac de Gras Region, Northwest Territories, Canada. University of Waterloo.

Stokes, C. R., Tarasov, L., & Dyke, A. S. (2012). Dynamics of the North American Ice Sheet Complex during its inception and build-up to the Last Glacial Maximum. *Quaternary Science Reviews*, *50*, 86–104. https://doi.org/10.1016/j.quascirev.2012.07.009

Stokes, C. R., Fowler, A. C., Clark, C. D., Hindmarsh, R. C. A., & Spagnolo, M. (2013). The instability theory of drumlin formation and its explanation of their varied composition and internal structure. *Quaternary Science Reviews*, *62*, 77–96. https://doi.org/10.1016/j.quascirev.2012.11.011

Stokes, C. R., Tarasov, L., Blomdin, R., Cronin, T. M., Fisher, T. G., Gyllencreutz, R., Hättestrand, C., Heyman, J., Hindmarsh, R. C. A., Hughes, A. L. C., Jakobsson, M., Kirchner, N., Livingstone, S. J., Margold, M., Murton, J. B., Noormets, R., Peltier, W. R., Peteet, D. M., Piper, D. J. W., … Teller, J. T. (2015). On the reconstruction of palaeo-ice sheets: Recent advances and future challenges. *Quaternary Science Reviews*, *125*, 15–49. https://doi.org/10.1016/j.quascirev.2015.07.016

Stokes, C. R., Margold, M., & Creyts, T. T. (2016). Ribbed bedforms on palaeo-ice stream beds resemble regular patterns of basal shear stress ('traction ribs') inferred from modern ice streams. *Journal of Glaciology*, *62*(234), 696–713. https://doi.org/10.1017/jog.2016.63

Trommelen, M. S., Ross, M., & Ismail, A. (2014). Ribbed moraines in northern Manitoba, Canada: Characteristics and preservation as part of a subglacial bed mosaic near the core regions of ice sheets. *Quaternary Science Reviews*, *87*, 135–155. https://doi.org/10.1016/j.quascirev.2014.01.010

Veillette, J. J., Dyke, A. S., & Roy, M. (1999). Ice-flow evolution of the Labrador Sector of the Laurentide Ice Sheet: a review, with new evidence from northern Quebec. *Quaternary Science Reviews*, *18*(8–9), 993–1019. https://doi.org/10.1016/S0277-3791(98)00076-6

Winkler, S. (2021). Terminal Moraine Formation Processes and Geomorphology of Glacier Forelands at the Selected Outlet Glaciers of Jostedalsbreen, South Norway. In A. A. Beylich (Ed.), *Landscapes and Landforms of Norway* (pp. 33–69). Springer International Publishing. https://doi.org/10.1007/978-3-030-52563-7_3

Appendix A

Grain Size Analysis

Sample ID	8mm	4mm	2mm	1mm	0.5mm	0.25mm	0.125mm	0.063mm	<0.063mm
20PXN001B	0	0	0	0.001993	0.012624	0.254476	57.40122	37.66806	4.661624
20PXN002B	2.12144	1.092924	2.13946	3.061854	4.748127	14.05817	17.90593	13.13577	41.73633
20PXN003B	0.179558	2.075529	8.300094	7.53133	6.766271	4.324552	3.816534	3.963415	63.04272
20PXN004B	6.404007	7.24612	9.45997	9.163541	7.737603	6.217317	5.037622	4.629781	44.10404
20PXN005B	0	0.226288	7.86483	23.76755	12.53887	6.724689	4.24423	2.012821	42.62072
20PXN006B	0.337158	1.755421	4.238463	5.383201	15.31037	20.29278	35.59782	3.457869	13.62691
20PXN007B	29.01431	14.1047	7.23298	4.589598	3.061195	5.701652	10.63252	13.72004	11.943
20PXN008B	0.190875	2.67732	3.168721	4.018519	10.41586	6.974029	6.151982	7.384883	59.01781
20PXN009B	4.820524	5.94043	4.402584	5.233504	9.57591	17.36037	15.57123	7.331468	29.76398
20PXN010B	0.394381	3.195999	3.254401	3.889775	6.500076	9.95452	9.108698	8.840519	54.86163
20PXN011B	0.216872	0.15201	0.110099	0.304353	3.073796	36.52399	57.26255	2.275494	0.080828
20PXN012B	15.66577	8.869152	9.818966	8.777202	12.68573	29.8247	10.87339	2.946722	0.538372

20PXN013B	**1.226559**	**2.000124**	**2.502992**	**3.499099**	**7.305009**	**11.2203**	**14.12469**	**11.28324**	**46.83798**
20PXN014B	**1.606202**	**2.574894**	**2.690102**	**3.552655**	**7.203053**	**10.96127**	**13.87977**	**10.91324**	**46.61881**
20PXN015B	**1.269748**	**1.539793**	**1.219578**	**1.6169**	**7.224534**	**18.56674**	**20.6106**	**12.36986**	**35.58225**
20PXN016B	**3.350378**	**6.823495**	**4.890456**	**5.87169**	**12.24002**	**30.95672**	**28.79225**	**5.534245**	**1.540746**
20PXN017B	**0.354976**	**0.871521**	**1.209561**	**1.824334**	**3.640539**	**3.482697**	**5.567166**	**11.47102**	**71.57819**
20PXN018B	**1.014505**	**3.868983**	**3.160009**	**3.4709**	**5.982683**	**8.640264**	**11.1281**	**10.5224**	**52.21215**
20PXN019B	**0.442642**	**0.972552**	**1.317972**	**6.937274**	**30.77525**	**46.32846**	**10.49301**	**0.991798**	**1.741038**
20PXN020B	**0**	**0.080852**	**0.095159**	**0.360339**	**4.116453**	**70.04525**	**24.65813**	**0.354018**	**0.289802**
20PXN021B	**3.078967**	**6.678107**	**6.579615**	**11.67751**	**35.08928**	**20.15118**	**9.109697**	**2.476662**	**5.15899**
20PXN022B	**1.024476**	**2.809559**	**3.661491**	**3.877508**	**4.723375**	**5.358617**	**7.893185**	**4.537351**	**66.11444**
20PXN023B	**2.879985**	**5.794099**	**6.240813**	**6.685837**	**6.750378**	**5.980286**	**7.529254**	**7.611028**	**50.52832**
20PXN024B	**3.246651**	**2.653878**	**3.932118**	**4.637401**	**6.57189**	**7.434014**	**7.894127**	**6.525543**	**57.10438**
20PXN025B	**0**	**0**	**0**	**0.003335**	**1.464448**	**34.30863**	**63.04562**	**1.170958**	**0.007004**
20PXN026B	**6.075639**	**7.316181**	**5.385395**	**5.695107**	**9.712551**	**16.9796**	**14.97121**	**7.153531**	**26.71079**
20PXN027B	**0**	**0.034414**	**0.129973**	**0.794205**	**2.433736**	**2.032122**	**4.225959**	**7.004173**	**83.34542**

20PXN028B	**15.26014**	**13.00083**	**9.285145**	**9.780593**	**27.88118**	**14.34894**	**7.33756**	**2.61829**	**0.487337**
20PXN029B	**3.47171**	**1.980078**	**2.343126**	**3.190238**	**5.889333**	**15.21094**	**11.87271**	**9.695437**	**46.34643**
20PXN030B	**2.337591**	**2.798383**	**3.289807**	**3.941375**	**6.336232**	**8.693466**	**14.50165**	**9.173237**	**48.92826**
20PXN031B	**3.085325**	**3.401896**	**2.670508**	**2.939114**	**4.38535**	**8.965538**	**9.24109**	**6.179913**	**59.13127**
20PXN032B	**1.07875**	**2.980729**	**3.520274**	**5.336401**	**13.79164**	**14.34612**	**14.16729**	**6.429742**	**38.34906**
20PXN033B	**7.966519**	**7.527112**	**7.24454**	**9.805744**	**18.36684**	**18.07156**	**7.591318**	**2.433127**	**20.99325**
20PXN034B	**12.08605**	**11.7517**	**13.17786**	**10.1788**	**10.69372**	**19.86713**	**5.954243**	**2.58398**	**13.70652**
20PXN035B	**0**	**0.89714**	**2.686075**	**12.65281**	**33.86852**	**43.69631**	**3.811674**	**1.417187**	**0.970287**
20PXN036B	**0**	**0.100118**	**0.026512**	**0.456634**	**2.067585**	**14.24007**	**52.15218**	**16.58672**	**14.37018**
20PXN037B	**0**	**0**	**0.279159**	**0.553322**	**4.234694**	**7.376402**	**3.570108**	**48.97647**	**35.00984**
20PXN038B	**12.80613**	**14.17578**	**12.11571**	**12.52134**	**17.22092**	**17.38521**	**5.8418**	**3.069915**	**4.863188**
20PXN039B	**2.964225**	**7.510822**	**10.52736**	**9.607576**	**7.901134**	**5.659188**	**5.849649**	**3.890713**	**46.08934**
20PXN040B	**0**	**0**	**0.077387**	**0.458316**	**2.866311**	**14.83424**	**70.94729**	**10.61132**	**0.205142**
20PXN041B	**4.763926**	**13.74257**	**18.64734**	**21.85698**	**15.41748**	**4.594448**	**2.596422**	**1.048542**	**17.33228**
20PXN042B	**18.77786**	**13.80329**	**14.14152**	**11.96283**	**12.09105**	**8.556918**	**4.159166**	**1.355792**	**15.15158**
20PXN043	**0**	**0.798943**	**1.591061**	**1.932003**	**2.95243**	**3.894038**	**7.053636**	**11.02515**	**70.75273**

B						9								
20PXN044B	18.86358	33.63444	16.70478	6.282397		2.778159	2.382531	3.086504	4.811944	11.45567				
20PXN045B	15.16061	12.3763	9.895475	7.519609		6.662486	6.09543	6.436804	4.165898	31.68738				
20PXN046B	0	3.922921	4.110216	2.872079		2.799482	2.810752	3.017274	4.180824	76.28645				
20PXN047B	1.497486	4.103936	5.213235	5.854967		7.8716	11.21457	13.7604	13.56078	36.92304				
20PXN048B	0	1.242744	1.396662	1.586461		4.038416	8.638514	18.22703	24.11212	40.75805				
20PXN049B	2.229937	4.176149	3.141248	4.337614		25.8233 5	43.5592	14.42948	1.8492	0.453828				
20PXN050B	5.53898	12.29461	18.63042	24.18832		25.2403 6	5.456675	3.72396	3.232787	1.693886				
20PXN051B	2.47417	2.486518	2.271271	4.728422		30.6241 2	41.23528	14.04477	1.72965	0.405799				
20PXN052B	9.577407	10.42946	14.85713	22.719		19.3271	7.777635	7.763423	4.955612	2.593238				
20PXN054B	0.846368	0.560573	0.807973	0.681435		2.534097	21.70242	33.13791	30.37611	9.353121				
20PXN056B	13.65	14.39786	10.35219	10.02091		22.49884	18.52685	6.005112	2.976499	1.571732				
20PXN057B	2.549939	3.067656	2.290415	2.845444		4.983609	9.312576	8.561986	7.65315	58.73522				
20PXN058B	2.587706	2.718445	2.252331	2.865569		4.410703	7.92696	9.910121	7.840692	59.48747				
				< 0.063	< 0.063	0.063	0.125	0.25	0.5	1	2	4	8	

Sample No.	W_T	W_{TO}	W_{T1}	W_1	W_{1D}	W_2	W_3	W_4	W_5	W_6	W_7	W_8	W_9	Loss (%)
21PXN001B	329.473	322.565	248.416	74.149	20.507	40.091	49.973	34.728	23.931	18.863	20.457	23.094	16.772	0.020967
21PXN002B	318.426	311.388	260.52	50.868	16.027	41.451	48.487	34.324	24.099	23.276	25.83	28.651	18.375	0.022102
21PXN003B	321.262	313.175	215.466	97.709	19.685	42.686	42.348	29.848	23.553	20.947	18.878	13.061	4.46	0.025173
21PXN004B	319.744	311.696	226.52	85.176	22.963	53.48	48.471	31.593	20.405	14.441	12.188	11.936	11.043	0.02517
21PXN005B	280.021	276.473	161.496	114.977	15.962	31.103	35.29	15.878	7.676	8.711	13.376	22.194	11.306	0.01267
21PXN006B	285.25	270.363	235.706	34.657	10.484	25.453	29.321	24.181	21.215	23.709	36.854	47.922	27.051	0.052189
21PXN007B	290.654	286.716	284.896	1.82	2.441	34.001	87.172	73.049	25.609	17.639	18.751	20.583	5.651	0.013549
21PXN008B	328.569	323.843	316.891	6.952	4.083	29.869	56.267	67.157	59.791	46.847	31.492	15.476	5.909	0.014384
21PXN009B	291.997	286.68	269.958	16.722	8.63	32.2	53.398	58.55	47.382	34.98	22.853	9.315	2.65	0.018209

21PXN010B	**281.358**	**273.707**	**173.118**	**100.589**	**55.831**	**48.536**	**19.414**	**15.481**	**14.536**	**9.909**	**5.568**	**2.472**	**1.371**	**0.027193**
21PXN011B	**290.393**	**281.062**	**139.742**	**141.32**	**25.501**	**66.388**	**38.42**	**7.032**	**1.231**	**0.769**	**0.266**	**0.135**	**0**	**0.032132**
21PXN012B	**325.661**	**319.086**	**167.047**	**152.039**	**7.439**	**32.383**	**24.363**	**35.992**	**27.169**	**17.603**	**13.002**	**6.981**	**2.115**	**0.02019**
21PXN013B	**273.175**	**263.609**	**158.124**	**105.485**	**8.076**	**22.832**	**27.613**	**36.695**	**23.569**	**14.831**	**11.892**	**11.921**	**0.695**	**0.035018**
21PXN014B	**262.836**	**258.195**	**194.124**	**64.071**	**9.333**	**21.48**	**26.438**	**31.932**	**29.54**	**19.692**	**19.475**	**25.037**	**11.197**	**0.017657**
21PXN015B	**300.21**	**290.473**	**116.801**	**173.672**	**14.493**	**34.857**	**19.105**	**27.767**	**19.649**	**0.888**	**0.042**	**0**	**0**	**0.032434**
21PXN016B	**318.52**	**308.937**	**132.785**	**176.152**	**9.962**	**19.25**	**36.009**	**27.15**	**14.66**	**16.882**	**5.825**	**1.944**	**1.103**	**0.030086**
21PXN017B	**292.445**	**281.909**	**113.03**	**168.879**	**10.503**	**16.596**	**19.79**	**29.528**	**18.153**	**8.762**	**5.398**	**1.575**	**2.725**	**0.036027**
21PXN018B	**256.108**	**253.219**	**251.692**	**1.527**	**0.634**	**4.312**	**20.949**	**59.076**	**37.222**	**23.711**	**32.247**	**43.834**	**29.707**	**0.01128**
21PXN019B	**324.544**	**317.111**	**123.534**	**193.577**	**6.15**	**25.341**	**29.756**	**30.685**	**13.618**	**6.595**	**5.452**	**5.172**	**0.765**	**0.022903**

21PXN020B	**314.717**	**303.075**	**297.512**	**5.563**	**1.166**	**3.96**	**17.775**	**195.97**	**38.692**	**10.69**	**10.959**	**14.986**	**3.314**	**0.036992**
21PXN021B	**273.721**	**266.428**	**178.459**	**87.969**	**8.252**	**24.741**	**39.428**	**54.163**	**24.714**	**10.364**	**8.574**	**6.894**	**1.329**	**0.026644**
21PXN022B	**306.189**	**297.214**	**157.208**	**140.006**	**6.838**	**25.905**	**32.39**	**38.589**	**18.888**	**11.426**	**9.488**	**10.303**	**3.381**	**0.029312**
21PXN023B	**287.961**	**279.826**	**150.223**	**129.603**	**9.059**	**29.21**	**28.581**	**30.084**	**18.22**	**13.077**	**10.268**	**8.481**	**3.243**	**0.02825**
21PXN024B	**317.378**	**311.757**	**305.647**	**6.11**	**3.395**	**9.527**	**20.793**	**100.885**	**60.092**	**23.315**	**25.506**	**36.902**	**25.232**	**0.017711**
21PXN025B	**272.6**	**266.3**	**207.34**	**58.96**	**8.34**	**26.45**	**44.29**	**49.41**	**32.99**	**16**	**7.24**	**8.17**	**14.45**	**0.023111**
21PXN026B	**280**	**268.97**	**152.49**	**116.48**	**8.5**	**29.025**	**30.615**	**32.575**	**19.37**	**11.305**	**10.6**	**7.81**	**2.69**	**0.039393**
21PXN027B	**274.69**	**267.48**	**156.175**	**111.305**	**11.47**	**28.265**	**31.56**	**34.275**	**18.725**	**9.29**	**7.88**	**9.66**	**5.05**	**0.026248**
21PXN028B	**284.94**	**279.538**	**169.463**	**110.075**	**8.86**	**25.71**	**34.11**	**38.06**	**27.255**	**11.78**	**10.01**	**8.9**	**4.778**	**0.018958**
21PXN029B	**282.488**	**278.48**	**186.78**	**91.7**	**13.105**	**33.345**	**37.45**	**42.5**	**27.75**	**11.045**	**11.445**	**10.14**	**0**	**0.014188**

21PXN030B	**291.28**	**286.355**	**189.19**	**97.165**	**14.235**	**30.755**	**34.485**	**38.505**	**29.152**	**14.98**	**8.978**	**11.76**	**6.34**	**0.016908**
21PXN031B	**288.325**	**282.87**	**165.25**	**117.62**	**8.99**	**27.14**	**27.19**	**31.075**	**19.71**	**10.494**	**9.846**	**7.94**	**22.865**	**0.01892**
21PXN032B	**297.97**	**295.29**	**173.12**	**122.17**	**10.76**	**29.685**	**33.95**	**38.175**	**23.61**	**11.85**	**9.43**	**7.32**	**8.34**	**0.008994**
21PXN033B	**245.043**	**236.951**	**175.286**	**61.665**	**8.118**	**22.787**	**37.233**	**48.049**	**23.486**	**11.037**	**7.103**	**11.157**	**6.316**	**0.033023**
21PXN034B	**299.592**	**293.686**	**200.377**	**93.309**	**12.907**	**31.161**	**40.106**	**51.27**	**26.582**	**14.49**	**8.969**	**9.236**	**5.656**	**0.019713**
21PXN035B	**322.338**	**313.888**	**246.961**	**66.927**	**15.728**	**34.555**	**52.524**	**75.119**	**29.116**	**16.305**	**10.366**	**9.841**	**3.407**	**0.026215**
21PXN036B	**299.036**	**291.845**	**224.381**	**67.464**	**17.433**	**35.865**	**52.303**	**59.29**	**22.643**	**10.778**	**9.462**	**7.074**	**9.533**	**0.024047**
21PXN037B	**287.923**	**281.468**	**162.912**	**118.556**	**6.438**	**28.875**	**32.406**	**38.008**	**21.884**	**10.735**	**8.44**	**11.503**	**4.623**	**0.022419**
21PXN038B	**302.884**	**296.329**	**197.77**	**98.559**	**11.776**	**31.756**	**40.825**	**45.238**	**21.628**	**10.397**	**10.458**	**6.237**	**19.455**	**0.021642**
21PXN039B	**296.283**	**267.995**	**160.563**	**107.432**	**6.186**	**28.927**	**28.333**	**29.744**	**18.027**	**11.101**	**13.363**	**12.286**	**12.596**	**0.095476**

21PXN040B	**311.512**	**303.631**	**165.263**	**138.368**	**6.984**	**25.327**	**33.323**	**34.528**	**22.071**	**12.529**	**11.745**	**12.085**	**6.671**	**0.025299**
21PXN042B	**294.577**	**99.888**	**99.888**		**2.433**	**14.792**	**18.819**	**16.569**	**12.635**	**10.657**	**10.056**	**7.127**	**6.8**	**0.66091**
21PXN045B	**314.073**	**310.847**	**307.779**	**3.068**	**1.93**	**11.077**	**33.961**	**109.097**	**55.646**	**8.351**	**19.888**	**37.411**	**30.418**	**0.010271**
21PXN046B	**290.901**	**286.553**	**279.961**	**6.592**	**10.247**	**25.419**	**26.937**	**49.456**	**102.141**	**65.739**	**0.022**	**0**	**0**	**0.014947**
21PXN047B	**285.218**	**282.072**	**280.989**	**1.083**	**2.459**	**12.408**	**11.743**	**29.548**	**97.801**	**67.665**	**29.905**	**18.895**	**10.565**	**0.01103**
21PXN048B	**323.975**	**317.087**	**177.429**	**139.658**	**3.829**	**19.411**	**23.218**	**29.371**	**21.869**	**19.924**	**19.797**	**19.317**	**20.693**	**0.021261**
21PXN074B	**313.752**	**308.972**	**303.27**	**5.702**	**1.234**	**8.658**	**28.418**	**84.376**	**54.672**	**36.415**	**39.117**	**39.587**	**10.793**	**0.015235**
21PXN075B	**277.632**	**282.019**	**254.04**	**27.979**	**6.682**	**8.291**	**10.069**	**27.693**	**54.052**	**39.35**	**43.022**	**40.257**	**24.624**	**-0.0158**
21PXN076B	**320.822**	**302.98**	**190.677**	**112.303**	**6.807**	**24.083**	**23.714**	**26.305**	**31.466**	**33.91**	**19.99**	**15.595**	**8.807**	**0.055613**
21PXN077B	**265.068**	**260.237**	**204.263**	**55.974**	**6.701**	**11.472**	**13.621**	**21.75**	**25.374**	**24.207**	**28.332**	**35.329**	**37.477**	**0.018226**

21PXN078B	**299.605**	**288.536**	**206.402**	**82.134**	**23.646**	**48.241**	**46.609**	**39.126**	**23.354**	**12.102**	**6.127**	**6.218**	**0.979**	**0.036945**
21PXN079B	**318.05**	**311.035**	**198.487**	**112.548**	**20.778**	**40.459**	**37.538**	**27.972**	**18.405**	**15.551**	**13.024**	**13.618**	**11.142**	**0.022056**
21PXN080B	**266.593**	**266.398**	**205.822**	**60.576**	**8.951**	**23.133**	**23.954**	**27.46**	**30.727**	**25.829**	**25.255**	**22.747**	**17.766**	**0.000731**
21WL01B	**330.039**	**321.298**	**227.961**	**93.337**	**8.47**	**23.383**	**39.305**	**62.655**	**52.901**	**19.833**	**8.553**	**6.36**	**6.501**	**0.026485**
21WL02B	**329.149**	**316.626**	**216.371**	**100.255**	**12.431**	**27.536**	**39.131**	**60.38**	**32.224**	**14.405**	**12.078**	**8.853**	**9.333**	**0.038047**
21WL03B	**334.819**	**326.535**	**218.902**	**107.633**	**11.72**	**32.127**	**39.49**	**52.649**	**27.554**	**13.792**	**12.617**	**14.145**	**14.808**	**0.024742**
21WL04B	**315.895**	**308.431**	**158.664**	**149.767**	**6.718**	**25.26**	**30.519**	**33.203**	**17.222**	**10.852**	**12.049**	**13.498**	**9.343**	**0.023628**

Additional Notes LEGEND FOR SUBSCRIPTS//

TO = total sum observed after sieving

T = total before sieving 1 = lowest grain size (< 0.063mm)

W1 = wet total 9 = highest grain size (> 8mm)

T1 = dry total 1D = from dry sieving

Appendix B

Clast Fabric Data

Stratigraphic section 1

2nd hole				6th hole				
Clast	**Trend (°)**	**Plunge (°)**		**Clast**	**Trend (°)**	**Plunge (°)**	**a-axis (cm)**	**b-axis (cm)**
1	**30**	**242**	**274**	**1**	**41**	**28**	**2**	**1**
2	**46**	**30**	**62**	**2**	**346**	**18**	**1.8**	**1.2**
3	**23**	**308**	**340**	**3**	**72**	**18**	**1.6**	**0.6**
4	**08**	**50**	**82**	**4**	**357**	**14**	**5**	**4**
5	**15**	**352**	**24**	**5**	**266**	**5**	**7.8**	**5**
6	**47**	**15**	**47**	**6**	**80**	**19**	**1.5**	**1.1**
7	**14**	**198**	**230**	**7**	**165**	**17**	**2.6**	**1.5**
8	**26**	**44**	**76**	**8**	**325**	**19**	**1.8**	**1**
9	**42**	**42**	**74**	**9**	**89**	**10**	**2**	**1.6**
10	**18**	**36**	**68**	**10**	**71**	**19**	**2.5**	**2**
11	**24**	**244**	**276**	**11**	**104**	**12**	**1.4**	**1**
12	**18**	**345**	**17**	**12**	**71**	**19**	**1.4**	**0.7**
13	**32**	**44**	**76**	**13**	**66**	**5**	**1.8**	**1**
14	**04**	**18**	**50**	**14**	**240**	**12**	**2.4**	**1.1**
15	**14**	**185**	**217**	**15**	**254**	**17**	**1.4**	**0.5**
16	**03**	**41**	**73**	**16**	**34**	**21**	**1.3**	**0.8**

17	**22**	**34**	**66**	**17**	**15**	**2**	**1.4**	**0.9**
18	**07**	**23**	**55**	**18**	**24**	**12**	**0.6**	**0.4**
19	**26**	**237**	**269**	**19**	**38**	**19**	**0.7**	**0.5**
20	**22**	**229**	**261**	**20**	**41**	**20**	**0**	**0**
21	**14**	**40**	**72**	**21**	**239**	**14**	**1.1**	**0.4**
22	**50**	**65**	**97**	**22**	**41**	**18**	**1.1**	**0.7**
23	**45**	**304**	**336**	**23**	**66**	**4**	**1.6**	**1.2**
24	**52**	**5**	**37**	**24**	**138**	**12**	**1.4**	**0.9**
25	**52**	**66**	**98**	**25**	**55**	**13**	**1.2**	**0.8**
26	**01**	**44**	**76**	**26**	**251**	**8**	**2.4**	**1.9**
27	**16**	**24**	**56**	**27**	**73**	**7**	**1**	**0.8**
28	**38**	**24**	**56**	**28**	**280**	**5**	**1**	**0.3**
29	**36**	**270**	**302**	**29**	**248**	**22**	**1.4**	**0.5**
30	**31**	**82**	**114**	**30**	**269**	**27**	**1.6**	**1**
31	**25**	**118**	**150**	**31**	**59**	**13**	**1**	**0.5**
32	**22**	**4**	**36**	**32**	**150**	**23**	**1.2**	**0.7**
33	**13**	**5**	**37**	**33**	**52**	**10**	**0.9**	**0.5**
34	**15**	**246**	**278**	**34**	**61**	**13**	**1.9**	**1.1**
35	**37**	**358**	**30**	**35**	**253**	**9**	**2.3**	**1.4**
36	**15**	**37**	**69**	**36**	**6**	**8**	**1.2**	**0.7**
37	**25**	**36**	**68**	**37**	**264**	**7**	**1**	**0.6**
38	**30**	**226**	**258**	**38**	**204**	**12**	**0.9**	**0.6**
39	**23**	**126**	**158**	**39**	**207**	**62**	**2.3**	**1.5**

40	**03**	**31**	**63**	**40**	**94**	**37**	**0.9**	**0.7**
41	**16**	**20**	**52**	**41**	**235**	**33**	**1.6**	**0.9**
42	**22**	**49**	**81**	**42**	**66**	**21**	**1.4**	**0.8**
43	**23**	**232**	**264**	**43**	**13**	**31**	**1**	**0.5**
44	**05**	**38**	**70**	**44**	**97**	**16**	**1.1**	**0.6**
45	**24**	**105**	**137**	**45**	**84**	**22**	**0**	**0**
46	**24**	**46**	**78**	**46**	**98**	**8**	**0.9**	**0.6**
47	**26**	**39**	**71**	**47**	**18**	**19**	**3.1**	**2.1**
48	**32**	**31**	**63**	**48**	**12**	**19**	**1**	**0.5**
49	**36**	**268**	**300**	**49**	**41**	**5**	**1.4**	**1**
50	**25**	**48**	**80**	**50**	**58**	**24**	**1.8**	**1**

9th hole					**13th hole**				
Clast	**Trend (°)**	**Plunge (°)**	**a-axis (cm)**	**b-axis (cm)**	**Clast**	**Trend (°)**	**Plunge (°)**	**a-axis (cm)**	**b-axis (cm)**
1	**53**	**17**	**1.7**	**1.4**	**1**	**05**	**37**	**8**	**5**
2	**58**	**1**	**1.5**	**1.1**	**2**	**22**	**13**	**4**	**2.2**
3	**271**	**12**	**2.4**	**1.3**	**3**	**18**	**14**	**2.3**	**1.6**
4	**333**	**18**	**2.6**	**1.6**	**4**	**28**	**36**	**3**	**1.8**
5	**320**	**20**	**2.5**	**1.8**	**5**	**39**	**76**	**2.6**	**1.5**
6	**52**	**6**	**1.1**	**0.7**	**6**	**13**	**276**	**2.4**	**1.5**
7	**210**	**3**	**1.8**	**1.4**	**7**	**14**	**37**	**3.8**	**2**

8	**258**	**12**	**2.4**	**1**	**8**	**36**	**18**	**1.3**	**0.6**
9	**62**	**4**	**2**	**1.5**	**9**	**1**	**21**	**2.7**	**1.1**
10	**22**	**4**	**2.4**	**1.7**	**10**	**16**	**140**	**1.5**	**0.7**
11	**56**	**15**	**1.1**	**0.5**	**11**	**12**	**14**	**5**	**3.5**
12	**7**	**2**	**2**	**1.7**	**12**	**15**	**46**	**1.5**	**0.4**
13	**290**	**12**	**3**	**2**	**13**	**18**	**68**		
14	**63**	**22**	**1.4**	**0.9**	**14**	**21**	**40**	**4.7**	**2.9**
15	**72**	**20**	**0.7**	**0.5**	**15**	**11**	**31**	**1.5**	**0.8**
16	**15**	**31**	**1.5**	**0.8**	**16**	**07**	**261**	**1**	**0.6**
17	**170**	**5**	**1.2**	**0.8**	**17**	**05**	**22**	**2.5**	**1.4**
18	**35**	**34**	**1**	**0.4**	**18**	**54**	**26**	**1.1**	**0.7**
19	**95**	**9**	**1**	**0.7**	**19**	**34**	**36**	**2.9**	**1.8**
20	**58**	**6**	**2.1**	**1.7**	**20**	**24**	**17**	**1.3**	**0.7**
21	**92**	**10**	**1.1**	**0.6**	**21**	**29**	**4**	**1.1**	**0.8**
22	**31**	**36**	**1.5**	**0.7**	**22**	**21**	**22**	**3.9**	**2.8**
23	**235**	**41**	**1**	**0.4**	**23**	**25**	**37**	**1.3**	**0.8**
24	**75**	**22**	**2.5**	**2**	**24**	**24**	**36**	**3.5**	**2.7**
25	**34**	**14**	**2.3**	**1.7**	**25**	**16**	**67**		
26	**264**	**26**	**2.5**	**1.9**	**26**	**03**	**18**	**2.1**	**1.2**
27	**73**	**46**	**1**	**0.5**	**27**	**22**	**65**	**2**	**1.5**
28	**196**	**17**	**2.3**	**1.7**	**28**	**18**	**63**	**2.4**	**1.4**
29	**65**	**38**	**3.8**	**2.5**	**29**	**35**	**287**	**1.5**	**1**
30	**45**	**12**	**2.3**	**1.7**	**30**	**14**	**42**	**2.2**	**1.3**

31	**245**	**31**	**1.3**	**0.9**	**31**	**02**	**72**	**1.6**	**1.1**
32	**267**	**10**	**1.2**	**1**	**32**	**17**	**20**	**1.8**	**0.5**
33	**222**	**36**	**5.7**	**3.7**	**33**	**14**	**31**	**1.2**	**0.8**
34	**44**	**23**	**0.9**	**0.5**	**34**	**62**	**22**	**2.4**	**1.6**
35	**62**	**29**	**0.7**	**0.4**	**35**	**16**	**54**	**2.9**	**2**
36	**168**	**17**	**1.3**	**0.8**	**36**	**16**	**63**	**7**	**4.3**
37	**89**	**8**	**1.3**	**1**	**37**	**57**	**344**	**1.8**	**1.2**
38	**89**	**10**	**0.9**	**0.6**	**38**	**28**	**355**	**2**	**0.6**
39	**192**	**35**	**1.1**	**0.7**	**39**	**08**	**170**	**1.3**	**0.8**
40	**74**	**14**	**1.4**	**0.6**	**40**	**25**	**346**	**5.6**	**3.2**
41	**264**	**3**	**2.6**	**1.8**	**41**	**28**	**19**	**2.3**	**1.6**
42	**59**	**23**	**1.2**	**0.5**	**42**	**21**	**38**	**1.3**	**0.5**
43	**182**	**4**	**1.6**	**1.1**	**43**	**34**	**74**	**1.8**	**1**
44	**94**	**27**	**1.8**	**0.8**	**44**	**28**	**30**	**1.8**	**0.9**
45	**215**	**11**	**1.9**	**1.2**	**45**	**31**	**344**	**2.2**	**1.4**
46	**211**	**24**	**1**	**0.6**	**46**	**16**	**116**	**1.7**	**0.9**
47	**24**	**2**	**0.9**	**0.5**	**47**	**05**	**97**	**2.8**	**1.8**
48	**70**	**4**	**1.4**	**1**	**48**	**20**	**357**	**2.6**	**1.8**
49	**200**	**40**	**2.9**	**1.8**	**49**	**72**	**355**	**3.1**	**2.6**
50	**95**	**40**	**1.1**	**0.6**	**50**	**41**	**54**	**7**	**4.5**

Stratigraphic section 2

2nd hole					6th hole					15th hole				
Clast	Trend (°)	Plunge (°)	a-axis (cm)	b-axis (cm)	Clast	Trend (°)	Plunge (°)	a-axis (cm)	b-axis (cm)	Clast	Trend (°)	Plunge (°)	a-axis (cm)	b-axis (cm)
1	25	88	2	1.3	1	07	12	4	3	1	10	200	1.5	0.9
2	34	120			2	20	205	2	1.1	2	07	244	1.8	1
3	77	12	4	2.5	3	07	312	1.2	0.7	3	26	35	1.9	1.2
4	23	100	1.8	0.9	4	41	86	2.2	1.6	4	15	4	1.2	0.8
5	29	105	2.9	1.6	5	36	36	0.8	0.5	5	10	65	1.8	1
6	22	86	1.2	0.8	6	02	6	1.4	0.7	6	12	258	1.9	1
7	52	81	1.4	0.9	7	24	48	1	0.6	7	06	313	0.6	0.3
8	24	75	3.9	2.6	8	05	348	2.3	1	8	05	59	1.2	0.7
9	12	254	2	0.8	9	30	114	2.3	1.5	9	26	254	0.8	0.4
10	15	236	1.6	1	10	20	96	2.8	2	10	26	338	1.5	0.6
11	14	248	2.7	1.6	11	52	82	3	1.7	11	33	23	2	1.4

12	**03**	**200**	**1**	**0.7**	**12**	**36**	**47**	**1.1**	**0.9**	**12**	**05**	**85**	**4.5**	**2.1**
13	**17**	**272**	**3.3**	**2.2**	**13**	**36**	**96**	**1.3**	**0.8**	**13**	**00**	**214**	**1.5**	**0.9**
14	**12**	**48**	**1.2**	**0.7**	**14**	**05**	**345**	**1.5**	**1**	**14**	**22**	**326**	**3.5**	**2**
15	**11**	**104**	**1.4**	**0.9**	**15**	**15**	**117**	**1.1**	**0.8**	**15**	**24**	**75**	**1.3**	**0.7**
16	**29**	**135**	**2.5**	**1.6**	**16**	**14**	**21**	**1**	**0.6**	**16**	**36**	**276**	**2.1**	**1.5**
17	**21**	**271**	**1.2**	**0.8**	**17**	**42**	**88**	**2**	**1.4**	**17**	**49**	**290**	**2.5**	**1.6**
18	**08**	**95**	**5.1**	**2**	**18**	**28**	**98**	**1.3**	**0.7**	**18**	**30**	**64**	**2.7**	**1.5**
19	**05**	**272**	**2**	**1.1**	**19**	**30**	**228**	**1.3**	**0.8**	**19**	**24**	**50**	**1.8**	**1**
20	**11**	**100**	**3.2**	**1.7**	**20**	**05**	**20**	**1.6**	**0.9**	**20**	**08**	**269**	**1.1**	**0.6**
21	**07**	**62**	**2.2**	**1.3**	**21**	**11**	**130**	**1.1**	**0.6**	**21**	**45**	**11**	**3.2**	**1.8**
22	**32**	**148**	**2**	**1.4**	**22**	**13**	**84**	**1.9**	**0.8**	**22**	**06**	**84**	**1.7**	**1.1**
23	**26**	**78**	**1.2**	**0.6**	**23**	**67**	**150**	**1.6**	**0.9**	**23**	**30**	**20**	**1.3**	**0.8**
24	**05**	**68**	**2.8**	**2**	**24**	**45**	**272**	**1.5**	**0.9**	**24**	**14**	**43**	**1.2**	**0.6**
25	**22**	**52**	**3**	**2**	**25**	**51**	**248**	**1.1**	**0.6**	**25**	**23**	**60**	**1.6**	**1**
26	**08**	**94**	**3.2**	**2.6**	**26**	**20**	**93**	**1.3**	**0.9**	**26**	**07**	**296**	**1**	**0.6**

27	**17**	**115**	**1.6**	**0.9**	**27**	**03**	**78**	**1**	**0.5**	**27**	**26**	**15**	**1.6**	**0.9**
28	**10**	**0**	**1.9**	**1**	**28**	**12**	**250**	**2.5**	**1.2**	**28**	**10**	**66**	**2**	**1.3**
29	**21**	**72**	**1.6**	**0.9**	**29**	**60**	**97**	**1.6**	**1**	**29**	**10**	**74**	**2.5**	**1.5**
30	**04**	**215**	**2.3**	**1.4**	**30**	**49**	**92**			**30**	**11**	**357**	**6.5**	**3.6**
31	**20**	**105**	**3.2**	**1.1**	**31**	**02**	**252**	**1.6**	**0.9**	**31**	**10**	**72**	**1.1**	**0.6**
32	**15**	**46**	**1.5**	**1**	**32**	**09**	**23**	**1.2**	**0.6**	**32**	**15**	**30**	**1.4**	**0.8**
33	**34**	**112**	**4**	**2.6**	**33**	**36**	**100**	**5.1**	**3.5**	**33**	**11**	**12**	**1.2**	**0.7**
34	**22**	**15**	**1.1**	**0.7**	**34**	**15**	**91**	**1.1**	**0.8**	**34**	**23**	**15**	**1.1**	**0.7**
35	**22**	**44**	**1**	**0.6**	**35**	**17**	**56**	**4.8**	**2.6**	**35**	**09**	**101**	**1.3**	**0.8**
36	**28**	**254**	**2**	**1.1**	**36**	**35**	**95**	**1**	**0.7**	**36**	**18**	**40**	**1.3**	**0.6**
37	**18**	**81**	**2.3**	**1.1**	**37**	**22**	**45**	**1.3**	**0.8**	**37**	**09**	**234**	**1.3**	**0.7**
38	**06**	**215**	**1.5**	**0.7**	**38**	**47**	**53**	**1.1**	**0.7**	**38**	**44**	**24**	**1.9**	**1.1**
39	**26**	**93**	**1.5**	**0.7**	**39**	**26**	**78**	**1.4**	**0.9**	**39**	**15**	**38**	**2**	**1**
40	**34**	**49**	**2.3**	**1.2**	**40**	**33**	**62**	**1**	**0.6**	**40**	**12**	**256**	**1.5**	**0.8**
41	**30**	**60**	**2.3**	**1.2**	**41**	**26**	**240**	**1.2**	**0.8**	**41**	**16**	**59**	**1.4**	**0.8**

42	**30**	**96**	**1.6**	**1**	**42**	**23**	**87**	**1**	**0.5**	**42**	**03**	**20**	**1**	**0.6**
43	**22**	**62**	**1.4**	**0.9**	**43**	**00**	**92**	**2.2**	**1.2**	**43**	**03**	**86**	**1**	**0.5**
44	**25**	**152**	**3**	**1.9**	**44**	**30**	**115**	**1.5**	**1**	**44**	**44**	**10**	**2.3**	**1.5**
45	**62**	**68**	**4.2**	**2.5**	**45**	**23**	**63**	**1**	**0.6**	**45**	**18**	**85**	**2.3**	**1.4**
46	**22**	**318**	**2**	**1**	**46**	**04**	**238**	**1.9**	**1.1**	**46**	**32**	**33**	**2.4**	**1.3**
47	**22**	**78**	**2.9**	**1.6**	**47**	**17**	**60**	**2.4**	**1.2**	**47**	**25**	**75**	**1.7**	**0.9**
48	**28**	**55**	**1.8**	**1.4**	**48**	**17**	**65**	**1.3**	**0.7**	**48**	**20**	**56**	**2.7**	**1.6**
49	**09**	**12**	**1.2**	**0.6**	**49**	**23**	**79**	**2.4**	**1.5**	**49**	**02**	**77**	**1**	**0.7**
50	**17**	**112**	**1.6**	**1.2**	**50**	**18**	**69**	**1**	**0.6**	**50**	**46**	**68**	**1.6**	**0.8**

Stratigraphic section 3

5th hole					8th hole				
Clast	Trend (°)	Plunge (°)	a-axis (cm)	b-axis (cm)	Clast	Trend (°)	Plunge (°)	a-axis (cm)	b-axis (cm)
1	11	145	1.1	0.8	1	115	15	1.4	0.4
2	19	45	2.1	1.5	2	124	19	4	2.6
3	21	90	1.5	0.9	3	130	14	2.3	1.7
4	00	100	0.7	0.4	4	300	77	2.4	1.6
5	10	75	0.8	0.4	5	126	6	0	0
6	12	182	9	3.3	6	110	11	1.4	0.9
7	07	33	2.3	1.5	7	124	5	0.9	0.4
8	08	32	1.3	0.6	8	83	51	4.1	1.8
9	08	305	1	0.6	9	250	23	3.7	2.5
10	11	84	2	0.9	10	283	0	2.4	2
11	09	10	2.4	1.3	11	260	10	2.8	1.4
12	07	210	1.9	1	12	269	10	1.7	1
13	04	35	2.8	2.2	13	328	7	1.2	0.7
14	01	266	1.6	1.2	14	222	30	1.5	0.9
15	38	178	2.2	1.3	15	356	76	3.6	2.4
16	09	42	1.7	1	16	265	7	0.9	0.7
17	16	58	2.6	1.4	17	333	5	2	0.6
18	12	31	1.8	1.1	18	338	7	1.4	0.6
19	22	45	1.8	0.7	19	200	66	1.5	1.2

20	**16**	**236**	**1.3**	**0.9**	**20**	**355**	**2**	**1.7**	**1.2**
21	**02**	**290**	**3.7**	**1.8**	**21**	**160**	**6**	**1**	**0.4**
22	**04**	**138**	**3.9**	**2.5**	**22**	**85**	**12**	**0.7**	**0.5**
23	**05**	**58**	**2.5**	**1.5**	**23**	**205**	**26**	**0.8**	**0.6**
24	**14**	**60**			**24**	**249**	**12**	**1.2**	**0.8**
25	**04**	**21**	**1.2**	**0.7**	**25**	**266**	**35**	**1**	**0.7**
26	**10**	**64**	**1.5**	**0.8**	**26**	**333**	**3**	**1.4**	**0.9**
27	**02**	**45**	**3.6**	**2.6**	**27**	**279**	**56**	**0.7**	**0.4**
28	**03**	**23**	**2.4**	**1.4**	**28**	**213**	**40**	**0.8**	**0.6**
29	**05**	**25**	**2.7**	**1.8**	**29**	**85**	**27**	**1.3**	**1**
30	**03**	**91**	**2.7**	**1.4**	**30**	**273**	**4**	**1.3**	**0.9**
31	**05**	**34**	**1.7**	**0.8**	**31**	**115**	**4**	**1.6**	**0.9**
32	**06**	**16**	**2.1**	**1.5**	**32**	**173**	**11**	**1.2**	**0.9**
33	**15**	**50**	**2.9**	**2.3**	**33**	**169**	**18**	**0.6**	**0.4**
34	**16**	**13**	**1.4**	**0.9**	**34**	**198**	**8**	**0.7**	**0.4**
35	**10**	**67**	**1.4**	**0.8**	**35**	**126**	**22**	**0.7**	**0.3**
36	**00**	**283**	**2.6**	**1.3**	**36**	**172**	**9**	**2.2**	**1.1**
37	**00**	**95**	**2**	**1.2**	**37**	**249**	**8**	**0.7**	**0.5**
38	**12**	**284**	**3**	**2.3**	**38**	**358**	**3**	**0.9**	**0.5**
39	**09**	**237**	**2.4**	**1.8**	**39**	**126**	**25**	**0.8**	**0.6**
40	**15**	**54**	**1.4**	**1**	**40**	**265**	**15**	**1.1**	**0.7**
41	**24**	**20**	**2.2**	**1.1**	**41**	**358**	**27**	**1.2**	**0.6**
42	**03**	**230**	**1.1**	**0.8**	**42**	**296**	**19**	**0.9**	**0.6**

43	**20**	**299**	**1.3**	**0.7**	**43**	**318**	**12**	**1.8**	**1**
44	**11**	**48**	**1.4**	**1**	**44**	**274**	**20**	**1.2**	**0.8**
45	**14**	**39**	**1.5**	**0.8**	**45**	**99**	**52**	**1.2**	**0.9**
46	**07**	**75**	**4.4**	**2**	**46**	**76**	**20**	**0.6**	**0.5**
47	**35**	**55**	**3.8**	**2.7**	**47**	**288**	**6**	**1.7**	**0.9**
48	**02**	**81**	**2.4**	**1.1**	**48**	**13**	**11**	**1.9**	**1.2**
49	**15**	**42**	**0.9**	**0.6**	**49**	**73**	**1**	**0.6**	**0.4**
50	**05**	**49**	**6.2**	**4.5**	**50**	**265**	**12**	**0.8**	**0.6**

12th hole					**16th hole**				
Clast	**Trend (°)**	**Plunge (°)**	**a-axis (cm)**	**b-axis (cm)**	**Clast**	**Trend (°)**	**Plunge (°)**	**a-axis (cm)**	**b-axis (cm)**
1	**32**	**15**	**4.5**	**2.8**	**1**	**59**	**53**	**3**	**1.5**
2	**19**	**10**	**0.7**	**0.5**	**2**	**05**	**32**	**2.5**	**1.5**
3	**283**	**2**	**0.6**	**0.3**	**3**	**20**	**85**	**2**	**1.5**
4	**275**	**14**	**0.6**	**0.4**	**4**	**19**	**45**	**1.7**	**1.1**
5	**50**	**20**	**2**	**0.5**	**5**	**51**	**288**	**1.9**	**0.5**
6	**8**	**10**	**1.2**	**0.8**	**6**	**33**	**62**	**1.7**	**0.8**
7	**10**	**16**	**1.2**	**0.8**	**7**	**28**	**289**	**1.9**	**0.9**
8	**7**	**42**	**1.8**	**1**	**8**	**43**	**76**	**3.5**	**2.1**
9	**5**	**4**	**1.8**	**1.2**	**9**	**17**	**1**	**2**	**1**
10	**53**	**25**	**1.1**	**0.7**	**10**	**72**	**159**	**1.5**	**1**

11	**64**	**39**	**0.6**	**0.4**	**11**	**39**	**350**	**2.3**	**1.3**
12	**355**	**74**	**1.4**	**0.9**	**12**	**13**	**31**	**1.6**	**1**
13	**79**	**11**	**0**	**0**	**13**	**24**	**50**	**1.8**	**1**
14	**6**	**7**	**0.6**	**0.4**	**14**	**21**	**25**	**4**	**2.2**
15	**76**	**62**	**4.5**	**3**	**15**	**30**	**12**	**3.2**	**2**
16	**358**	**35**	**3.3**	**2.8**	**16**	**40**	**252**	**2**	**1**
17	**189**	**51**	**0.8**	**0.6**	**17**	**60**	**177**	**1.4**	**0.7**
18	**89**	**4**	**1.3**	**1**	**18**	**02**	**260**	**1.5**	**1.1**
19	**353**	**6**	**0.7**	**0.5**	**19**	**46**	**355**	**2**	**1.2**
20	**174**	**5**	**1.2**	**0.8**	**20**	**24**	**24**	**2.2**	**1.3**
21	**115**	**36**	**0.8**	**0.5**	**21**	**31**	**352**	**1.8**	**1.1**
22	**4**	**20**	**1.3**	**0.7**	**22**	**22**	**25**	**3.8**	**2.5**
23	**9**	**54**	**1.7**	**1.2**	**23**	**32**	**312**	**1.2**	**0.8**
24	**75**	**6**	**0.5**	**0.4**	**24**	**20**	**24**	**1.3**	**0.6**
25	**8**	**18**	**1.1**	**0.7**	**25**	**27**	**359**	**3.3**	**1.7**
26	**72**	**34**	**2.7**	**1.7**	**26**	**20**	**29**	**2**	**1.4**
27	**6**	**11**	**0.7**	**0.5**	**27**	**00**	**69**	**1.5**	**1**
28	**50**	**38**	**0.8**	**0.5**	**28**	**46**	**322**	**2.5**	**1**
29	**135**	**12**	**0.9**	**0.6**	**29**	**38**	**31**	**4**	**2**
30	**83**	**2**	**0.6**	**0.4**	**30**	**15**	**332**	**2.8**	**1.6**
31	**87**	**4**	**1**	**0.6**	**31**	**33**	**314**	**1.3**	**0.9**
32	**85**	**5**	**0.8**	**0.6**	**32**	**34**	**15**	**3.1**	**2**

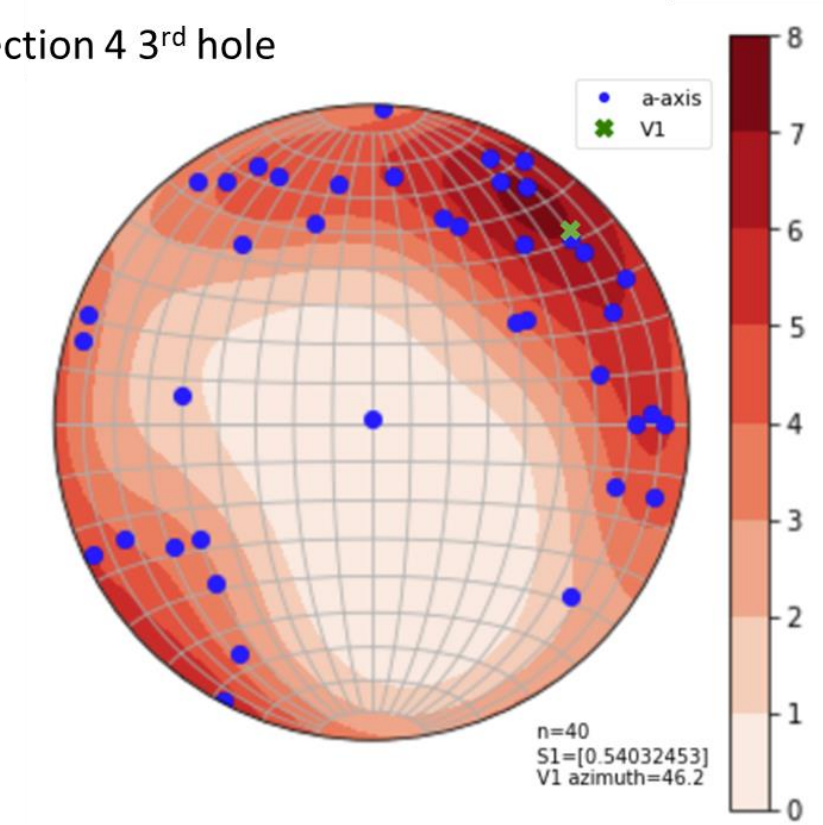
33	**172**	**5**	**0.8**	**0.6**	**33**	**20**	**320**	**0.9**	**0.6**
34	**65**	**36**	**0.5**	**0.4**	**34**	**42**	**22**	**3.6**	**1.5**
35	**48**	**28**	**1.3**	**0.6**	**35**	**26**	**39**	**2.2**	**1**
36	**8**	**10**	**0.7**	**0.35**	**36**	**30**	**288**	**2.1**	**1.6**
37	**174**	**2**	**1**	**0.7**	**37**	**52**	**189**	**1.5**	**1**
38	**10**	**14**	**0.9**	**0.6**	**38**	**25**	**326**	**1.9**	**1.1**
39	**72**	**21**	**0.7**	**0.4**	**39**	**09**	**1**	**1.8**	**0.9**
40	**67**	**12**	**1.2**	**0.7**	**40**	**51**	**21**	**0.8**	**0.5**
41	**31**	**0**	**2.2**	**1.6**	**41**	**15**	**4**	**1.9**	**1.4**
42	**78**	**38**	**1.5**	**1**	**42**	**58**	**290**	**1.5**	**1**
43	**33**	**0**	**1.2**	**0.8**	**43**	**32**	**32**	**1**	**0.6**
44	**12**	**26**	**1.2**	**1**	**44**	**27**	**0**	**2.8**	**2.2**
45	**220**	**28**	**1.3**	**0.7**	**45**	**35**	**124**	**2**	**0.8**
46	**262**	**90**	**2.3**	**1.3**	**46**	**28**	**2**	**1.8**	**1.1**
47	**0**	**5**	**1.7**	**1.4**	**47**	**20**	**5**	**1.8**	**1.1**
48	**358**	**15**	**1.4**	**0.7**	**48**	**62**	**70**	**1.1**	**0.8**
49	**350**	**3**	**0.6**	**0.4**	**49**	**34**	**322**	**1.2**	**0.7**
50	**165**	**2**	**0.9**	**0.5**	**50**	**23**	**30**	**2.4**	**1.8**

Stratigraphic section 4

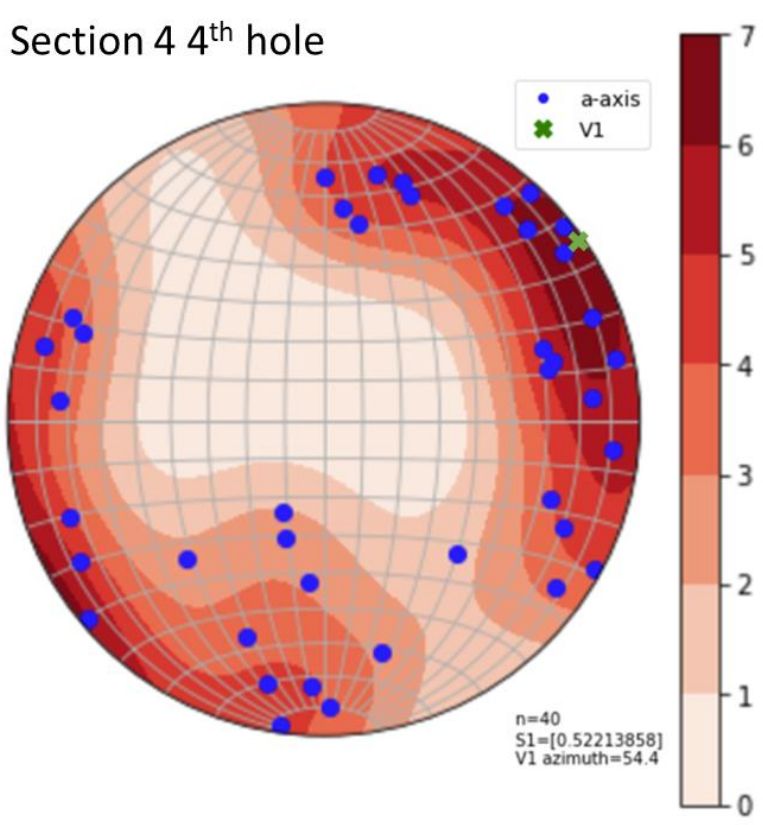
3rd hole					4th hole				
Clast	Trend (°)	Plunge (°)	a-axis (cm)	b-axis (cm)	Clast	Trend (°)	Plunge (°)	a-axis (cm)	b-axis (cm)
1	35	236	2.2	1.4	1	20	290	2.3	1.2
2	22	105	2.6	2.1	2	15	249	2.7	2
3	27	238	0.9	0.5	3	09	285	2.2	1.1
4	09	90	0.6	0.4	4	07	78	1.5	1
5	16	47	7.7	4.5	5	04	42	6.2	4.8
6	18	90	2	1.3	6	38	225	1.3	1
7	15	245	3.6	2	7	47	185	1.1	0.8
8	39	278	4.8	3	8	17	274	4	3.2
9	06	286	4.2	2.6	9	10	69	4	2
10	30	224	1.8	1.2	10	03	119	2.6	1.4
11	03	245	1.5	0.8	11	09	96	1	0.8
12	89	355	2.9	1.8	12	22	12	2.1	1.8
13	23	5	2	1.2	13	25	109	1.7	1.2
14	15	28	1.7	1	14	25	166	1.6	0.8
15	01	2	4.3	3	15	28	77	2.1	1.3
16	35	344	4.7	3.5	16	64	205	2.7	2.1
17	25	352	4.5	2.2	17	37	10	2	1.3
18	17	210	2.1	1.1	18	12	240	2.5	1.7

19	**05**	**30**	**2.4**	**1.5**	**19**	**15**	**292**	**4.6**	**2.7**
20	**18**	**339**	**0.8**	**0.4**	**20**	**13**	**47**	**6**	**3.5**
21	**41**	**56**	**1.9**	**1.1**	**21**	**03**	**230**	**2.9**	**1.6**
22	**33**	**24**	**1.3**	**0.7**	**22**	**10**	**179**	**1.1**	**0.7**
23	**13**	**88**	**0.8**	**0.4**	**23**	**17**	**183**	**1.2**	**0.9**
24	**32**	**19**	**4.2**	**1.6**	**24**	**16**	**192**	**3.2**	**2.2**
25	**31**	**324**	**2.3**	**1.5**	**25**	**09**	**55**	**12**	**7.5**
26	**01**	**208**	**1.3**	**0.7**	**26**	**25**	**21**	**1.5**	**1**
27	**07**	**324**	**4**	**2.2**	**27**	**11**	**126**	**1.2**	**0.9**
28	**18**	**65**	**1.1**	**0.8**	**28**	**13**	**40**	**1.9**	**1.3**
29	**18**	**131**	**3.5**	**2.4**	**29**	**28**	**200**	**1.9**	**1.1**
30	**05**	**291**	**2.5**	**1.6**	**30**	**22**	**18**	**1.2**	**0.4**
31	**28**	**78**	**1**	**0.5**	**31**	**03**	**51**	**4**	**2**
32	**12**	**336**	**3.8**	**2.7**	**32**	**16**	**85**	**1**	**0.5**
33	**44**	**55**	**3**	**1.7**	**33**	**28**	**72**	**2.2**	**1.4**
34	**09**	**105**	**2.7**	**1.7**	**34**	**03**	**188**	**1.5**	**0.5**
35	**09**	**60**	**3.6**	**2.5**	**35**	**40**	**135**	**2.3**	**1.5**
36	**15**	**51**	**0.8**	**0.5**	**36**	**18**	**114**	**3.3**	**1**
37	**27**	**40**	**0.8**	**0.5**	**37**	**26**	**76**	**1.2**	**0.8**
38	**12**	**33**	**2.1**	**1**	**38**	**58**	**198**	**2.1**	**1.5**
39	**12**	**329**	**2**	**1.4**	**39**	**24**	**0**	**2.5**	**1.5**
40	**10**	**24**	**2**	**1.4**	**40**	**33**	**5**	**2.9**	**1.6**

Section 4 3rd hole



Section 4 4th hole



Appendix C

Clast Lithology Counts Data

Drumlin					Canadian Shield							WCSB				
	Sample number	Felsic	Mafic	Quartzite	Total	Per (%)	Carbonate	Red dolostone	Sand/Silt/Mudstone	Shale	Dark siltstone	Total	Per (%)	other	Total	Comment
Section 1	21-PXN-025A	49	43	2	94	33.45	126	20	33	8	0	187	66.55		281	
	21-PXN-026A	103	62	2	167	45.88	126	14	41	16	0	197	54.12		364	
	21-PXN-027A	137	64	3	204	44.35	166	19	47	24	0	256	55.65		460	
	21-PXN-	117	79	2	198	43.	153	18	52	30	0	253	56.1		451	

	028A					90							0			
	21-PXN-029A	99	86	5	190	42.70	136	18	61	40	0	255	57.30		445	
	21-PXN-030A	72	67	8	147	37.03	145	24	63	18	0	250	62.97		397	
	21-PXN-031A	104	80	4	188	39.00	193	21	55	25	0	294	61.00		482	
	21-PXN-032A	97	81	5	183	35.40	212	34	56	32	0	334	64.60		517	
Section 2	21-PXN-033A	64	45	5	114	31.32	166	15	57	12	0	250	68.68		364	
	21-PXN-	74	48	5	127	33.87	167	21	48	12	0	248	66.13		375	

	034A															
	21-PXN-035A	**88**	**79**	**5**	**172**	**38.65**	**169**	**24**	**62**	**18**	**0**	**273**	**61.35**		**445**	
	21-PXN-036A	**78**	**70**	**5**	**153**	**37.78**	**157**	**13**	**58**	**23**	**0**	**251**	**61.98**	**1**	**405**	**One chert**
	21-PXN-037A	**63**	**95**	**2**	**160**	**38.37**	**155**	**18**	**53**	**31**	**0**	**257**	**61.63**		**417**	
	21-PXN-038A	**104**	**85**	**7**	**196**	**43.56**	**154**	**18**	**56**	**26**	**0**	**254**	**56.44**		**450**	
	21-PXN-039A	**63**	**72**	**6**	**141**	**31.69**	**174**	**18**	**66**	**46**	**0**	**304**	**68.31**		**445**	
	21-PXN-	**96**	**82**	**4**	**182**	**36.25**	**173**	**23**	**86**	**38**	**0**	**320**	**63.75**		**502**	

	040A															
Section 3	21-WL-001A	54	48	3	105	35.12	103	18	52	21	0	194	64.88		299	One quartz vein
	21-WL-002A	66	47	4	117	30.15	142	23	54	52	0	271	69.85		388	
	21-WL-003A	118	96	9	223	43.39	149	22	85	35	0	291	56.61		514	
	21-WL-004A	74	62	3	139	39.15	92	17	67	40	0	216	60.85		355	
Section 4	21-PXN-062A	66	51	0	117	30.79	168	12	54	29	0	263	69.21		380	
	21-PXN-063A	68	64	6	138	27.99	240	21	51	43	0	355	72.01		493	
	21-PXN-	71	73	1	145	28.66	223	16	73	49	0	361	71.34		506	

	064A															
	21-PXN-065A	81	93	3	177	34.77	221	19	55	37	0	332	65.23		509	
Other samples	21-PXN-012A	90	68	8	166	47.98	64	14	74	28	0	180	52.02		346	
	21-PXN-024A	209	109	21	339	70.77	0	22	83	35	0	140	29.23		479	One quartz vein
	21-PXN-021A	90	56	5	151	49.35	103	9	41	2	0	155	50.65		306	No carbonate
	21-PXN-016A	10	3	0	13	4.73	258	0	4	0	0	262	95.27		275	
	21-PXN-	38	21	1	60	15.42	84	10	110	58	65	327	84.06	2	389	1/2 total

	042A															
	21-PXN-022A	72	70	9	151	42.90	125	20	53	0	0	198	56.25	3	352	
	21-PXN-023A	75	64	11	150	32.19	180	34	99	1	0	314	67.38	2	466	
	21-PXN-013A	74	31	6	111	31.62	142	12	84	0	0	238	67.81	2	351	
	21-PXN-014A	78	46	5	129	32.09	160	24	85	0	0	269	66.92	4	402	
	21-PXN-020A	94	7	2	103	37.18	39	18	40	40	35	172	62.09	2	277	1/2 total
	21-PXN-	22	12	3	37	38.95	36	4	15	1	2	58	61.05		95	1/2 total

	019A															
	21-PXN-018A	**75**	**36**	**7**	**118**	**37.46**	**91**	**8**	**48**	**38**	**12**	**197**	**62.54**		**315**	
	21-PXN-060A	**72**	**39**	**6**	**117**	**41.05**	**62**	**5**	**40**	**51**	**8**	**166**	**58.25**	**2**	**285**	**1/8 total**
	21-PXN-017A	**51**	**11**	**6**	**68**	**86.08**	**1**	**0**	**9**	**1**	**0**	**11**	**13.92**		**79**	
	21-PXN-070A	**135**	**65**	**8**	**208**	**44.26**	**108**	**16**	**88**	**26**	**21**	**259**	**55.11**	**3**	**470**	
	21-PXN-074A	**56**	**38**	**2**	**96**	**29.72**	**71**	**7**	**95**	**43**	**11**	**227**	**70.28**		**323**	
	21-PXN-	**18**	**8**	**0**	**26**	**38.81**	**19**	**5**	**15**	**2**	**0**	**41**	**61.19**		**67**	**1/4 total**

	059A															
	21-PXN-071A	**156**	**69**	**3**	**228**	**48.82**	**18**	**25**	**178**	**2**	**16**	**239**	**51.18**		**467**	
	21-PXN-072A	**0**	**0**	**0**	**0**	**0.00**	**301**	**0**	**0**	**0**	**0**	**301**	**100.00**		**301**	**1/4 total**
	20-PXN-058A	**41**	**24**	**3**	**68**	**29.82**	**100**	**4**	**40**	**8**	**6**	**158**	**69.30**	**2**	**228**	**1/8 total**
	20-PXN-057A	**32**	**22**	**1**	**55**	**25.00**	**81**	**4**	**25**	**48**	**4**	**162**	**73.64**	**3**	**220**	
	20-PXN-048A	**68**	**44**	**5**	**117**	**38.87**	**92**	**17**	**73**	**0**	**0**	**182**	**60.47**	**2**	**301**	
	20-PXN-	**5**	**3**	**2**	**10**	**52.63**	**3**	**0**	**6**	**0**	**0**	**9**	**47.37**	**0**	**19**	

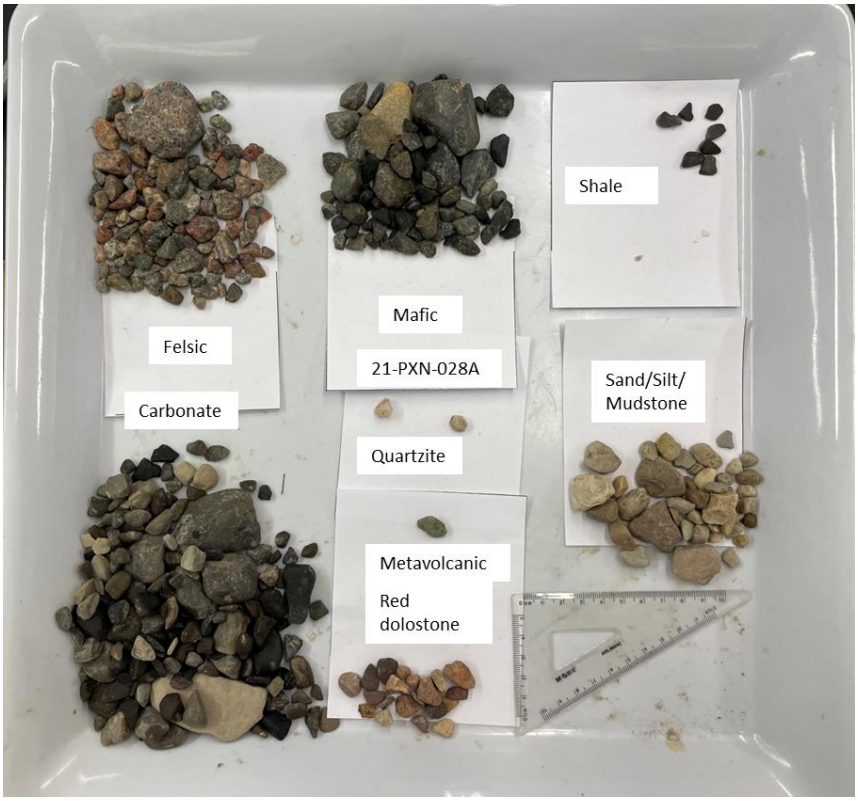
	037A															
	20-PXN-029A	**78**	**25**	**5**	**108**	**24.77**	**254**	**11**	**58**	**4**	**0**	**327**	**75.00**	**1**	**436**	
	20-PXN-028A	**80**	**24**	**3**	**107**	**36.90**	**102**	**6**	**67**	**0**	**8**	**183**	**63.10**	**0**	**290**	
	20-PXN-010A	**86**	**31**	**3**	**120**	**33.15**	**36**	**8**	**192**	**0**	**6**	**242**	**66.85**	**0**	**362**	**1/8 total**
	20-PXN-009A	**116**	**34**	**2**	**152**	**33.70**	**75**	**7**	**207**	**0**	**10**	**299**	**66.30**	**0**	**451**	
	20-PXN-030A	**81**	**18**	**5**	**104**	**28.65**	**140**	**5**	**109**	**0**	**5**	**259**	**71.35**	**0**	**363**	**1/2 total**
	20-PXN-	**57**	**16**	**0**	**73**	**23.70**	**124**	**12**	**99**	**0**	**0**	**235**	**76.30**	**0**	**308**	**1/2 total**

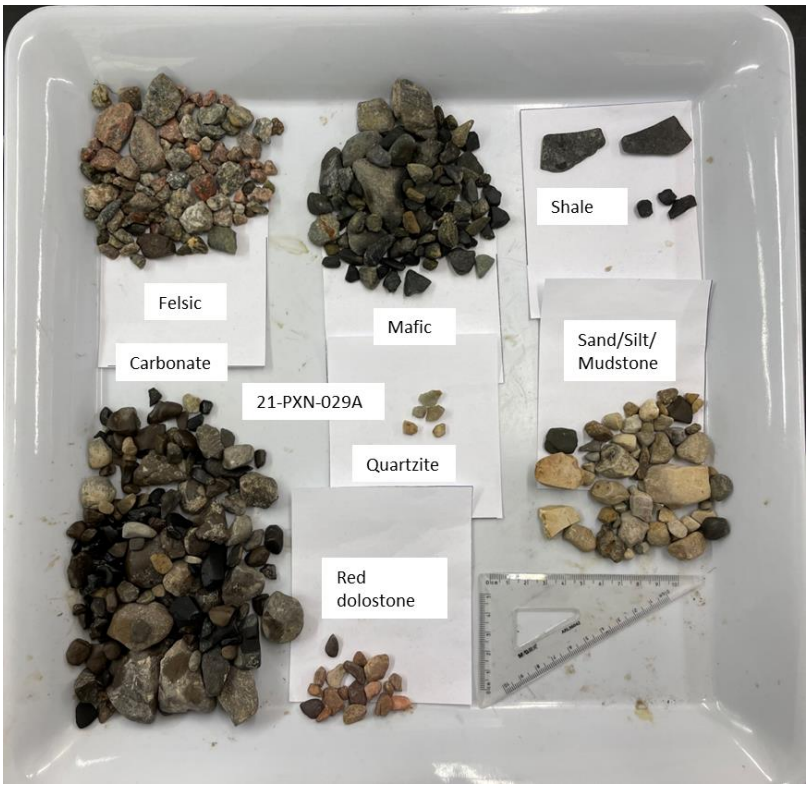
	047A															
	20-PXN-021A	**61**	**10**	**1**	**72**	**19.62**	**211**	**7**	**77**	**0**	**0**	**295**	**80.38**	**0**	**367**	**1/4 total**
	20-PXN-038A	**74**	**27**	**5**	**106**	**36.18**	**5**	**9**	**166**	**0**	**7**	**187**	**63.82**	**0**	**293**	
	20-PXN-031A	**56**	**17**	**2**	**75**	**26.69**	**127**	**7**	**43**	**15**	**14**	**206**	**73.31**	**0**	**281**	**1/4 total**
	21-PXN-044A	**53**	**22**	**4**	**79**	**20.41**	**205**	**11**	**82**	**8**	**2**	**308**	**79.59**	**0**	**387**	**1/2 total**

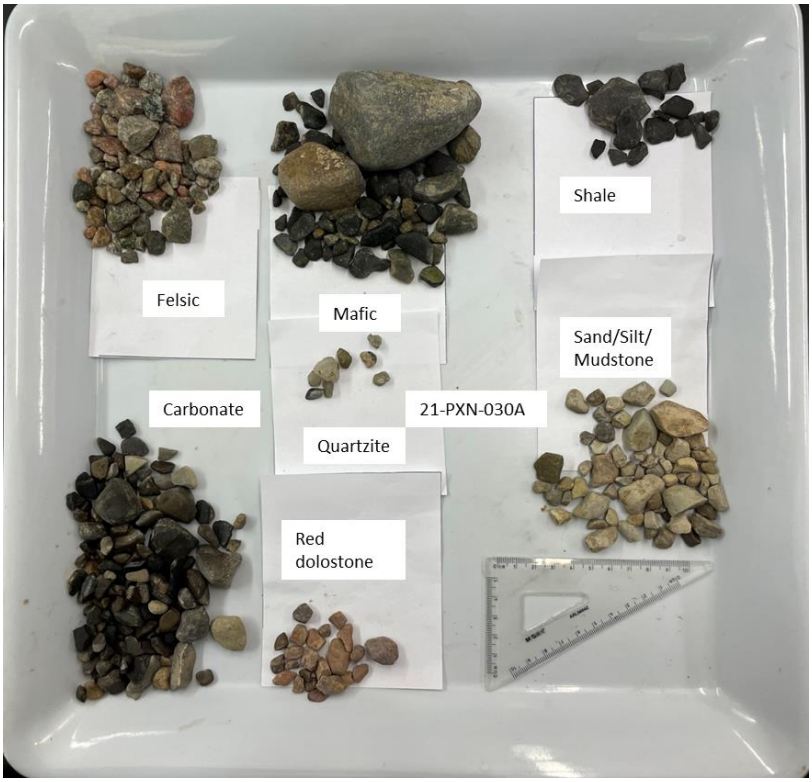

Felsic
Mafic
Shale
Carbonate
21-PXN-025A
Quartzite
Sandstone
/Siltstone


Shale
Mafic
Felsic
Sand/Silt/
Mudstone
Quartzite
Carbonate
21-PXN-026A
Red
dolostone

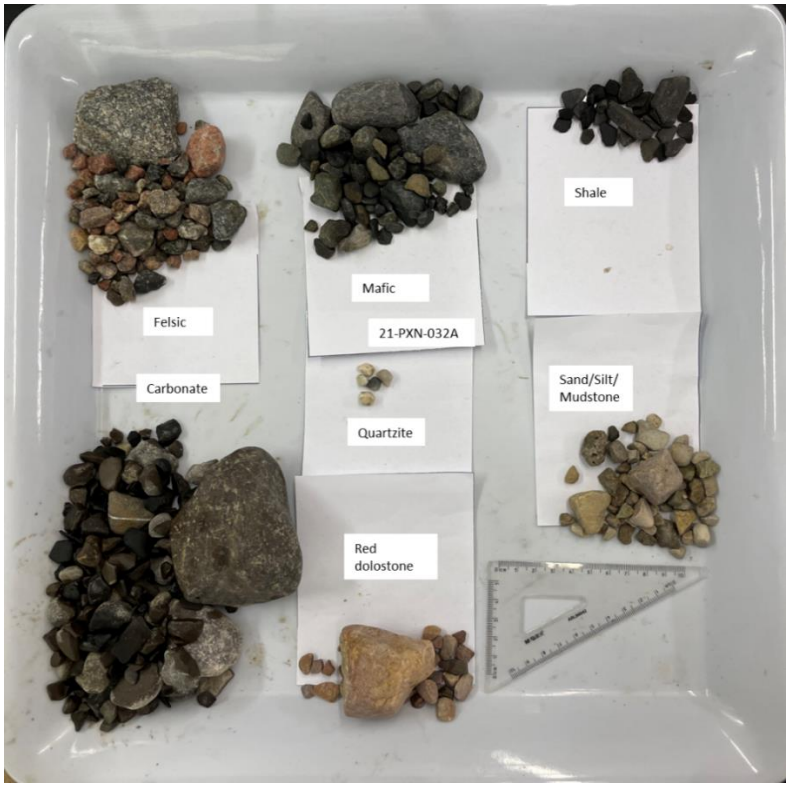

Felsic
Carbonate
Mafic
Quartzite
21-PXN-027A
Red
dolostone
Shale
Sand/Silt/
Mudstone

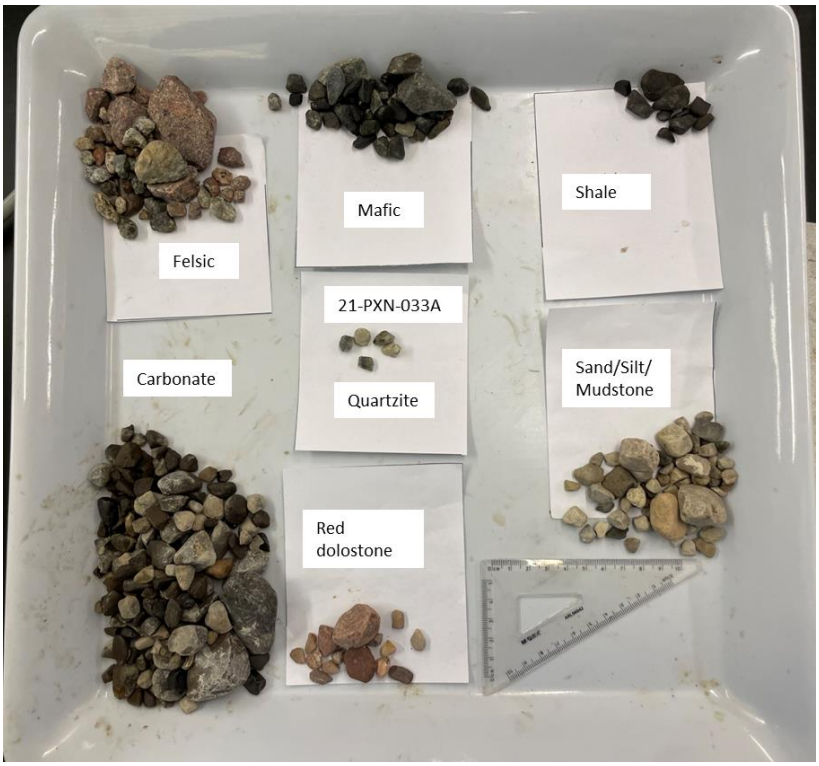

Felsic
Carbonate
Mafic
21-PXN-028A
Quartzite
Metavolcanic
Red
dolostone
Shale
Sand/Silt/
Mudstone

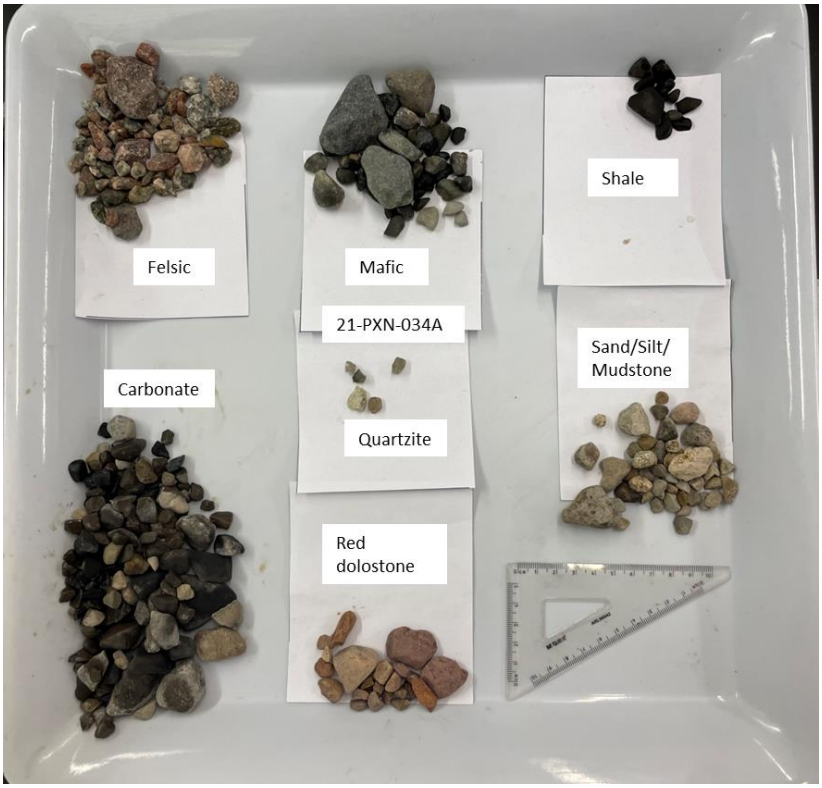

Felsic
Mafic
Shale
Carbonate
21-PXN-029A
Sand/Silt/
Mudstone
Quartzite
Red
dolostone


Felsic
Mafic
Shale
Carbonate
21-PXN-030A
Sand/Silt/
Mudstone
Quartzite
Red
dolostone

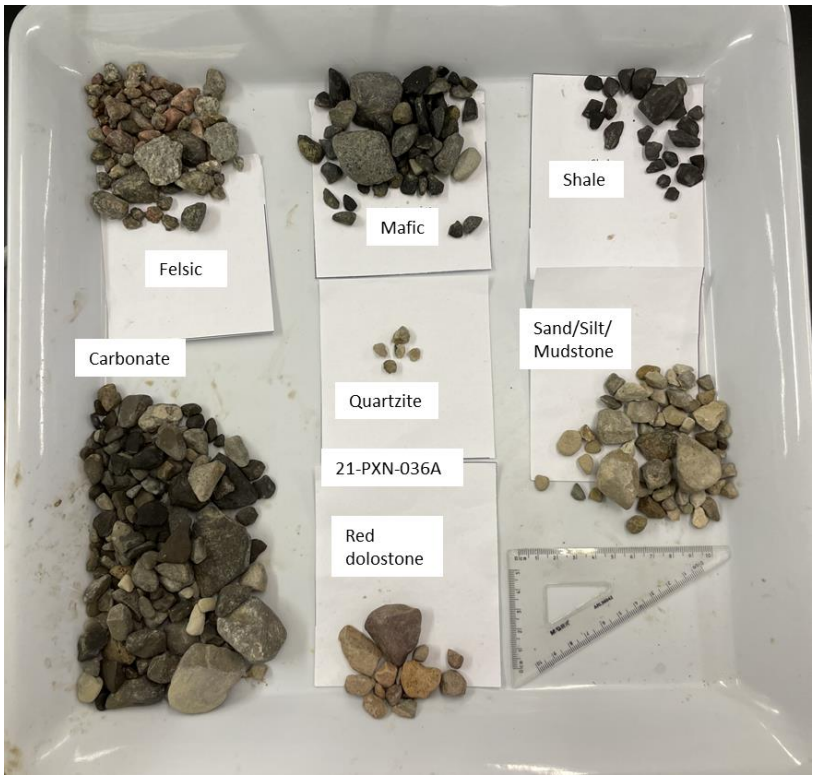

Felsic
Mafic
Shale
21-PXN-031A
Carbonate
Quartzite
Sand/Silt/
Mudstone
Red
dolostone

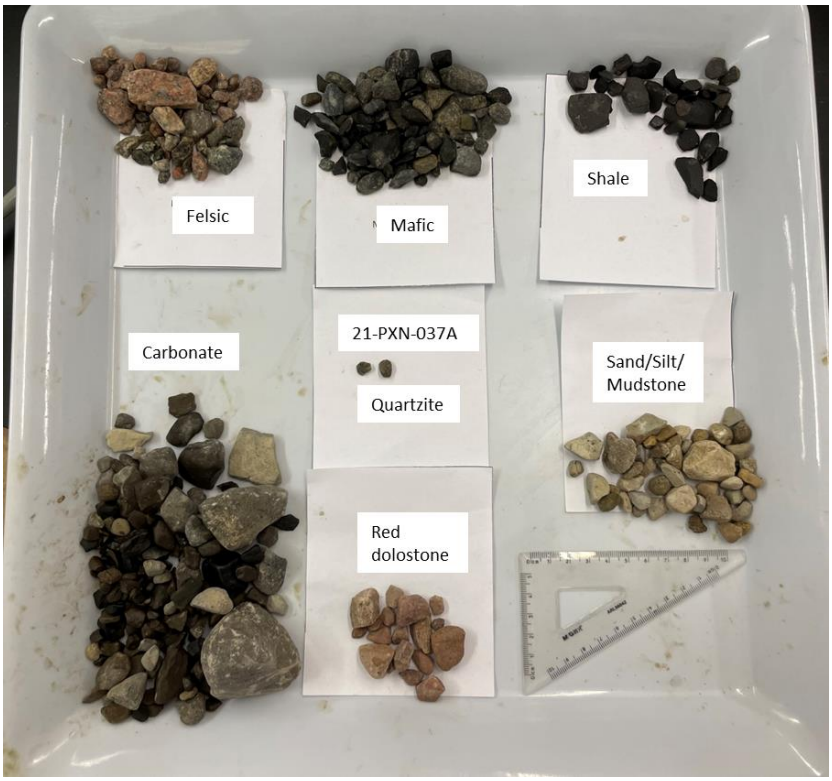

Felsic
Mafic
Shale
21-PXN-032A
Carbonate
Quartzite
Sand/Silt/
Mudstone
Red
dolostone

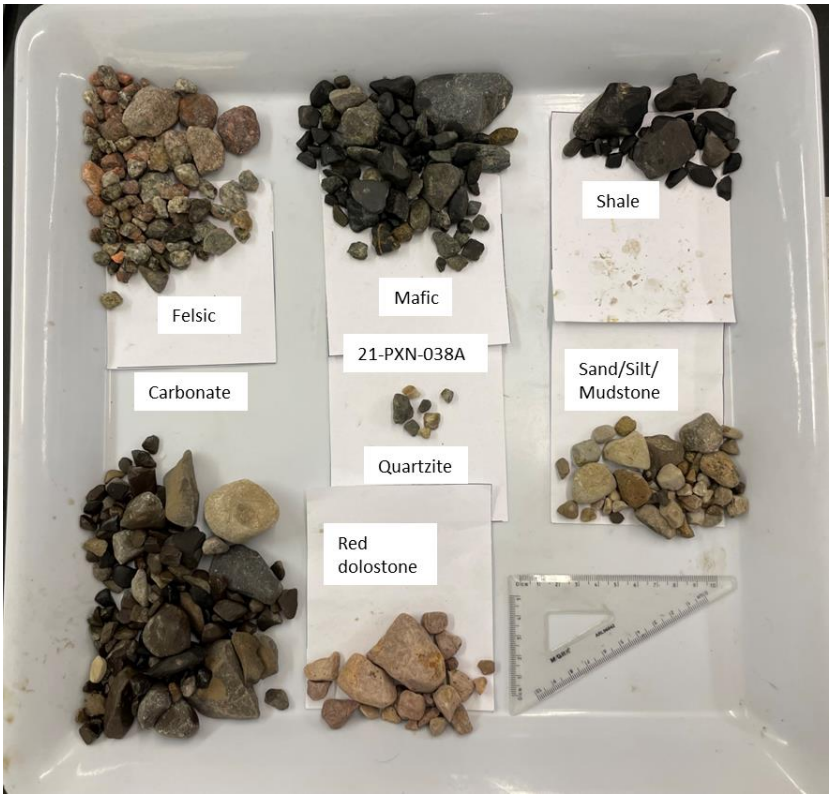

Felsic
Mafic
Shale
21-PXN-033A
Carbonate
Quartzite
Sand/Silt/
Mudstone
Red
dolostone


Felsic
Mafic
Shale
21-PXN-034A
Carbonate
Quartzite
Sand/Silt/
Mudstone
Red
dolostone


Felsic
Mafic
Shale
Carbonate
Quartzite
21-PXN-035A
Sand/Silt/
Mudstone
Red
dolostone


Felsic
Mafic
Shale
Carbonate
Quartzite
Sand/Silt/
Mudstone
21-PXN-036A
Red
dolostone

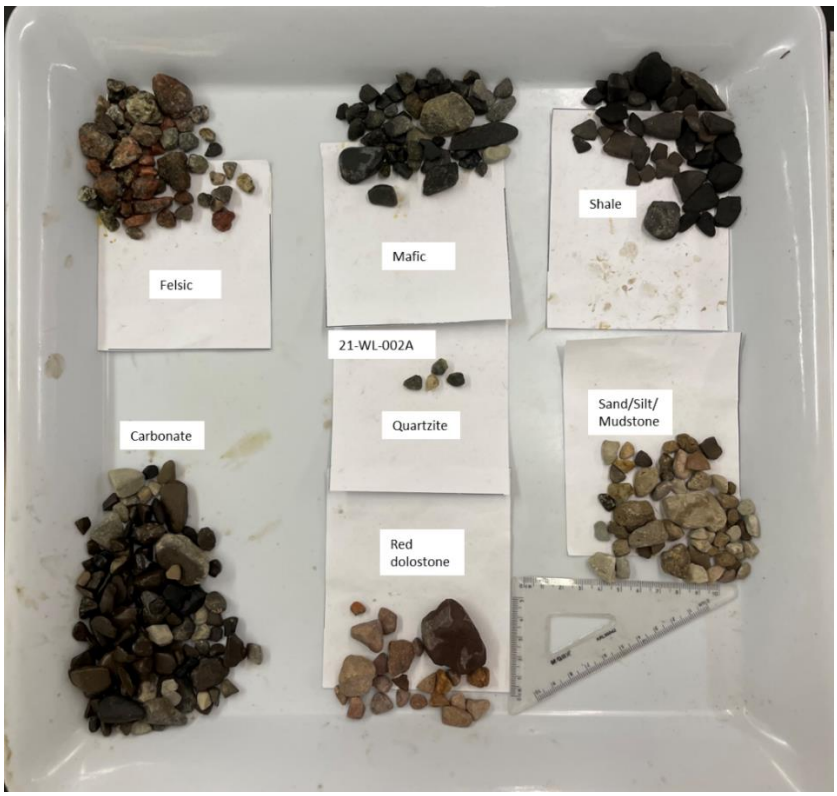

Felsic
Mafic
Shale
Carbonate
21-PXN-037A
Quartzite
Sand/Silt/
Mudstone
Red
dolostone

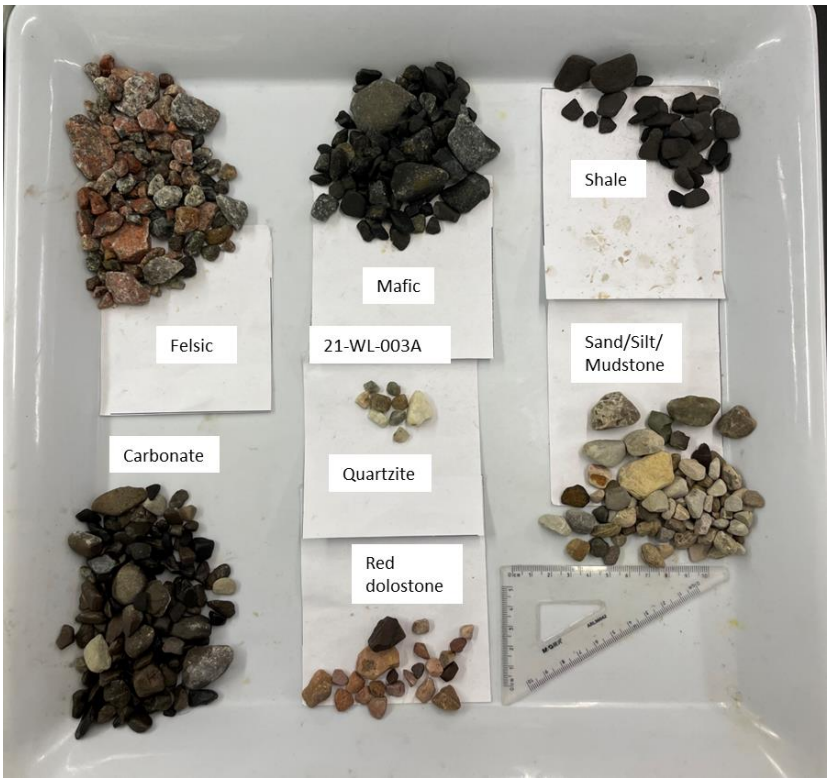

Felsic
Mafic
Shale
Carbonate
21-PXN-038A
Quartzite
Sand/Silt/
Mudstone
Red
dolostone

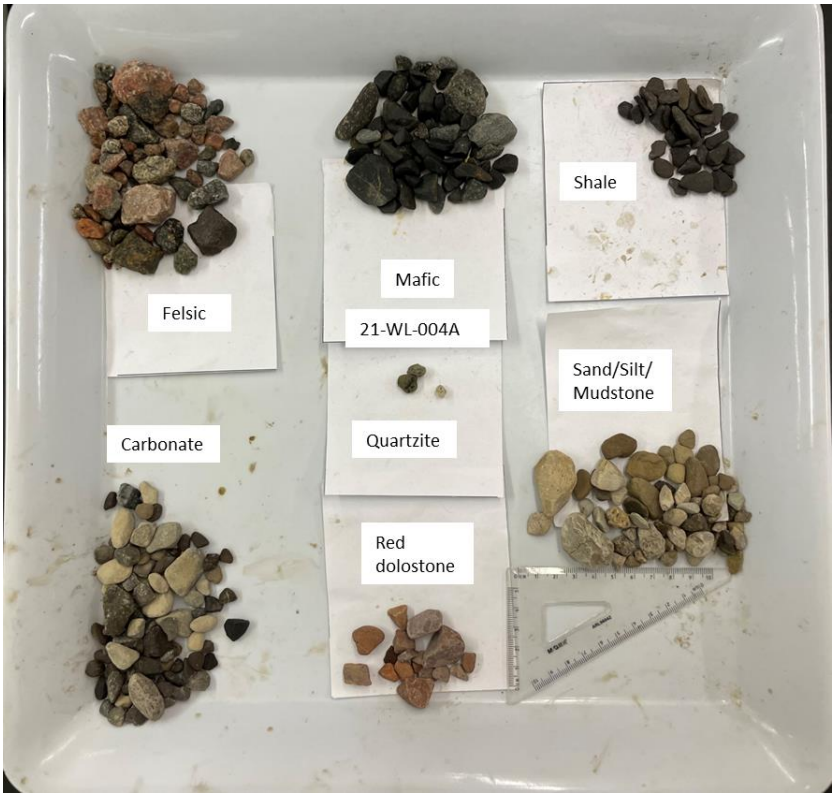

Felsic
Mafic
Shale
21-PXN-039A
Carbonate
Sand/Silt/
Mudstone
Quartzite
Red
dolostone

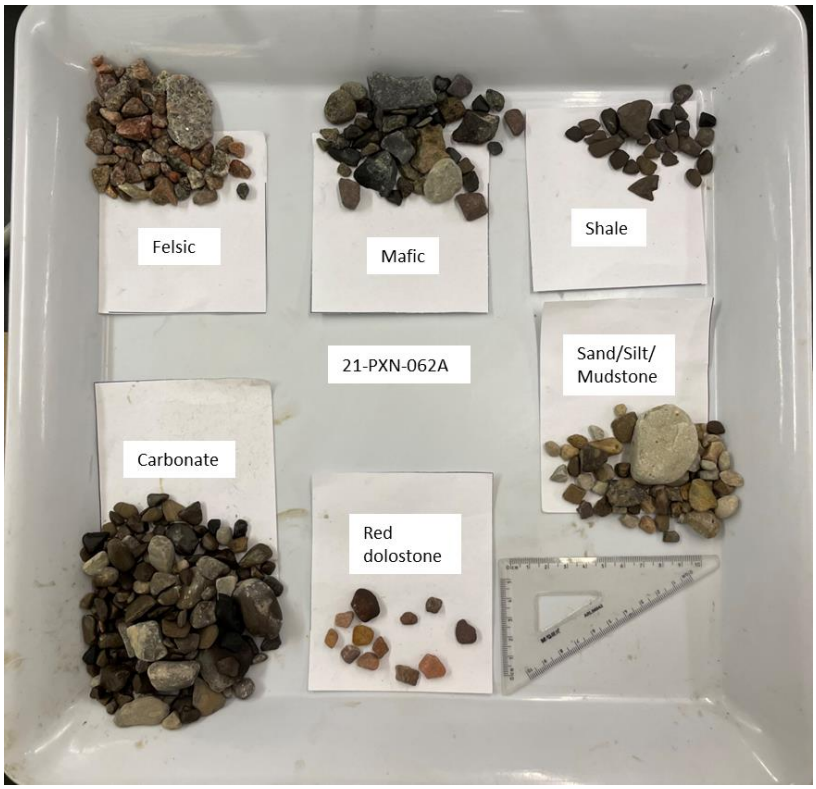

Shale
Mafic
Felsic
21-PXN-040A
Sand/Silt/
Mudstone
Carbonate
Quartzite
Red
dolostone

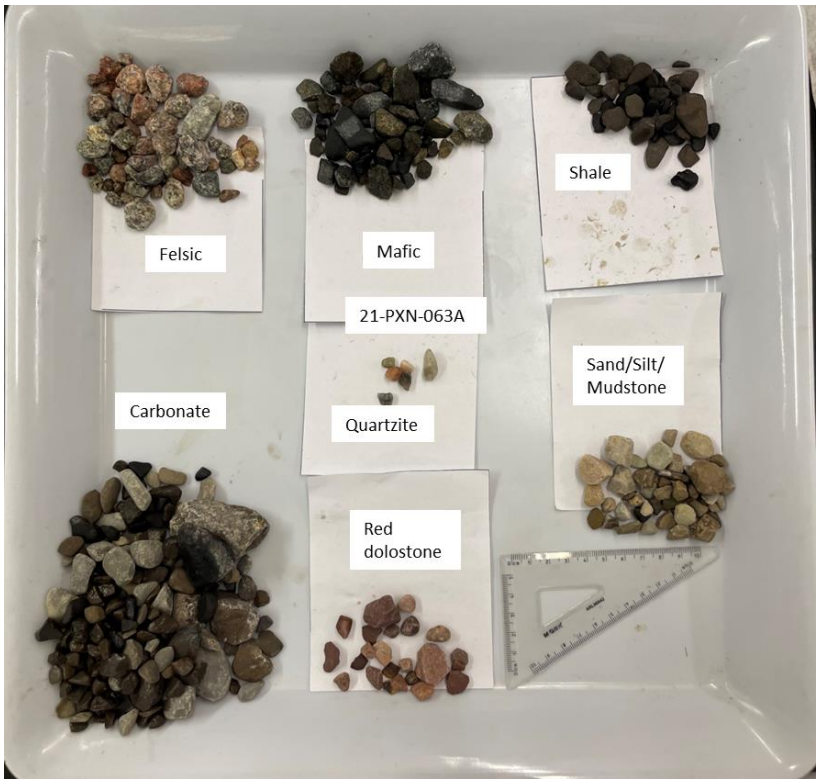

Felsic
Mafic
Shale
Sand/Silt/
Mudstone
Quartzite
Carbonate
21-WL-001A
Red
dolostone

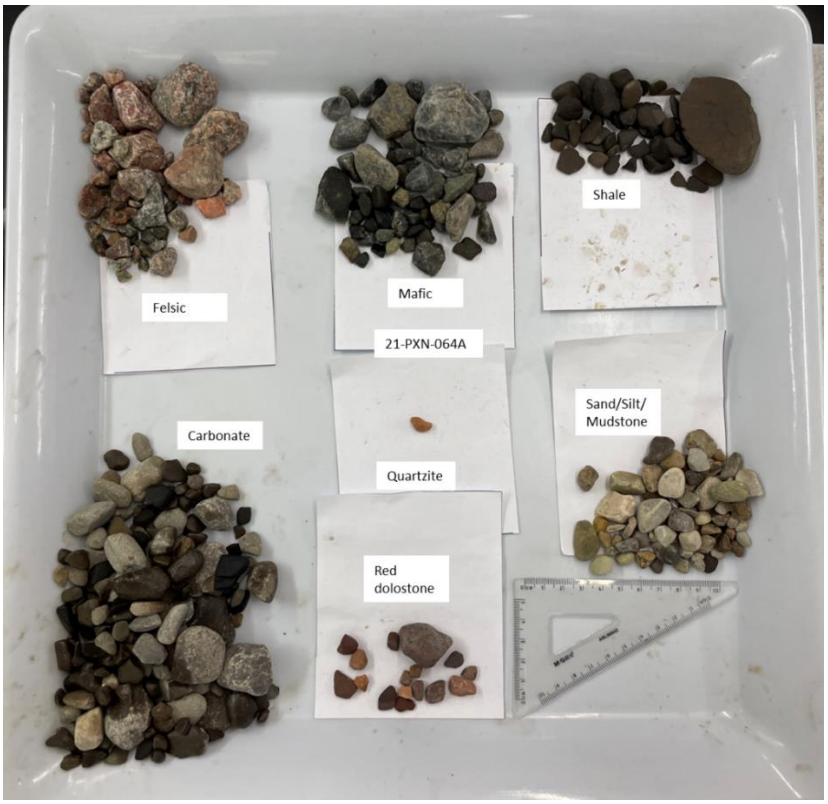

Felsic
Mafic
Shale
21-WL-002A
Sand/Silt/
Mudstone
Quartzite
Carbonate
Red
dolostone


Felsic
Mafic
21-WL-003A
Shale
Sand/Silt/
Mudstone
Carbonate
Quartzite
Red
dolostone


Felsic
Mafic
21-WL-004A
Shale
Sand/Silt/
Mudstone
Carbonate
Quartzite
Red
dolostone


Felsic
Mafic
Shale
21-PXN-062A
Sand/Silt/
Mudstone
Carbonate
Red
dolostone

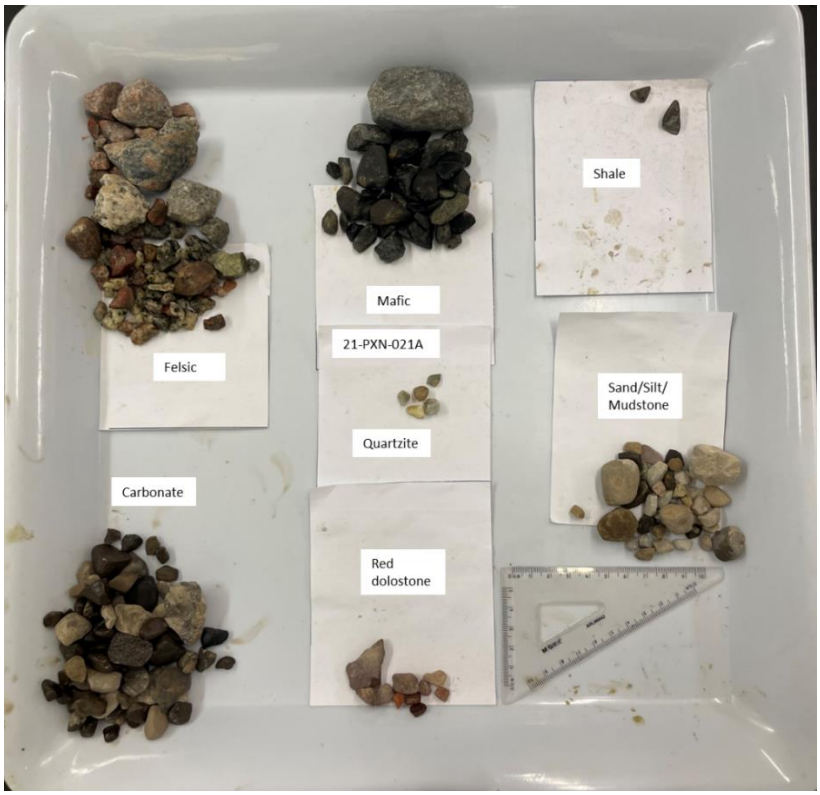

Felsic
Mafic
Shale
21-PXN-063A
Sand/Silt/
Mudstone
Carbonate
Quartzite
Red
dolostone

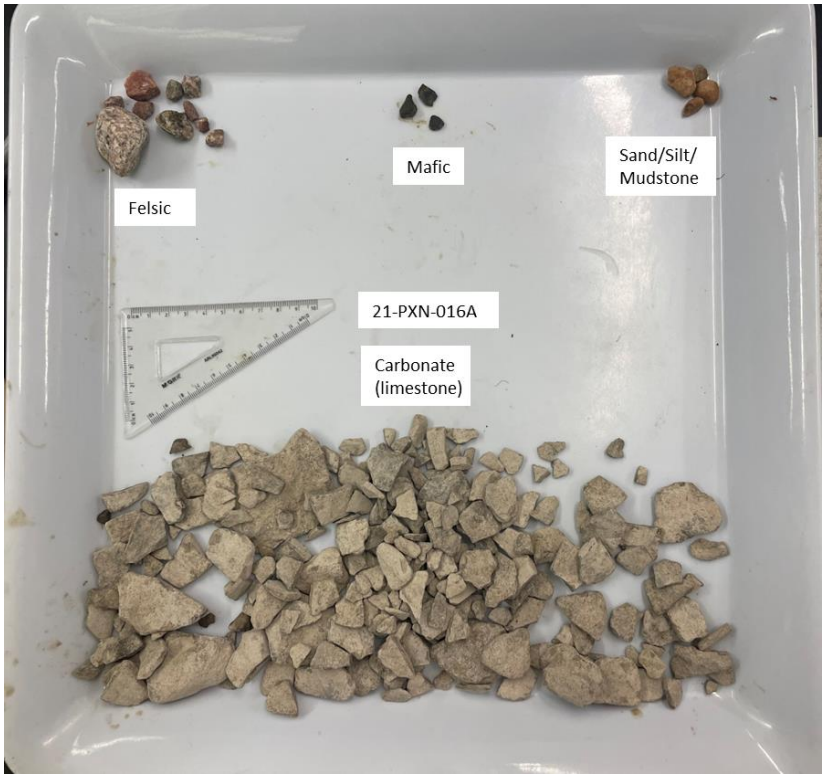

Felsic
Mafic
Shale
21-PXN-064A
Carbonate
Quartzite
Sand/Silt/
Mudstone
Red
dolostone

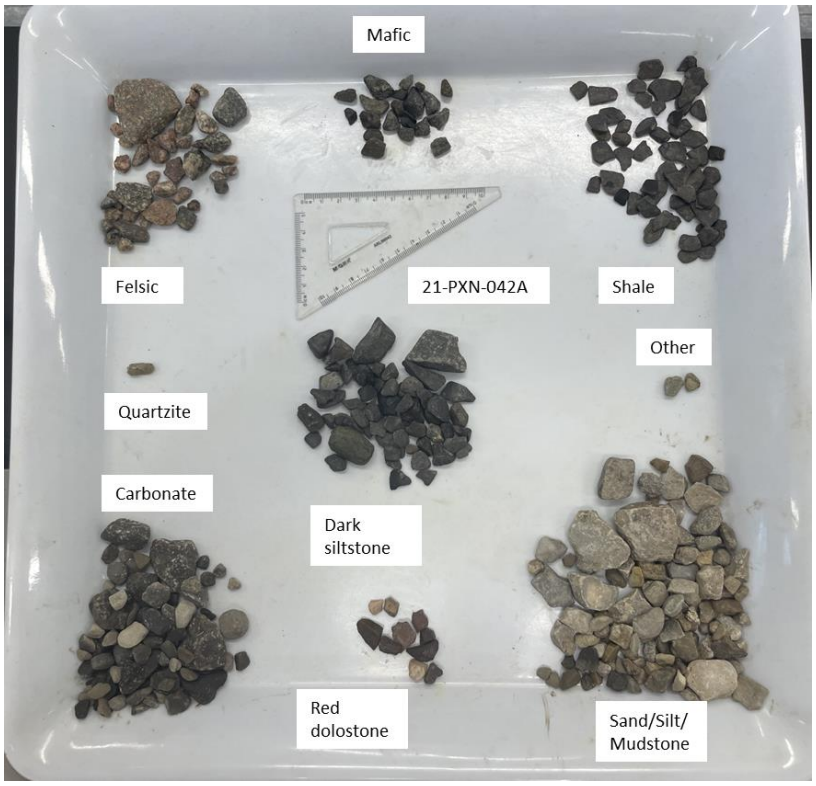

Felsic
Mafic
Shale
21-PXN-065A
Carbonate
Quartzite
Sand/Silt/
Mudstone
Red
dolostone

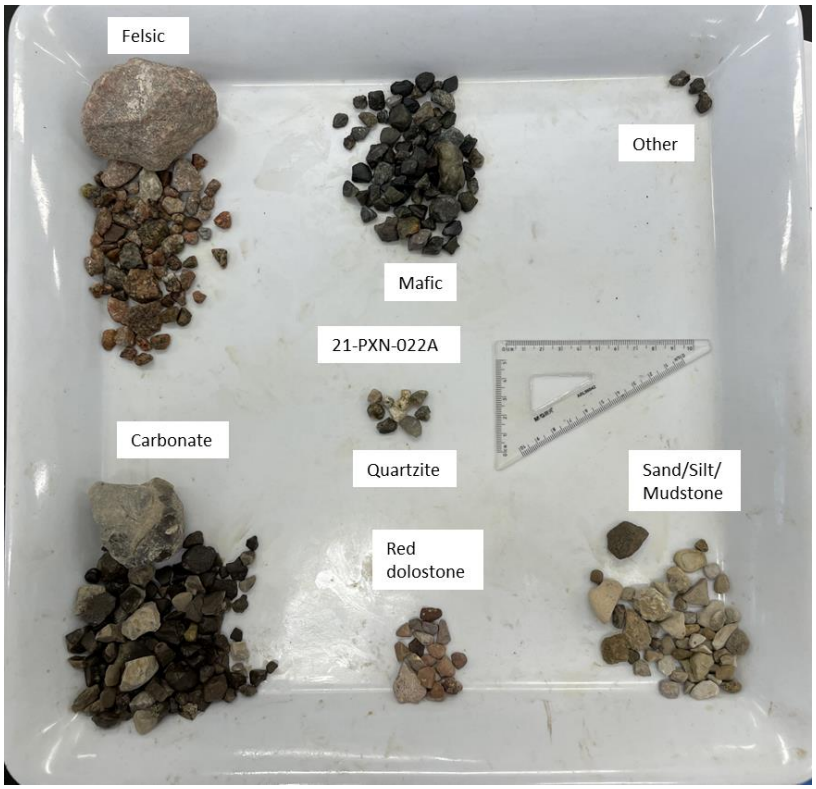

Felsic
Mafic
Shale
Sand/Silt/
Mudstone
Quartzite
Carbonate
21-PXN-012A
Red
dolostone

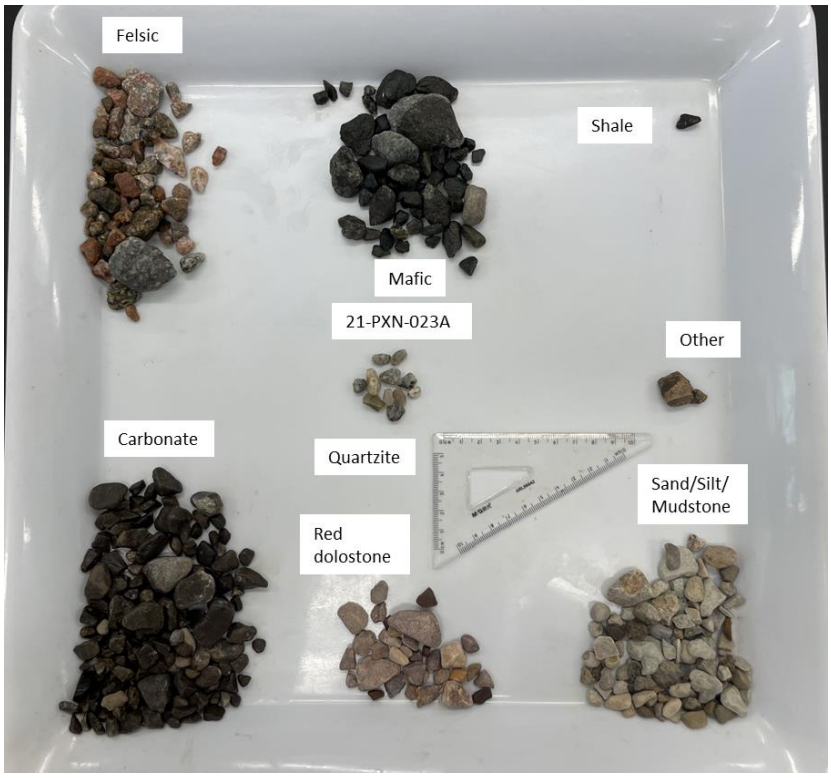

Shale
Mafic
Sand/Silt/
Mudstone
Felsic
Quartzite
Red
dolostone
21-PXN-024A

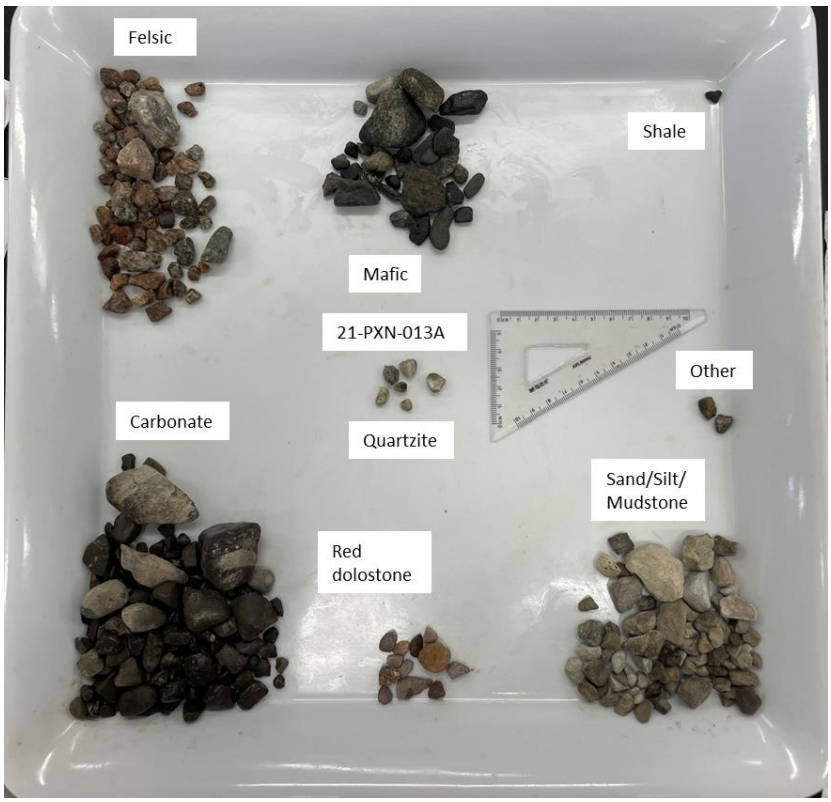

Shale
Mafic
21-PXN-021A
Felsic
Sand/Silt/
Mudstone
Quartzite
Carbonate
Red
dolostone

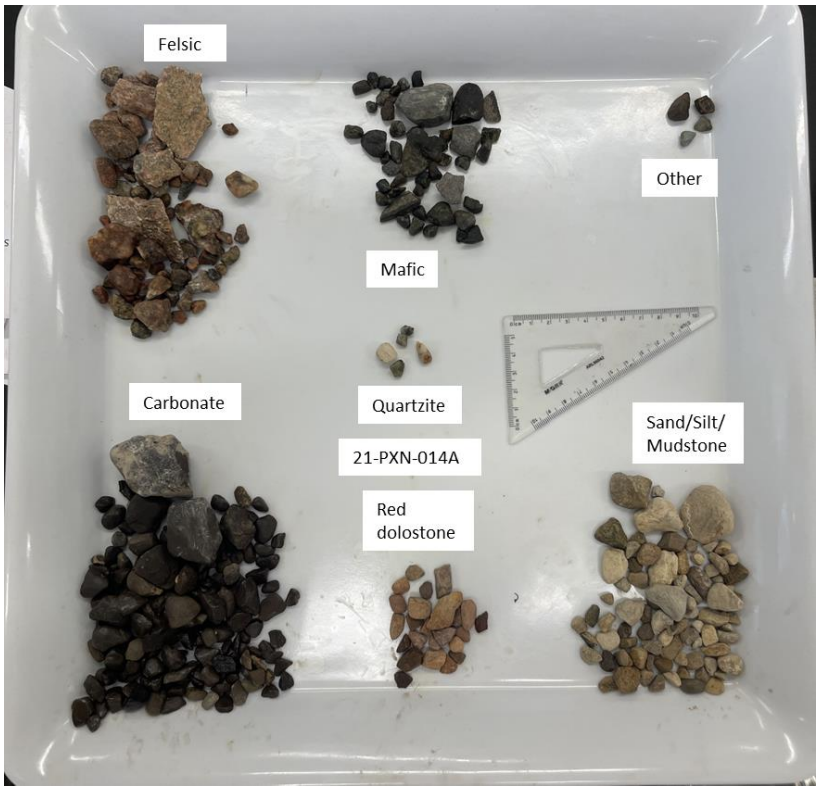

Mafic
Sand/Silt/
Mudstone
Felsic
21-PXN-016A
Carbonate
(limestone)

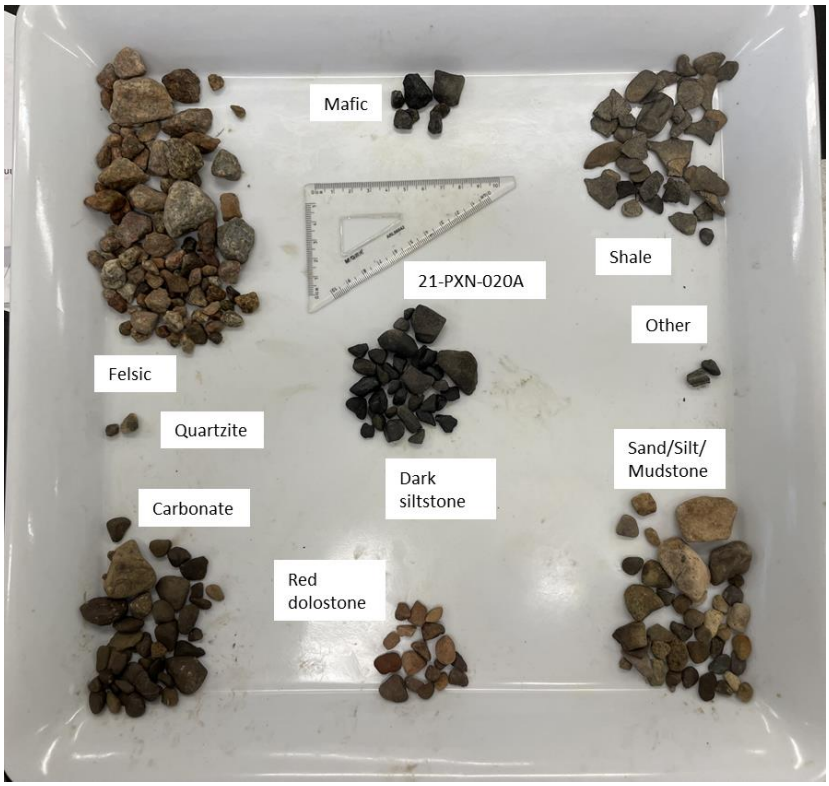

Mafic
Felsic
21-PXN-042A
Shale
Other
Quartzite
Carbonate
Dark siltstone
Red dolostone
Sand/Silt/ Mudstone

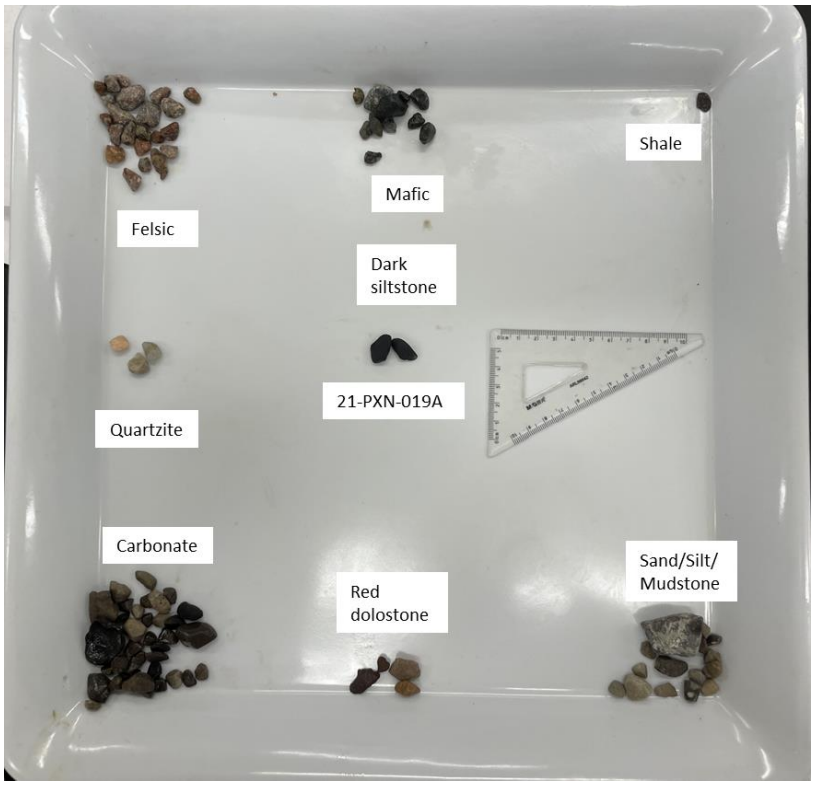

Felsic
Other
Mafic
21-PXN-022A
Carbonate
Quartzite
Sand/Silt/ Mudstone
Red dolostone

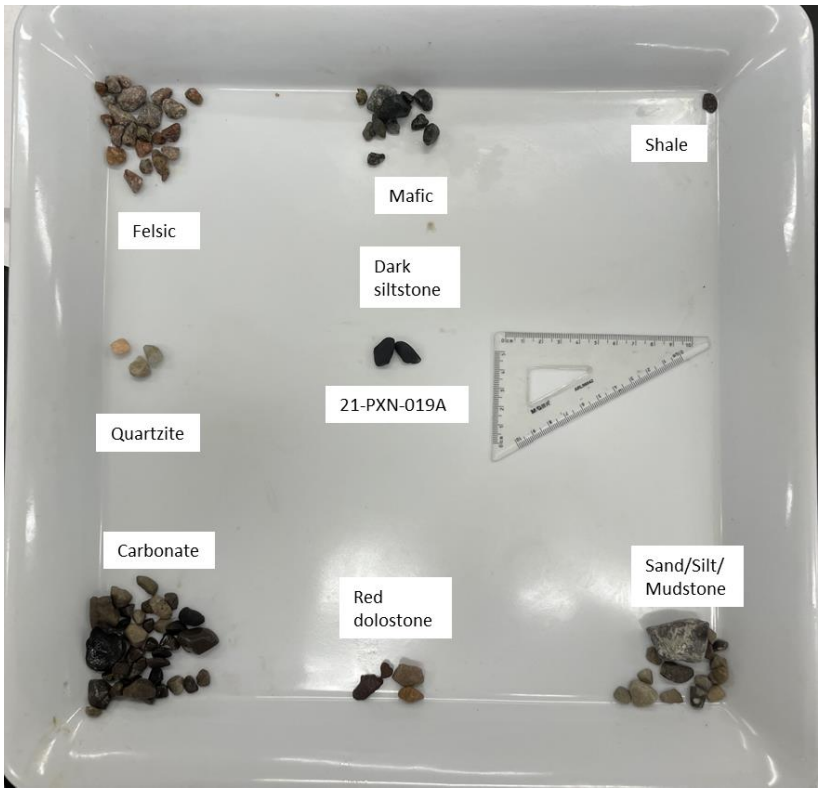

Felsic
Shale
Mafic
21-PXN-023A
Other
Carbonate
Quartzite
Sand/Silt/
Mudstone
Red
dolostone

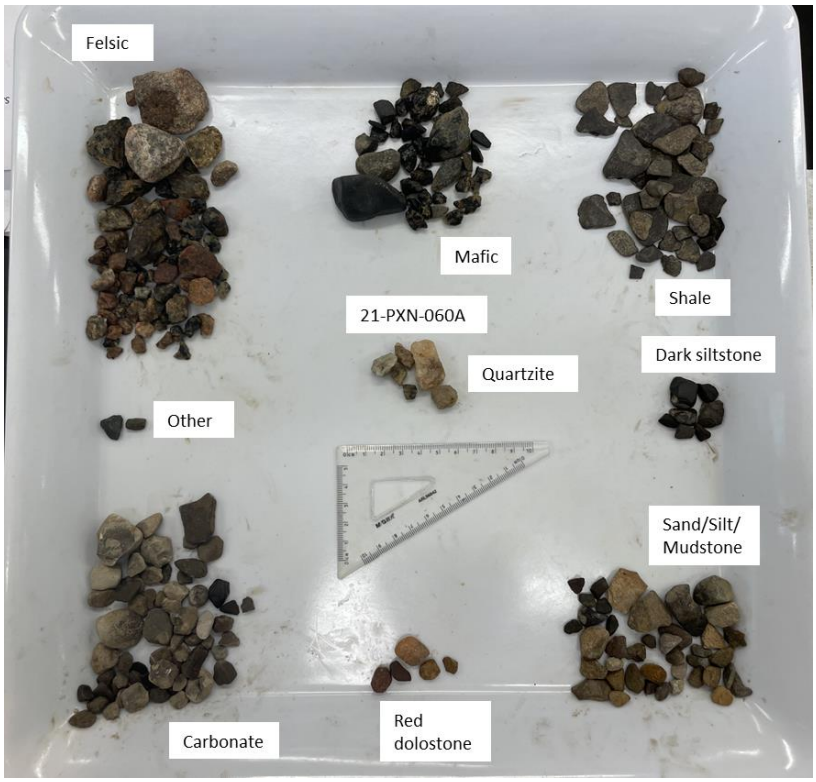

Felsic
Shale
Mafic
21-PXN-013A
Other
Carbonate
Quartzite
Sand/Silt/
Mudstone
Red
dolostone

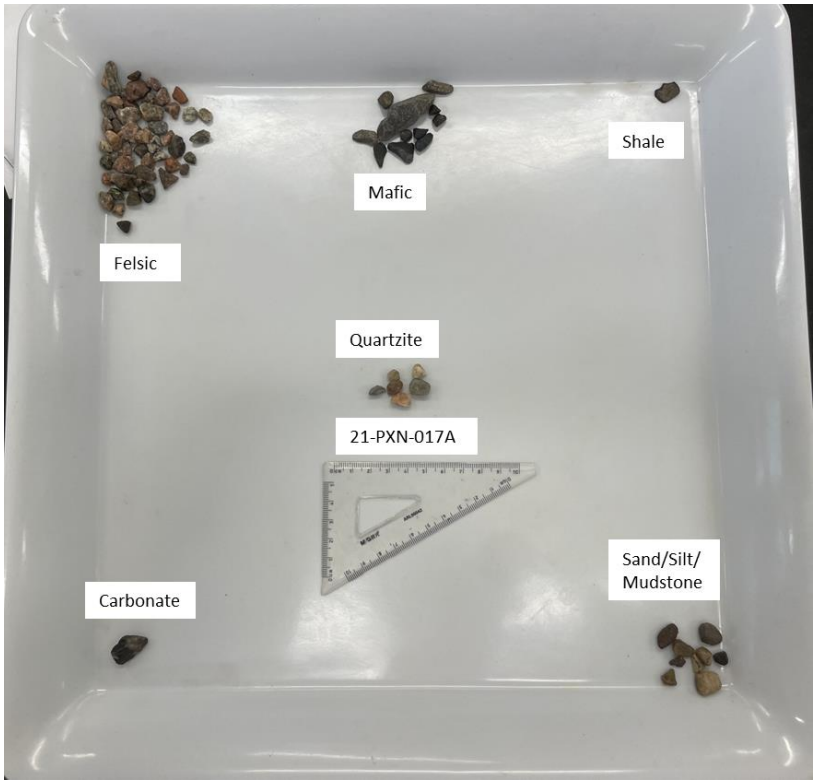

Felsic
Other
Mafic
Carbonate
Quartzite
Sand/Silt/
Mudstone
21-PXN-014A
Red
dolostone

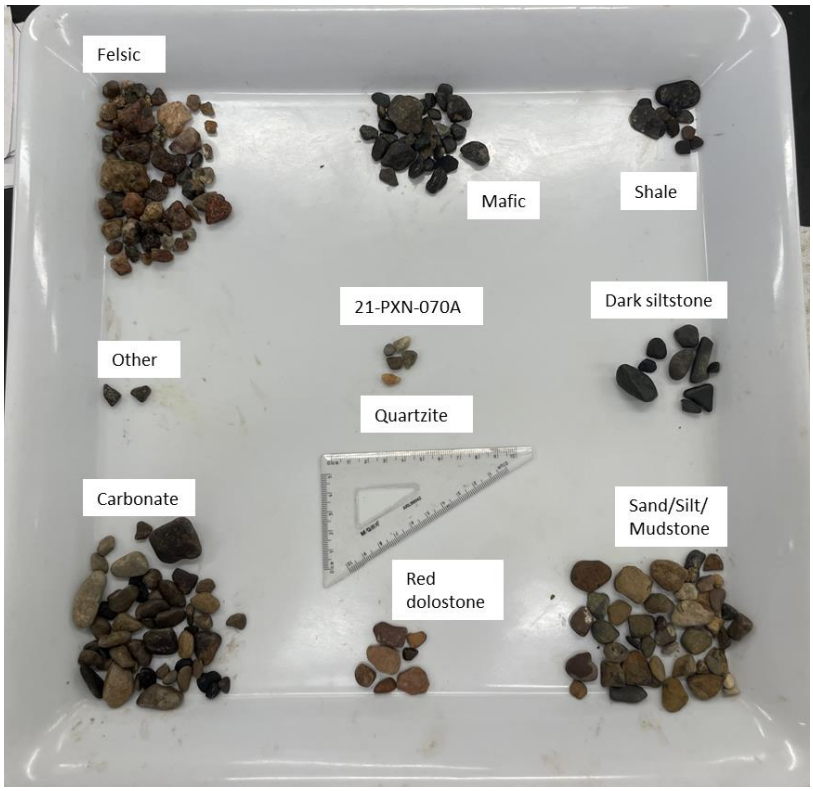

Mafic
Shale
21-PXN-020A
Other
Felsic
Quartzite
Sand/Silt/
Mudstone
Dark
siltstone
Carbonate
Red
dolostone

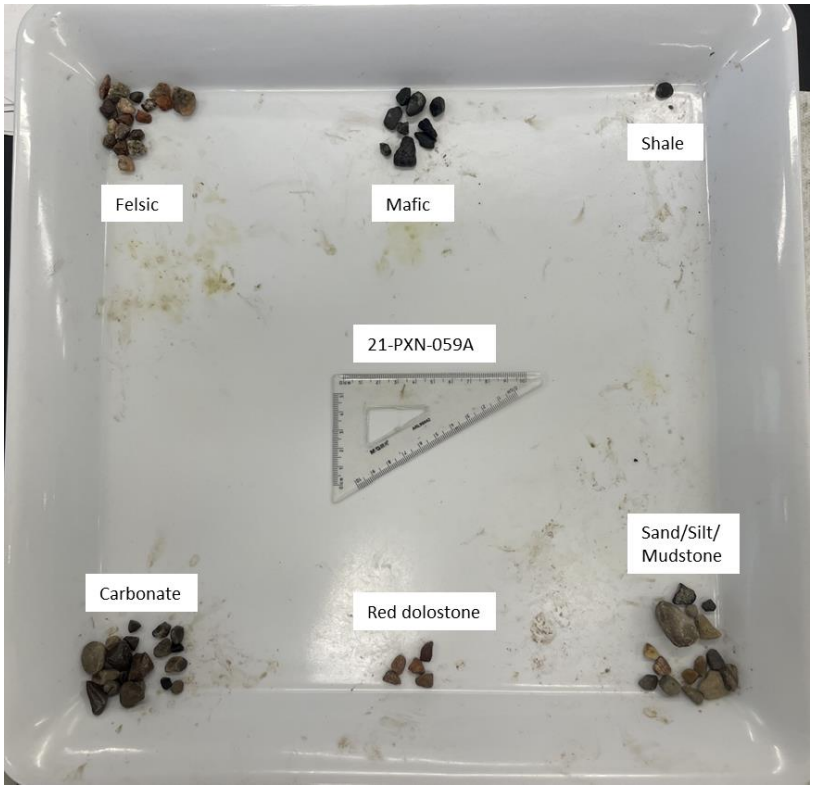

Shale
Mafic
Felsic
Dark siltstone
21-PXN-019A
Quartzite
Carbonate
Sand/Silt/ Mudstone
Red dolostone

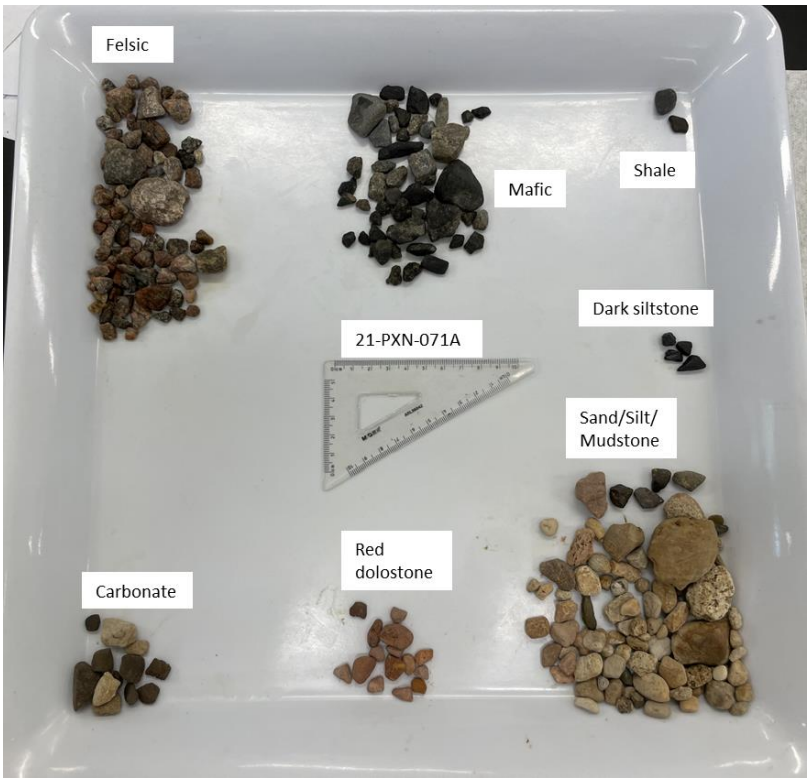

Shale
Mafic
Felsic
Dark siltstone
21-PXN-019A
Quartzite
Carbonate
Sand/Silt/ Mudstone
Red dolostone

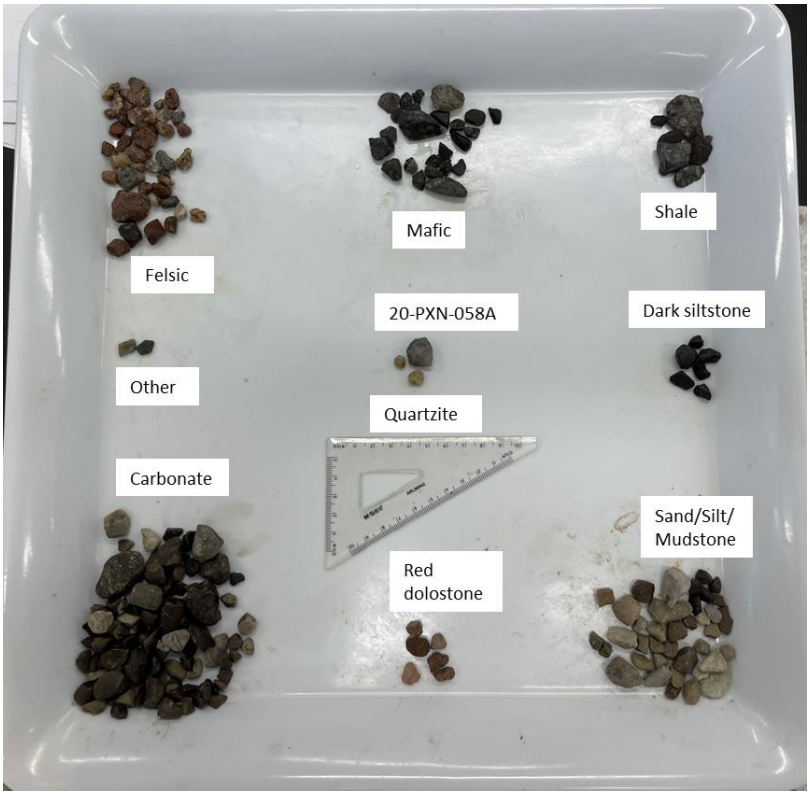

Felsic
Mafic
Shale
21-PXN-060A
Quartzite
Dark siltstone
Other
Sand/Silt/
Mudstone
Carbonate
Red
dolostone

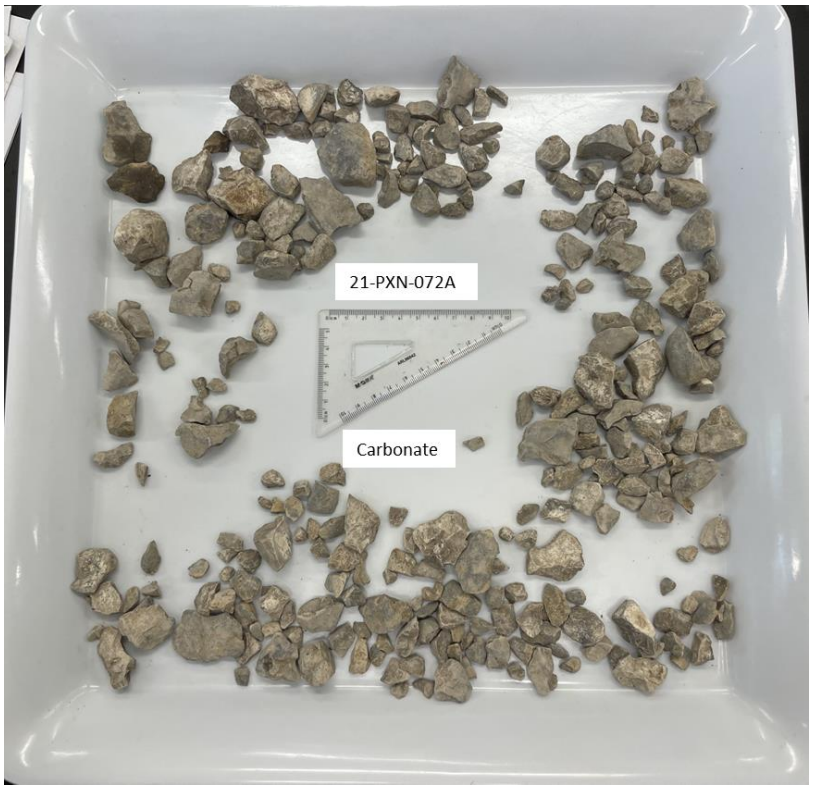

Shale
Mafic
Felsic
Quartzite
21-PXN-017A
Sand/Silt/
Mudstone
Carbonate

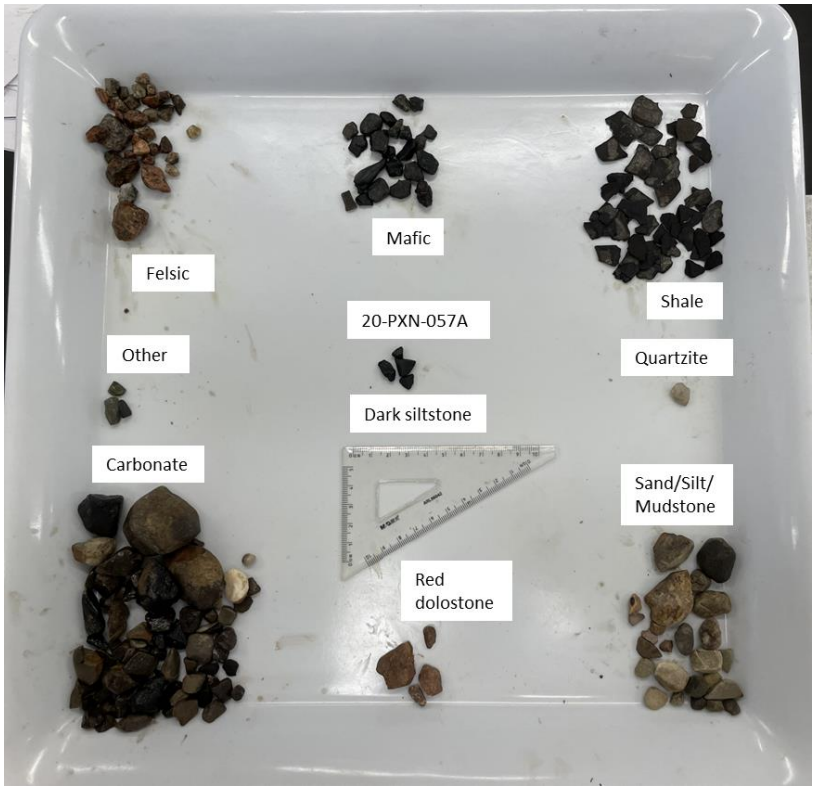

Felsic
Mafic
Shale
21-PXN-070A
Dark siltstone
Other
Quartzite
Carbonate
Sand/Silt/
Mudstone
Red
dolostone

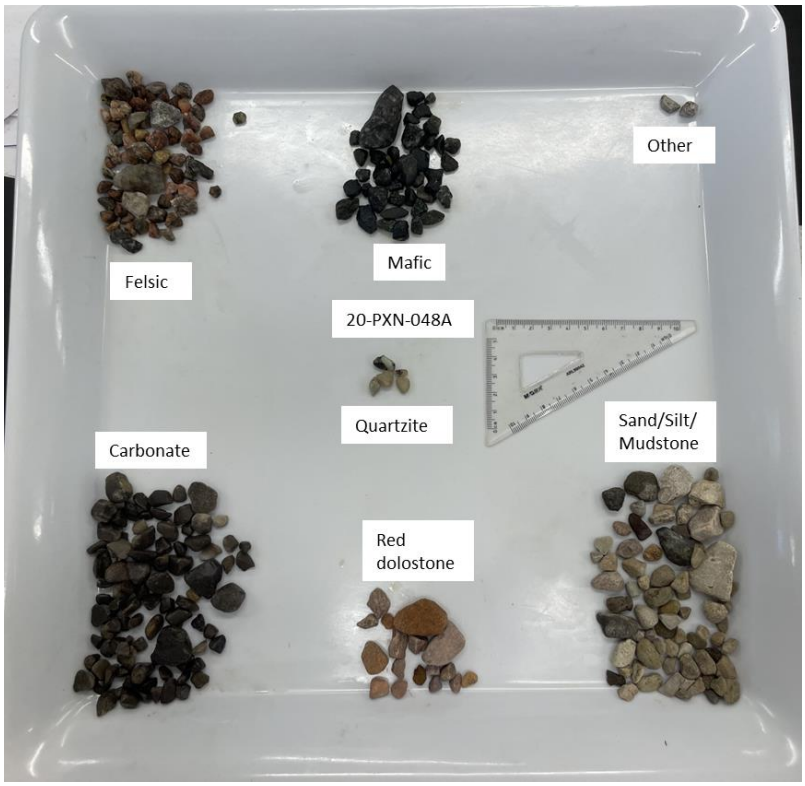

Shale
Felsic
Mafic
21-PXN-059A
Sand/Silt/
Mudstone
Carbonate
Red dolostone

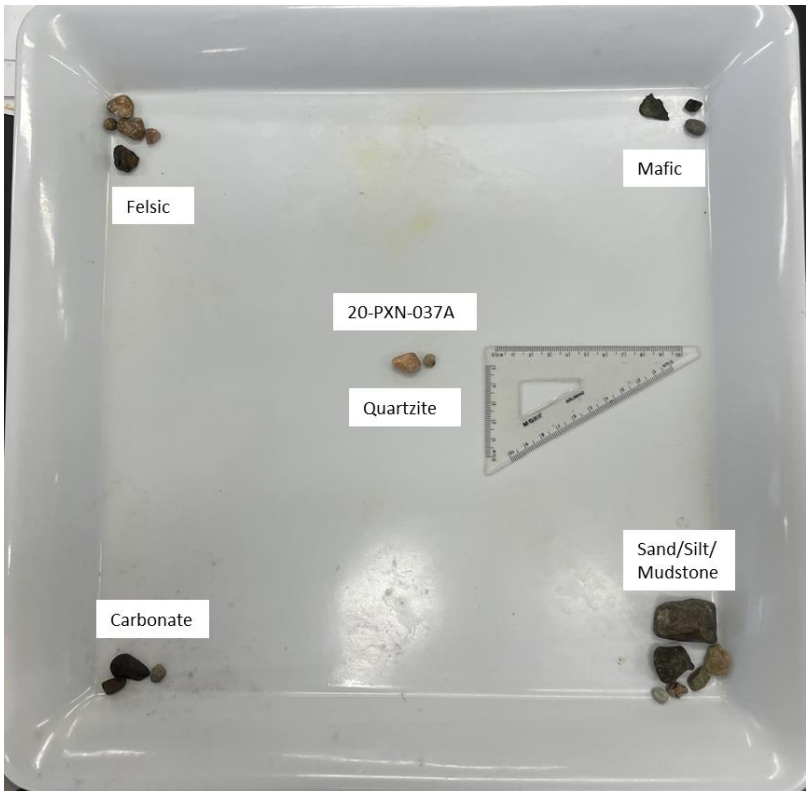

Felsic
Mafic
Shale
Dark siltstone
21-PXN-071A
Sand/Silt/
Mudstone
Red
dolostone
Carbonate

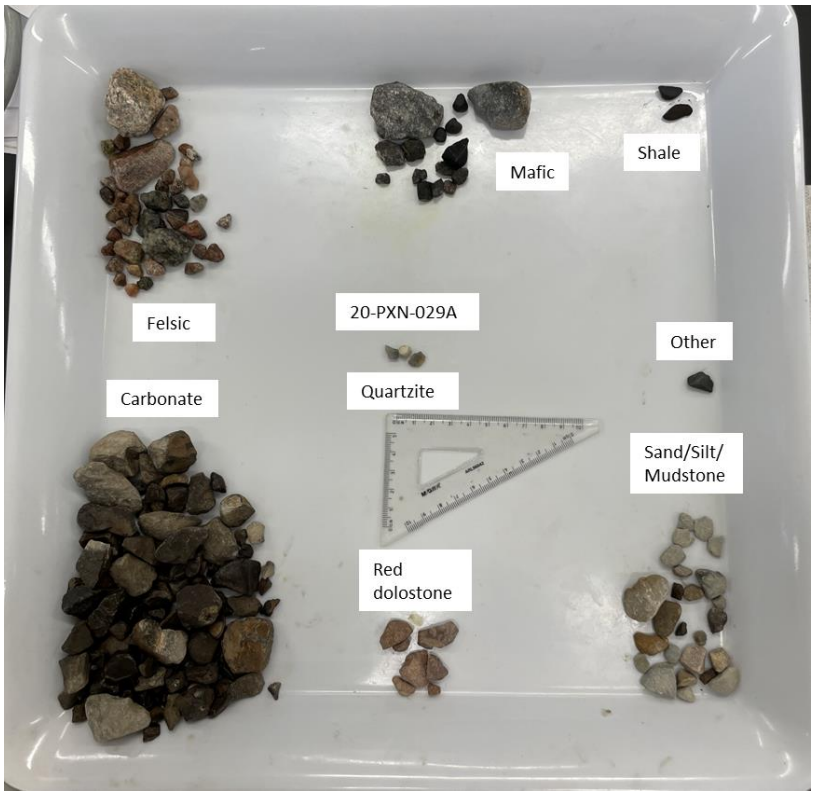

Mafic
Shale
Felsic
20-PXN-058A
Dark siltstone
Other
Quartzite
Carbonate
Sand/Silt/
Mudstone
Red
dolostone

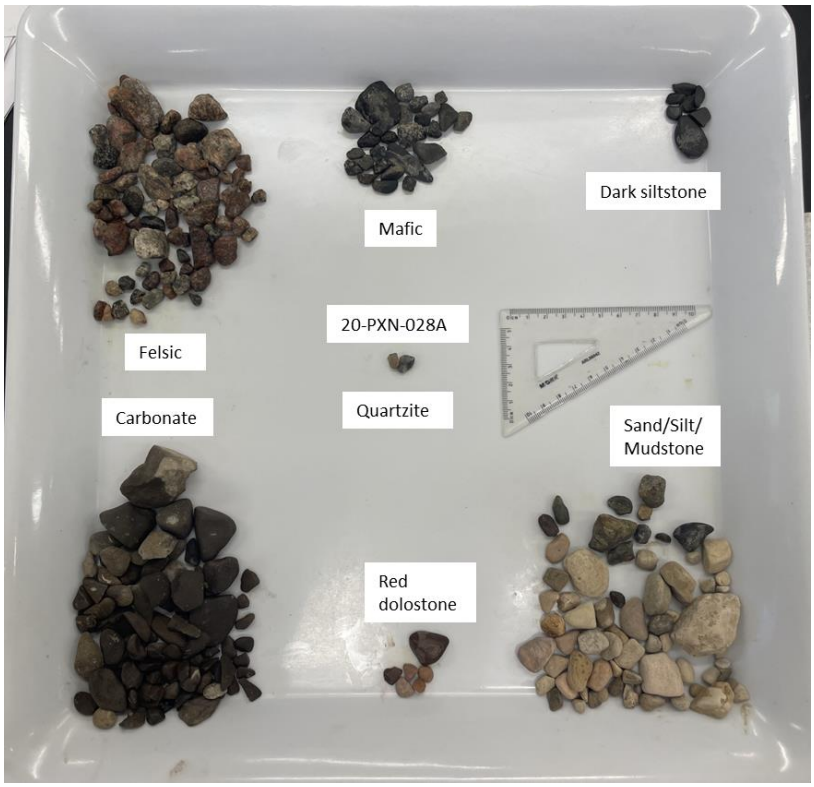

21-PXN-072A
Carbonate


Felsic
Mafic
Shale
20-PXN-057A
Other
Quartzite
Dark siltstone
Carbonate
Sand/Silt/
Mudstone
Red
dolostone

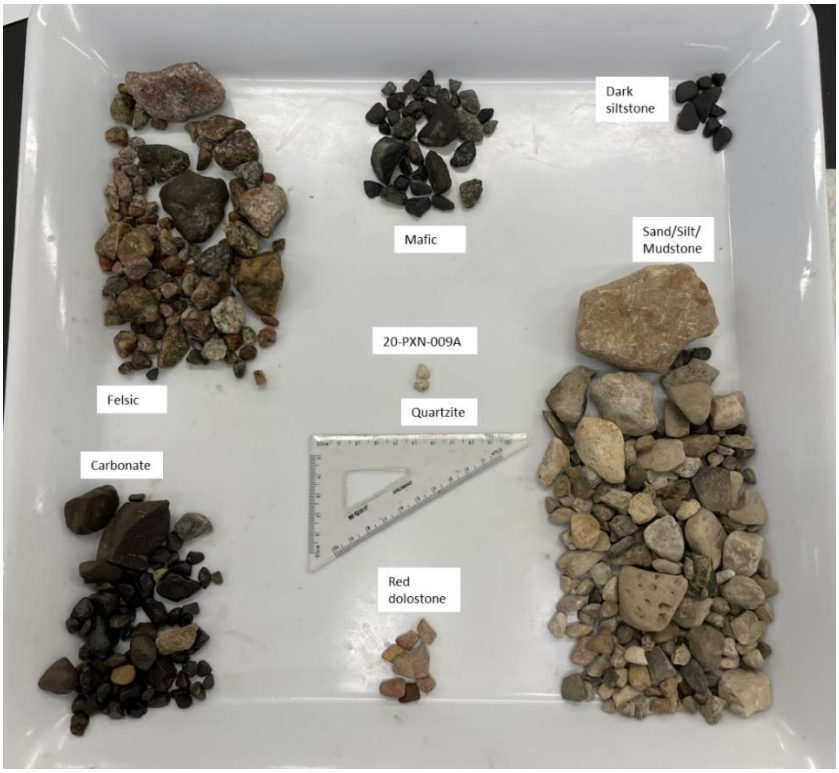

Other
Felsic
Mafic
20-PXN-048A
Quartzite
Sand/Silt/
Mudstone
Carbonate
Red
dolostone

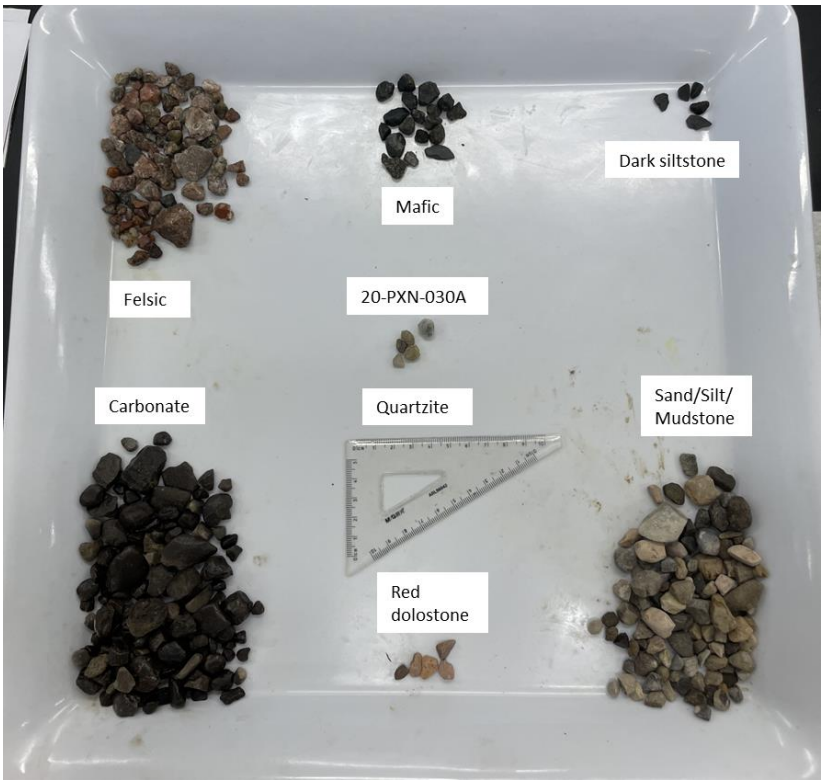

Mafic
Felsic
20-PXN-037A
Quartzite
Sand/Silt/
Mudstone
Carbonate


Mafic
Shale
Felsic
20-PXN-029A
Other
Quartzite
Carbonate
Sand/Silt/
Mudstone
Red
dolostone

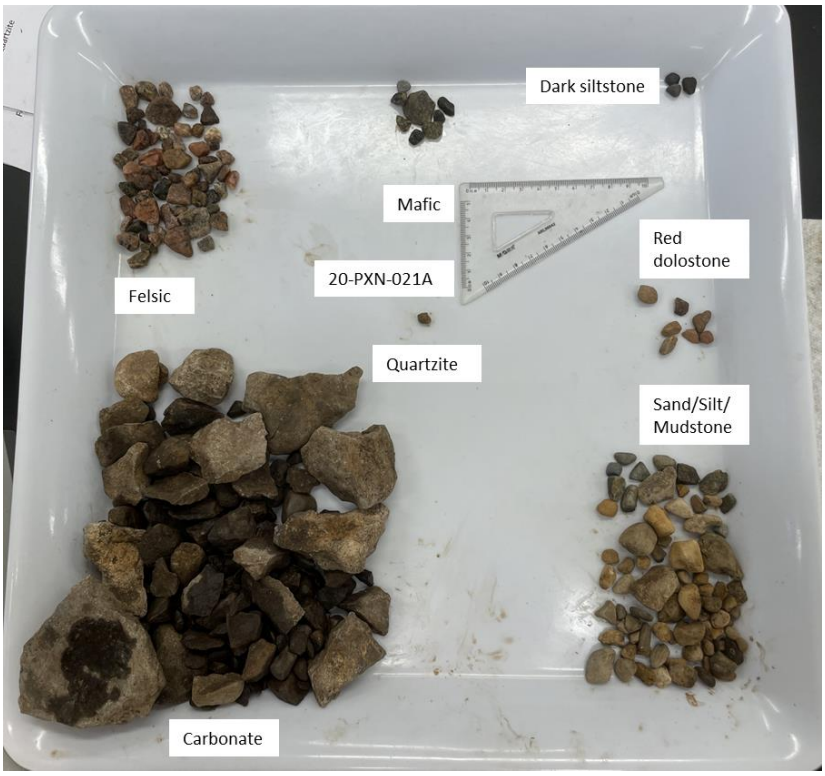

Mafic
Dark siltstone
Felsic
20-PXN-028A
Quartzite
Carbonate
Sand/Silt/
Mudstone
Red
dolostone

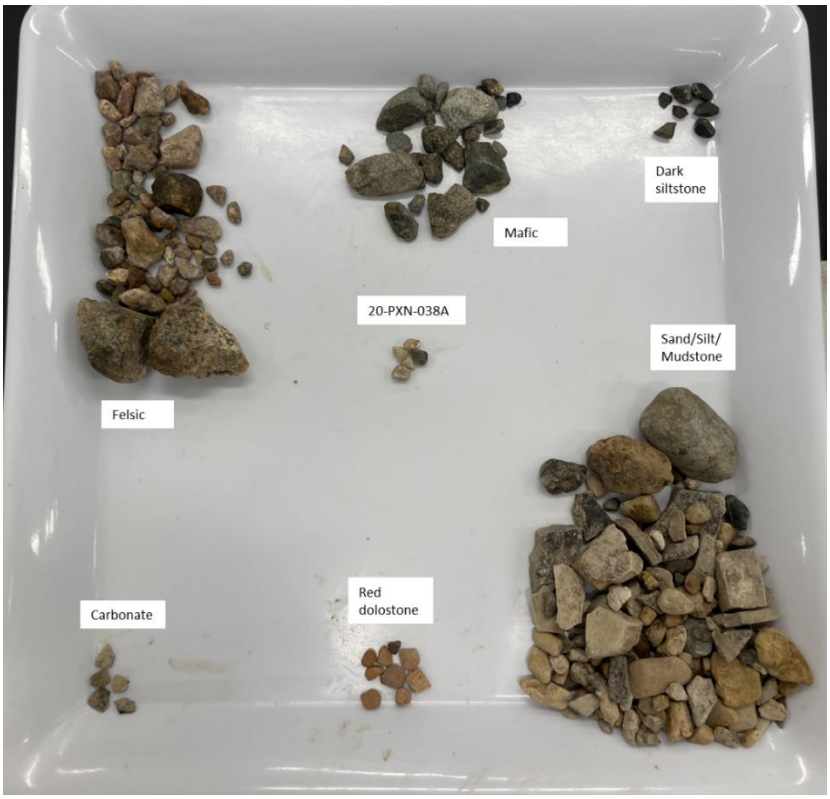

Dark siltstone
Mafic
Sand/Silt/
Mudstone
20-PXN-010A
Felsic
Quartzite
Carbonate
Red
dolostone

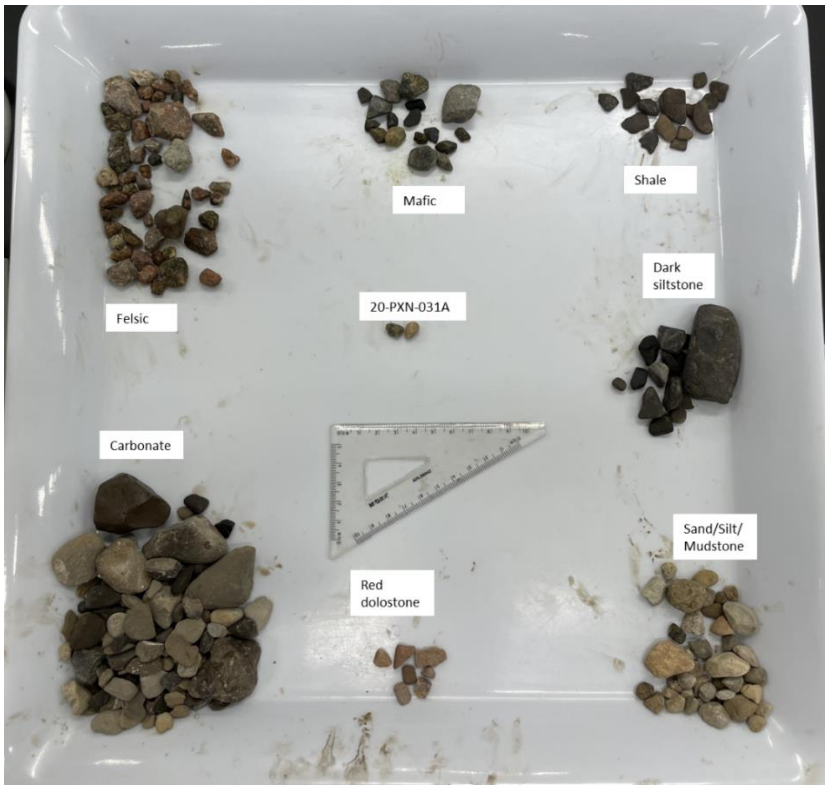

Dark
siltstone
Mafic
Sand/Silt/
Mudstone
20-PXN-009A
Felsic
Quartzite
Carbonate
Red
dolostone

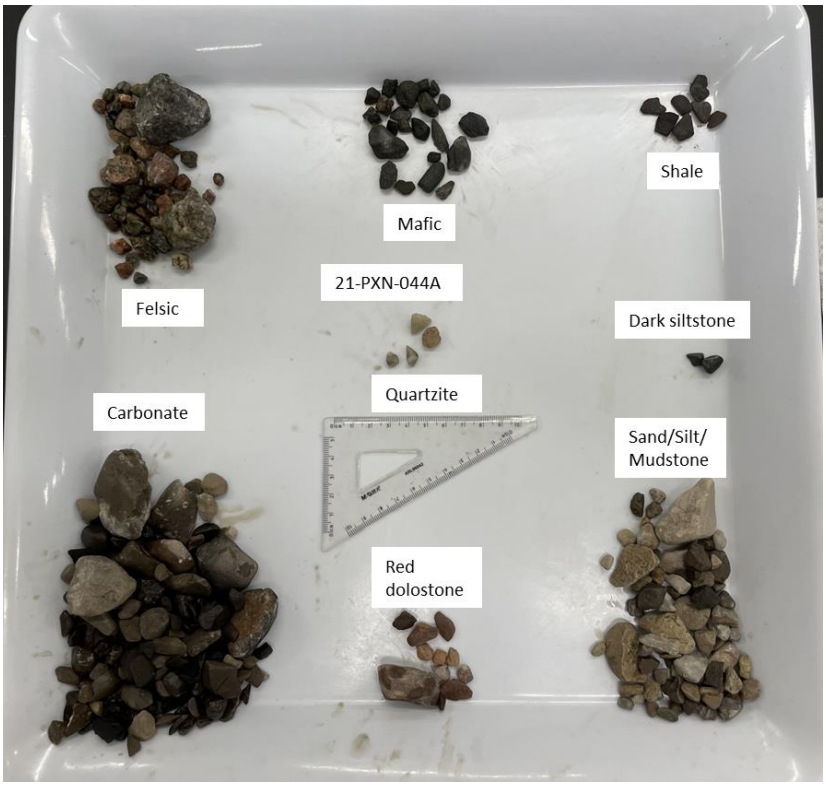

Dark siltstone
Mafic
Felsic
20-PXN-030A
Carbonate
Quartzite
Sand/Silt/
Mudstone
Red
dolostone


Mafic
Felsic
20-PXN-047A
Carbonate
Sand/Silt/
Mudstone
Red
dolostone


Dark siltstone
Mafic
Red dolostone
20-PXN-021A
Felsic
Quartzite
Sand/Silt/ Mudstone
Carbonate


Dark siltstone
Mafic
20-PXN-038A
Sand/Silt/ Mudstone
Felsic
Carbonate
Red dolostone


Mafic
Shale
Dark siltstone
Felsic
20-PXN-031A
Carbonate
Sand/Silt/ Mudstone
Red dolostone


Shale
Mafic
21-PXN-044A
Felsic
Dark siltstone
Quartzite
Carbonate
Sand/Silt/ Mudstone
Red dolostone

Appendix D

Stratigraphic Logging Data

Strat section 01		West side of Hwy 3	
Bottom: 22°		Top: 24°	
Height: 6m			
1st hole: 1.4m from top, poorly sorted			
Clast	Sphericity	Roundness	
1	0.9	0.5	
2	0.7	0.1	
3	0.7	0.9	
4	0.3	0.9	
5	0.5	0.3	
6	0.9	0.7	
7	0.9	0.3	
8	0.9	0.5	
9	0.7	0.5	
10	0.5	0.1	
11	0.7	0.3	
12	0.5	0.1	
Color: 10yr, 3/3			
2nd hole: 0.7m below 1st hole			
Clast	Sphericity	Roundness	
1	0.7	0.5	
2	0.9	0.9	
3	0.5	0.3	
4	0.5	0.3	
5	0.5	0.3	
6	0.9	0.9	
7	0.5	0.5	
8	0.9	0.7	
9	0.9	0.7	
10	0.9	0.5	
11	0.5	0.5	
12	0.3	0.1	
13	0.7	0.9	
Color: 10YR, 4/3			

Strat section 02		East side of Hwy 3	
Dip angle: 27°			
Height: 6.8m			
1st hole: 0.8m from top			
Clast	Sphericity	Roundness	
1	0.9	0.3	
2	0.7	0.5	
3	0.9	0.3	
4	0.9	0.3	
5	0.9	0.7	
6	0.3	0.5	
Color: 10yr, 6/3			
Till: 10yr, 4/3			
2nd hole: 0.5m below 1st hole			
Clast	Sphericity	Roundness	
1	0.7	0.3	
2	0.5	0.9	
3	0.7	0.5	
4	0.5	0.1	
5	0.7	0.9	
6	0.9	0.5	
Color: 10yr, 4/3			
3rd hole: 0.5m below 2nd hole			
Clast	Sphericity	Roundness	
1	0.9	0.3	
2	0.5	0.7	
3	0.9	0.3	
4	0.9	0.9	
5	0.9	0.7	
6	0.9	0.5	
Color: 10yr, 4/3			

3rd hole: 0.6m below 2nd hole		
Clast	Sphericity	Roundness
1	0.7	0.3
2	0.3	0.7
3	0.7	0.9
4	0.5	0.9
5	0.7	0.5
6	0.3	0.5
7	0.9	0.7
8	0.7	0.9
Color: 10yr, 3/3		

4th hole: 0.6m brlow 3rd hole		
Clast	Sphericity	Roundness
1	0.7	0.9
2	0.5	0.3
3	0.7	0.3
4	0.9	0.7
5	0.3	0.3
6	0.3	0.1
7	0.5	0.3
8	0.7	0.5
9	0.7	0.5
10	0.9	0.7
11	0.5	0.3
12	0.5	0.7
Color: 10yr, 3/3		

5th hole: 0.5m brlow 4th hole		
Clast	Sphericity	Roundness
1	0.9	0.5
2	0.7	0.3
3	0.5	0.3
4	0.9	0.9
5	0.7	0.1
6	0.9	0.9

4th hole: 0.55m below 3rd hole		
Clast	Sphericity	Roundness
1	0.7	0.5
2	0.7	0.9
3	0.9	0.3
4	0.5	0.7
5	0.7	0.1
Color: 10yr, 4/3		

5th hole: 0.5m below 4th hole		
Clast	Sphericity	Roundness
1	0.5	0.3
2	0.9	0.7
3	0.9	0.3
4	0.5	0.9
5	0.9	0.7
Color: 10yr, 4/3		

6th hole: 0.5m below 5th hole		
Clast	Sphericity	Roundness
1	0.9	0.3
2	0.9	0.9
3	0.9	0.7
4	0.9	0.3
5	0.9	0.7
6	0.9	0.7
Color: 10yr, 4/3		

7th hole: 0.45m below 6th hole		
Clast	Sphericity	Roundness
1	0.9	0.7
2	0.5	0.9
3	0.9	0.7
4	0.7	0.3
5	0.7	0.1
Color: 10yr, 4/3		

7	0.5	0.9				
8	0.7	0.1		8th hole: 0.5m below		
9	0.9	0.5		Clast	Sphericity	Roundness
10	0.3	0.3		1	0.7	0.3
11	0.3	0.5		2	0.9	0.5
12	0.3	0.5		3	0.9	0.7
Color: 10yr, 4/3				4	0.9	0.3
				5	0.5	0.1
6th hole: 0.6m below 5th hole				Color: 10yr, 4/3		
Clast	Sphericity	Roundness				
1	0.7	0.5		9th hole: 0.5m below 8th hole		
2	0.5	0.9		Clast	Sphericity	Roundness
3	0.5	0.3		1	0.7	0.1
4	0.3	0.3		2	0.5	0.5
5	0.3	0.1		3	0.7	0.5
6	0.7	0.5		4	0.9	0.1
7	0.7	0.5		5	0.7	0.1
8	0.7	0.1		Color: 10yr, 4/3		
9	0.5	0.3				
10	0.5	0.3		10th hole: 0.45m below 9th hole		
11	0.9	0.7		Clast	Sphericity	Roundness
12	0.7	0.9		1	0.3	0.5
13	0.5	0.3		2	0.9	0.7
Color: 10yr, 4/3				3	0.7	0.1
				4	0.9	0.5
7th hole: 0.4m below 6th hole				5	0.5	0.3
Clast	Sphericity	Roundness		6	0.9	0.3
1	0.7	0.1		Color: 10yr, 4/3		
2	0.7	0.3				
3	0.7	0.5		11th hole: 0.4m below 10th hole		
4	0.5	0.5		Clast	Sphericity	Roundness
5	0.5	0.9		1	0.3	0.3
6	0.7	0.1		2	0.9	0.9
7	0.3	0.1		3	0.7	0.9
8	0.7	0.3		4	0.5	0.3
9	0.7	0.9		Color: 10yr, 4/3		

10	0.3	0.5				
11	0.5	0.9		12th hole: 0.4m below 11th hole		
12	0.7	0.9		Clast	Sphericity	Roundness
Color: 10yr, 4/3				1	0.9	0.7
				2	0.9	0.9
8th hole: 0.6m below 7th hole				3	0.9	0.7
Clast	Sphericity	Roundness		4	0.9	0.5
1	0.9	0.7		5	0.3	0.5
2	0.9	0.7		6	0.5	0.3
3	0.3	0.3		Color: 1oyr, 4/3		
4	0.5	0.3				
5	0.9	0.5		13th hole: 0.4m below 12th hole		
6	0.7	0.9		Clast	Sphericity	Roundness
7	0.9	0.7		1	0.7	0.7
8	0.7	0.5		2	0.3	0.7
9	0.7	0.9		3	0.7	0.1
10	0.7	0.1		4	0.9	0.5
11	0.9	0.3		5	0.9	0.7
12	0.7	0.3		Color: 10yr, 4/3		
13	0.9	0.5				
Color: 10yr, 4/3				14th hole: 0.4m below 13th hole		
				Clast	Sphericity	Roundness
9th hole: 0.6m below 8th hole				1	0.9	0.7
Clast	Sphericity	Roundness		2	0.9	0.7
1	0.5	0.3		3	0.3	0.7
2	0.9	0.7		4	0.9	0.1
3	0.7	0.5		5	0.5	0.9
4	0.7	0.3		Color: 10yr, 4/3		
5	0.9	0.5				
6	0.9	0.7		15th hole: 0.4m below 14th hole		
7	0.7	0.9		Clast	Sphericity	Roundness
8	0.5	0.3		1	0.3	0.3
Colorl: 10yr, 4/3				2	0.9	0.3
				3	0.9	0.5
10th hole: 0.4m below 9th hole				4	0.9	0.5
Clast	Sphericity	Roundness		5	0.3	0.7

1	0.9	0.5		Color: 10yr, 3/3		
2	0.9	0.3				
3	0.7	0.9		16th hole: 0.5m below 15th hole		
4	0.7	0.1		Clast	Sphericity	Roundness
5	0.9	0.5		1	0.3	0.7
6	0.7	0.9		2	0.9	0.7
7	0.3	0.1		3	0.7	0.1
8	0.7	0.5		4	0.5	0.1
Colorl: 10yr, 4/3				5	0.7	0.3
				Color: 10yr, 3/3		

11th hole: 0.35m below 10th hole		
Clast	Sphericity	Roundness
1	0.9	0.1
2	0.9	0.7
3	0.3	0.9
4	0.7	0.5
5	0.5	0.3
6	0.7	0.5
7	0.7	0.5
8	0.9	0.3
9	0.7	0.5
10	0.7	0.3
Color: 10yr, 4/3		
12th hole: 0.3m below 11th hole		
Clast	Sphericity	Roundness
1	0.3	0.3
2	0.5	0.3
3	0.7	0.3
4	0.7	0.5
5	0.9	0.5
6	0.7	0.3
7	0.9	0.3
8	0.9	0.7
9	0.3	0.3
10	0.7	0.9

11	0.7	0.5
Color: 10yr, 4/3		
13th hole: 0.5m below 12th hole		
Clast	Sphericity	Roundness
1	0.7	0.9
2	0.7	0.9
3	0.9	0.7
4	0.9	0.5
5	0.9	0.9
6	0.7	0.1
7	0.9	0.5
8	0.7	0.9
9	0.7	0.9
10	0.9	0.5
Color: 10y	0.8	0.68
14th hole: 0.5m below 13th hole		
Clast	Sphericity	Roundness
1	0.5	0.9
2	0.3	0.5
3	0.3	0.9
4	0.9	0.7
5	0.5	0.7
6	0.9	0.7
7	0.7	0.9
8	0.3	0.5
9	0.7	0.9
10	0.5	0.1
Color: 10yr, 3/3		

Strat section 03		West side of Hwy 3
Top: 16°	Middle: 22	Bottom: 25°
Height: 5.3m		
1st hole: 0.45m from top		
Clast	Sphericity	Roundness
1	0.7	0.5
2	0.9	0.5
3	0.9	0.7
4	0.7	0.9
5	0.9	0.5
6	0.3	0.9
7	0.3	0.7
8	0.9	0.7
9	0.9	0.3
10	0.5	0.3
2nd hole: 0.3m below 1st hole		
Clast	Sphericity	Roundness
1	0.9	0.3
2	0.5	0.7
3	0.3	0.5
4	0.5	0.3
5	0.5	0.3
6	0.9	0.3
7	0.9	0.5
8	0.5	0.3
7.5yr, 4/4		
3rd hole: 0.35m below 2nd hole		
Clast	Sphericity	Roundness
1	0.5	0.5
2	0.5	0.1
3	0.5	0.3
4	0.9	0.7
5	0.7	0.1
6	0.9	0.7
7	0.7	0.1
8	0.5	0.5

Strat section 04		West side of Hwy 3
Height: 5m		South of Chan Lake
New drumlin site		
1st hole: 1.35m from top		
Clast	Sphericity	Roundness
1	0.5	0.5
2	0.9	0.3
3	0.9	0.5
4	0.7	0.3
5	0.9	0.5
6	0.9	0.5
7	0.7	0.1
8	0.7	0.1
Color: 10yr, 4/3		
2nd hole: 1.1m below 1st holw		
Clast	Sphericity	Roundness
1	0.3	0.3
2	0.9	0.9
3	0.9	0.3
4	0.9	0.9
5	0.7	0.7
6	0.9	0.3
7	0.9	0.7
8	0.5	0.5
Color: 10yr, 4/3		
3rd hole: 1.4m below 2nd hole		
Clast	Sphericity	Roundness
1	0.3	0.1
2	0.7	0.9
3	0.7	0.3
4	0.3	0.5
5	0.7	0.3
6	0.9	0.3
7	0.3	0.9
8	0.7	0.1
Color: 10yr, 4/3		

9	0.9	0.7				
10	0.3	0.3		4th hole: 0.9m below 3rd hole		
11	0.7	0.3		Clast	Sphericity	Roundness
12	0.5	0.9		1	0.5	0.3
First 0.2m: 7.5yr, 4/4				2	0.3	0.5
Till: 10yr, 4/3				3	0.3	0.3
				4	0.7	0.3
4th hole: 0.35m below 3th hole				5	0.9	0.5
Clast	Sphericity	Roundness		6	0.9	0.3
1	0.3	0.7		7	0.9	0.1
2	0.9	0.3		8	0.9	0.5
3	0.5	0.7		9	0.3	0.3
4	0.3	0.3		10	0.3	0.5
5	0.7	0.1		11	0.9	0.5
6	0.7	0.3		12	0.9	0.3
7	0.9	0.7		13	0.9	0.7
8	0.5	0.3		14	0.3	0.3
Color: 10yr, 3/3				15	0.7	0.7
				16	0.9	0.3
5th hole: 0.28m below 4th hole				17	0.3	0.3
Clast	Sphericity	Roundness		18	0.7	0.2
1	0.9	0.5		19	0.5	0.9
2	0.9	0.7		20	0.5	0.9
3	0.9	0.3		21	0.3	0.7
4	0.9	0.9		22	0.5	0.5
5	0.7	0.7		23	0.3	0.5
6	0.3	0.3		24	0.7	0.9
Color: 10yr, 3/3				25	0.7	0.7
				26	0.3	0.3
6th hole: 0.35m below 5th hoe				27	0.7	0.3
Clast	Sphericity	Roundness		28	0.5	0.3
1	0.7	0.1		29	0.7	0.9
2	0.5	0.3		30	0.3	0.9
3	0.3	0.1				
4	0.5	0.7				
5	0.5	0.1				
6	0.3	0.7				
7	0.5	0.9				

8	0.5	0.3
9	0.3	0.7
10	0.9	0.3
Color: 10yr, 3/3		
7th hole: 0.3m below 6th hole		
Clast	Sphericity	Roundness
1	0.7	0.5
2	0.9	0.7
3	0.9	0.9
4	0.7	0.7
5	0.9	0.7
6	0.5	0.3
7	0.9	0.5
8	0.9	0.3
9	0.7	0.1
10	0.5	0.3
Color: 10yr, 4/3		
8th hole: 0.3m below 7th hole		
Clast	Sphericity	Roundness
1	0.9	0.1
2	0.9	0.7
3	0.9	0.7
4	0.9	0.7
5	0.9	0.7
6	0.9	0.7
7	0.5	0.9
8	0.9	0.5
9	0.9	0.5
10	0.3	0.7
11	0.9	0.5
12	0.9	0.3
Color: 10yr, 4/3		
9th hole: 0.28m below 8th hole		
Clast	Sphericity	Roundness
1	0.7	0.5

2	0.9	0.7
3	0.9	0.3
4	0.9	0.7
5	0.9	0.7
6	0.9	0.7
7	0.5	0.9
8	0.9	0.5
9	0.9	0.5
10	0.3	0.7
11	0.9	0.5
12	0.9	0.3
Color: 10yr, 4/3		
10th hole: 0.45m below 9th hole		
Clast	Sphericity	Roundness
1	0.7	0.1
2	0.9	0.5
3	0.9	0.7
4	0.7	0.3
5	0.5	0.9
6	0.3	0.3
7	0.9	0.3
8	0.9	0.5
Color: 10yr, 4/3		
11th hole: 0.4m below 10th hole		
Clast	Sphericity	Roundness
1	0.9	0.7
2	0.7	0.1
3	0.5	0.3
4	0.9	0.9
5	0.9	0.5
6	0.9	0.1
7	0.7	0.3
8	0.5	0.7
9	0.7	0.9
10	0.7	0.9

12th hole: 0.3m below 11th hole		
Clast	Sphericity	Roundness
1	0.3	0.9
2	0.7	0.9
3	0.9	0.3
4	0.9	0.5
5	0.5	0.3
6	0.9	0.5
7	0.5	0.3
8	0.7	0.7
13th hole: 0.4m below 12th hole		
Clast	Sphericity	Roundness
1	0.9	0.7
2	0.9	0.1
3	0.3	0.3
4	0.5	0.5
5	0.5	0.3
6	0.3	0.5
7	0.3	0.1
8	0.5	0.3
Color: 10yr, 4/3		
14th hole: 0.35m below 13th hole		
Clast	Sphericity	Roundness
1	0.5	0.9
2	0.9	0.7
3	0.5	0.3
4	0.5	0.3
5	0.7	0.1
6	0.5	0.3
7	0.9	0.7
8	0.5	0.3
Color: 10yr, 4/3		

15th hole: 0.4m below 14th hole		
Clast	Sphericity	Roundness
1	0.9	0.7
2	0.5	0.3
3	0.9	0.7
4	0.9	0.5
5	0.9	0.7
6	0.3	0.5
7	0.7	0.1
8	0.5	0.3
Color: 10yr, 3/3		
16th hole: 0.4m below 15th hole		
Clast	Sphericity	Roundness
1	0.5	0.9
2	0.9	0.5
3	0.7	0.1
4	0.5	0.3
5	0.5	0.1
6	0.5	0.1
Color: 10yr, 3/3		
17th hole: 0.4m below 16th hole		
Clast	Sphericity	Roundness
1	0.7	0.1
2	0.9	0.3
3	0.9	0.3
4	0.5	0.3
5	0.3	0.3
6	0.5	0.7
7	0.7	0.5
8	0.3	0.5
Color: 10yr, 3/3		